

UNIVERSITÉ DU QUÉBEC À MONTRÉAL

PALÉOCÉANOGRAPHIE DU NORD-EST DU DÉTROIT DE FRAM DEPUIS LE  
DERNIER MAXIMUM GLACIAIRE

MÉMOIRE  
PRÉSENTÉ  
COMME EXIGENCE PARTIELLE  
DE LA MAÎTRISE EN SCIENCES DE LA TERRE

PAR  
JADE FALARDEAU

MAI 2017

UNIVERSITÉ DU QUÉBEC À MONTRÉAL  
Service des bibliothèques

Avertissement

La diffusion de ce mémoire se fait dans le respect des droits de son auteur, qui a signé le formulaire *Autorisation de reproduire et de diffuser un travail de recherche de cycles supérieurs* (SDU-522 – Rév.01-2006). Cette autorisation stipule que «conformément à l'article 11 du Règlement no 8 des études de cycles supérieurs, [l'auteur] concède à l'Université du Québec à Montréal une licence non exclusive d'utilisation et de publication de la totalité ou d'une partie importante de [son] travail de recherche pour des fins pédagogiques et non commerciales. Plus précisément, [l'auteur] autorise l'Université du Québec à Montréal à reproduire, diffuser, prêter, distribuer ou vendre des copies de [son] travail de recherche à des fins non commerciales sur quelque support que ce soit, y compris l'Internet. Cette licence et cette autorisation n'entraînent pas une renonciation de [la] part [de l'auteur] à [ses] droits moraux ni à [ses] droits de propriété intellectuelle. Sauf entente contraire, [l'auteur] conserve la liberté de diffuser et de commercialiser ou non ce travail dont [il] possède un exemplaire.»

## REMERCIEMENTS

Je tiens à remercier d'abord ma directrice Anne de Vernal pour son écoute et sa grande compréhension. Je la remercie pour sa patience et pour sa générosité. Elle m'a toujours bien guidée en respectant mes idées. Je ne lui serai jamais assez reconnaissante pour toutes les belles opportunités qu'elle m'a offertes durant ces trois dernières années. J'ai vécu certainement les meilleurs moments de ma vie. Jamais je ne regretterai le jour où je suis passée à son bureau en septembre 2013 avec un futur des plus incertains. Je dois bien évidemment souligner l'aide essentiel de Maryse Henry au laboratoire. Je dois la remercier pour son soutien technique, mais aussi pour son soutien moral. Après avoir passé des mois entiers consécutifs au laboratoire, je la considérais un peu comme ma troisième mère. Grâce à sa merveilleuse disponibilité, elle m'a enseignée tout ce que je sais aujourd'hui sur les pratiques au laboratoire et l'identification des palynomorphes, en plus de m'avoir aidée à travers toutes les étapes de ma recherche. J'ai aussi une pensée pour Robert Spielhagen que j'ai eu la chance de rencontrer à bord du RV Polarstern. Je dois le remercier pour sa grande sagesse avec les sédiments du Détroit de Fram, ses conseils pour les chronologies de mes carottes, ainsi que pour ses trucs et astuces avec le *box core*.

Merci à celles au laboratoire qui me rendent heureuses et me donnent le goût de me lever le matin pour aller au bureau. Je pense notamment à la belle dame Estelle Allan pour toutes ses petites attentions qui me réchauffent le cœur et les nombreux repas partagés ensemble. Je pense à Claudie Giguère-Croteau pour les pauses-café au Fractal bien méritées et son grand encouragement. Je pense aussi à Alice Morard, pour sa joie de vivre, ses coucous quotidiens à mon bureau et ses conseils. Finalement, il y a aussi cette chère Camille Brice avec qui une grande amitié a commencé au laboratoire

entre l'acide fluorhydrique et les tamis 106 µm. Merci pour les chasses au trésor à mon anniversaire et tous ces innombrables fous rires. Je dois aussi la remercier d'avoir épargné ma tendinite pendant 1 semaine.

Merci à mon amie, et aussi colocataire, qui tente à chaque matin de me sortir du lit pour que j'aille travailler, la grandiose Dominique Trudel-Grégoire, sans qui la vie au quotidien serait tellement plus plate. Merci pour tous ces beaux moments de complicité à aimer, mais aussi haïr la vie ensemble. Merci à Anthony Boulais mon technicien informatique personnel, mais surtout mon merveilleux ami. Finalement, un dernier merci à mes parents et ma sœur, qui ne savent certainement pas encore ce qu'est un dinokyste, mais qui ont certainement su être présents et réconfortants pour moi pendant la création du mémoire.

## AVANT-PROPOS

Ce mémoire de recherche porte sur l'étude de trois carottes sédimentaires, c'est-à-dire les carottes PS2863-2BC, PS2863-1 et MSM5/5-712-2. Plusieurs enregistrements paléocéanographiques ont déjà été publiés sur la carotte MSM5/5-712-2 notamment basés sur les biomarqueurs (Müller *et al.*, 2012; Müller et Stein, 2014) et les assemblages de foraminifères planctoniques, incluant l'analyse des isotopes stables sur les tests des foraminifères (Aagaard-Sørensen *et al.*, 2014a-b; Werner *et al.*, 2013, 2011; Zamelczyk *et al.*, 2014). Le modèle d'âge de la carotte MSM5/5-712-2 repose principalement sur celui de Müller et Stein (2014). Le modèle d'âge de la carotte PS2863-1 est original. Les âges  $^{14}\text{C}$  de cette dernière ont été transmis par M. Robert Spielhagen du centre Helmholtz pour la recherche océanique GEOMAR à l'exception d'un échantillon qui fut analysé au *National Ocean Sciences Accelerator Mass Spectrometry* (NOSAMS). Les 315 centimètres de la partie supérieure de la carotte MSM5/5-712-2 utilisés dans ce mémoire ont été analysés pour leur contenu palynologique par Sophie Bonnet et Maryse Henry. J'ai analysé la partie inférieure de la carotte (315-777 cm) et c'est la première fois que les résultats palynologiques de la carotte sont publiés. Dans cet article la carotte boîte PS2863-2BC est juxtaposée à la carotte par gravité PS2863-1 prélevée au même site et sont ainsi considérées comme une séquence composite (PS2863).

Le mémoire a été construit sous forme d'un article scientifique et a été soumis à la revue *Quaternary Science Reviews* le 12 mai 2017. Le cœur de l'article a donc été produit selon les directives de la revue et a été rédigé en anglais.

## TABLE DES MATIÈRES

AVANT-PROPOS .....	iv
LISTE DES FIGURES .....	vii
LISTE DES TABLEAUX .....	xi
LISTE DES ABRÉVIATIONS .....	xii
LISTE DES SYMBOLES .....	xv
RÉSUMÉ .....	xvii
INTRODUCTION .....	1
CHAPITRE I	
PALEOCEANOGRAPHY OF NORTHEASTERN FRAM STRAIT SINCE THE LAST GLACIAL MAXIMUM: PALYNNOLOGICAL EVIDENCE OF LARGE AMPLITUDE CHANGES .....	3
ABSTRACT .....	4
1.1 Introduction.....	5
1.2 Regional hydrography .....	7
1.3 Methods .....	9
1.4 Chronology of the cores.....	11
1.5 Results .....	12
1.5.1 Palynological assemblages .....	12
1.5.2 Reconstructions of sea-surface conditions .....	16
1.6 Discussion .....	18
1.6.1 The LGM paradox .....	18
1.6.2 Transition from the LGM to the postglacial.....	21
1.6.3 The setting of full “interglacial” conditions .....	29
1.7 Conclusion .....	31
1.8 Acknowledgements.....	33

1.9 References.....	34
CONCLUSION .....	68
APPENDICE A DÉNOMBREMENT ET CONCENTRATIONS DES PALYNOmorphes .....	72
APPENDICE B RÉSULTATS DES RECONSTITUTIONS .....	101
BIBLIOGRAPHIE GÉNÉRALE .....	107

## LISTE DES FIGURES

Figure	Page
1.1 Map of the main surface currents in Fram Strait and around Svalbard and location of the study sites MSM5/5-712-2 and PS2863 (yellow stars). Limits of minimum (September) and maximum (March) median sea-ice cover extent from 1979 to 2016 are represented by blue and gray dotted lines, respectively, from the Sea Ice Index (Fetterer et al., 2016). Red arrows indicate the warmer Atlantic waters derived from the North Atlantic Drift and were reproduced with respect to Walczowski et al. (2005). Blue arrows indicate cold surface water currents. In the Svalbard close up, the Arctic Coastal Front and the Polar Front are depicted, shown by a dotted and a uniform black line, respectively. The locations of other cores discussed in the text are indicated by black dots. Main features of the sea-floor such as the Yermak Plateau (YP), the Storfjorden and the Mohn and Knipovich Ridges are also indicated on the map. EGC: East Greenland Current, WSC: West Spitsbergen Current, NwASC: Norwegian Atlantic Slope Current, NwAC: Norwegian Atlantic Current, ESC: East Spitsbergen Current, SCC: South Cape Current, RAC: Return Atlantic Current, SB: Svalbard Branch, YB: Yermak Branch .....	54
1.2 Age model for cores MSM5/5-712-2, PS2863-1 and PS2837-5 (see Table 1.2 for data and text section 1.4). The red line corresponds to the weighted average. The darker gray areas show the most probable ages. The dates are indicated yellow and the correlated tie points are indicated in blue, with numbering as follows : (1) correlations with core PS2837-5 based on total	

organic carbon (cf. Müller and Stein, 2014), (2) correlations with the western Svalbard magnetic susceptibility stack of Jessen et al. (2010) from Müller and Stein (2014), (3) sedimentological correlation with core PS2837-5 based on IRD (this study; see triangle and dotted lines), (4) correlation of a fine-grained layer in core PS2863-1 with the rapidly deposited layer in the western Svalbard (Jessen et al., 2010). The vertical shaded zone corresponds to the interval of the rapidly deposited sediment layer defined by Jessen et al. (2010) including its 95% probability. Since the rapid sedimentation rate interval is a well-documented regional event (Jessen et al., 2010; Lucchi et al., 2015), we added hiatuses at the depths of the first and last age of the event so the model would interpret the accumulation rate of this interval separately.....	56
1.3 Palynomorph concentrations at sites PS2863 and MSM5/5-712-2. Dinocyst fluxes are represented by a thick line.....	58
1.4 Percentages of dinocyst taxa at site MSM5/5-712-2. Zones described in the text are delimited by dotted lines. The age of the LGM is established according to the MARGO working group (Kucera et al., 2005). The age of the Heinrich event 1 (H1), is determined according to Gibb et al. (2014). Limits of the Bølling-Allerød (BA) and the Younger Dryas (YD) intervals are set according to Rasmussen et al. (2006); the divisions between Early, Mid- and Late Holocene follow suggestions by Walker et al. (2012). On the calibrated age axis, the black bar indicates the interval of the rapidly deposited sediment layer described by Jessen et al. (2010), including its 95% probability while the gray bar represents the rapidly deposited sediment layer at the site. ....	59

1.5	Percentages of dinocysts taxa at site PS2863. For explanations see Fig. 1.4 .....	60
1.6	Light micrographs and SEM photographs of the morphological variations of <i>Spiniferites ramosus</i> and <i>Nematosphaeropsis labyrinthus</i> during the 14.5-11.5 ka interval in cores PS2863-1 and MSM5/5-712-2. ....	61
1.7	Reconstructions of sea-surface conditions at site MSM5/5-712-2 including summer and winter SSTs in red and blue, respectively, summer and winter SSSs in red and blue, respectively, sea-ice cover duration, and productivity. Mean values are represented by a thin line, the thick line shows a five-point running average. Maximum and minimum values are represented in brighter shading. At the right is the distance of the five closest analogues. The calculated threshold value for poor analogue is 1.2. Black triangles indicate modern values at the core site (SSTs and SSSs in summer) from the World Ocean Atlas 2001 (Conkright et al., 2002) and the average sea-ice cover extent from NSIDC data. Zones as described in the text are divided by horizontal black dotted lines. On the calibrated age axis, the black bar indicates the interval of the rapidly deposited sediment layer as defined by Jessen et al. (2010), including its 95% probability while the gray bar represents the rapidly deposited sediment layer at the site. ....	64
1.8	Close-up of sea-surface conditions at site MSM5/5-712-2 during the Bølling-Allerød interstadial. The two finer dotted lines indicate the limits of a cooling event. For explanations see Fig. 1.7 and text section 1.6.2.....	65
1.9	Reconstructions of the sea-surface conditions at site PS2863 including summer and winter SSTs in red and blue, respectively, summer and winter SSSs in red and blue, respectively, sea-ice cover duration, and productivity. For explanations see Fig. 1.7.....	66

1.10 Sea-surface reconstructions at site MSM5/5-712-2 including sea-ice cover seasonal duration, SSTs in summer (red) and winter (blue), SSSs in summer (red) and winter (blue) in correlation with the $^{231}\text{Pa}/^{230}\text{Th}$ record (green) as a proxy of AMOC strength (McManus et al., 2004), and $\delta^{18}\text{O}$ data (gray) from the NGRIP ice core (Andersen et al., 2004b). On the calibrated age axis, the black bar indicates the interval of the rapidly deposited sediment layer defined by Jessen et al. (2010), including its 95% probability. ....	67
--	----

## LISTE DES TABLEAUX

1.2	Infomation on cores .....	50
1.2	Radiocarbon chronology of cores MSM5/5-712-2, PS2863-1 and PS2837- 5 .....	51

## LISTE DES ABRÉVIATIONS

AMOC	<i>Atlantic meridional overturning circulation</i> Circulation méridienne de retournement de l'Atlantique
AMS	<i>Accelerator mass spectrometry</i> Accélérateur par spectrométrie de masse
AW	<i>Atlantic Water</i> Eau atlantique
BP	<i>Before Present</i> Avant l'actuel
C	Carbone
cal. yr	<i>Calibrated year</i> Année calibrée
<i>cf.</i>	<i>Confer</i> Se reporter à
E	Est
<i>e.g.</i>	<i>Exempli gratia</i>

## Par exemple

EGC	<i>East Greenland Current</i> Courant est groenlandais
<i>et al.</i>	<i>Et alli</i> Et autres
H1	<i>Heinrich event 1</i> Événement d'Heinrich 1
HCl	Acide chlorhydrique
HF	Acide fluorhydrique
<i>i.a.</i>	<i>Inter alia</i> Entre autres
LGM	<i>Last Glacial Maximum</i> Dernier maximum glaciaire
N	Nord
NAD	<i>North Atlantic Drift</i> Dérive nord atlantique
O	Oxygène
Pa	Protactinium

Th	Thorium
WSC	<i>West Spitsbergen Current</i> Courant ouest du Spitzberg
YD	<i>Younger Dryas</i> Dryas Récent

## LISTE DES SYMBOLES

% Pourcent

< Plus petit que

> Plus grand que

~ Environ

± Plus ou moins

δ Delta

° Degrés

°C Degrés celsius

µm Micron

cm Centimètre

km Kilomètre

kyr            *Thousand years*

Millier d'années

m            Mètre

mg            Milligramme

psu            *Practical salinity unit*  
Unité de salinité pratique

Sv            Sverdrup

TW            Térawatt

yr            *Year*  
Année

## RÉSUMÉ

L'est du Détroit de Fram est le principal lieu de passage des eaux nord-atlantiques vers l'océan Arctique. Le transport des eaux atlantiques s'accompagne de flux de chaleur qui ont une incidence immédiate sur la couverture de glace de mer et par conséquent sur le bilan énergétique dans le domaine arctique. Les conditions des eaux de surface des derniers 23 000 ans dans le nord-est du Détroit de Fram ont été reconstituées à partir des résultats de l'analyse palynologique de sédiments marins aux sites MSM5/5-712-2 ( $78^{\circ}54.94'N$  -  $6^{\circ}46.04'E$ ) et PS2863 ( $80^{\circ}33.46'N$  -  $10^{\circ}17.96'E$ ). La technique des analogues modernes appliquée aux assemblages de dinokystes démontrent des variations de grande amplitude semblables aux deux sites en ce qui a trait à la température, la salinité, la couverture de glace de mer et la productivité des eaux de surface.

Le dernier maximum glaciaire se caractérise par un faible couvert de glace mer saisonnier (< 2 mois/an) et des températures relativement élevées dans les eaux de surface en été (jusqu'à  $16^{\circ}C$ ), soulignant une grande amplitude saisonnière. Une telle reconstitution des conditions de surface lors du dernier maximum glaciaire doit être néanmoins considérée avec précaution étant donné une situation de mauvais analogues, ainsi que de faibles concentrations de dinokystes. Les conditions relativement douces que l'on reconstitue pourraient correspondre à une advection occasionnelle des eaux nord-atlantiques dans un milieu généralement froid, occupé par un couvert de glace de mer quasi-péren et une productivité primaire presque nulle. Entre ~19 000 et 14 700 ans calibrés (cal.) BP (*Before Present*), les températures des eaux de surface sont basses ( $\pm 4.5^{\circ}C$  en été) et s'accompagnent d'une hausse de la concentration en palynomorphes remaniés indiquant une augmentation de l'érosion et de l'apport de matériel fluvioglaciaire aux deux sites. Cet intervalle est interrompu par une augmentation rapide de la température des eaux de surface atteignant  $14^{\circ}C$  entre 14 700 ans et 14 500 ans cal. BP. Elle est suivie par un événement froid marqué par une baisse des températures estivales d'environ  $4^{\circ}C$  et par une augmentation du couvert de glace de mer qui se prolonge jusque vers 14 100 ans cal. BP. Durant l'Allerød, des températures estivales relativement élevées (moyenne de  $12,5^{\circ}C$ ) et des salinités faibles (< 31 psu) caractérisaient les eaux de surface. De telles conditions pourraient correspondre à une advection prononcée des eaux nord-atlantiques et à la stratification de masses d'eau de surface moins denses. Peu après le début Dryas Récent, à 12 600 ans BP, une baisse de  $10^{\circ}C$  des températures des eaux de surface est notée, ainsi qu'une hausse de la salinité de 2 psu en été. Cette transition indiquerait une réduction de l'apport d'eaux de fonte, ainsi qu'une réorganisation majeure des courants de surface dans le Détroit de Fram

qui s'illustre entre autres par l'installation de fronts océaniques à l'ouest et au nord-ouest du Svalbard. La salinité continue d'augmenter jusqu'à 7 600 ans BP. Une transition est alors enregistrée dans les assemblages de dinokystes, dorénavant semblables à ceux de l'actuel dans l'ouest du Svalbard, marquant ainsi l'installation des conditions océaniques modernes. Durant l'Holocène moyen et tardif, un léger refroidissement est enregistré. Il est principalement défini par une baisse des températures des eaux de surface en hiver de ~ 1,5°C.

MOTS-CLÉS: Détrit de Fram, dinokystes, dernier maximum glaciaire, déglaciation, Dryas Récent, Holocène

## INTRODUCTION

Les eaux nord-atlantiques, qui sont relativement chaudes et salines, circulent vers le nord et atteignent l'océan Arctique en suivant différentes trajectoires, notamment via le Détroit de Fram (Figure 1.1). Le Détroit de Fram est l'unique corridor profond entre l'océan Arctique et l'océan Atlantique et constitue ainsi le lieu de passage de la plus importante source de chaleur de l'Océan Arctique (Maslowski et al., 2004). Des variations dans l'intensité de ces masses d'eau nord-atlantiques jouent conséquemment un rôle décisif quant aux limites du couvert de glace de mer et par la suite, sur l'albédo et le bilan énergétique dans le domaine arctique. Au début du 21<sup>ème</sup> siècle, les eaux nord-atlantiques circulant dans le Détroit de Fram auraient atteint les températures les plus élevées des derniers 2000 ans (Spielhagen *et al.*, 2011). En considérant la sensibilité de l'Arctique vis-à-vis les changements du climat, généralement désignée comme le phénomène d'amplification arctique, il est essentiel de bien circonscrire la relation entre l'advection de chaleur des eaux nord-atlantiques et les changements du climat. L'étude du passé permet de retracer les causes et effets des flux d'eaux atlantiques selon différents scénarios climatiques et dans des contextes environnementaux diversifiés.

Au cours des derniers 23 000 ans, des variations importantes ont déjà été enregistrées dans le Détroit de Fram à partir de traceurs micropaléontologiques des masses d'eau profondes et intermédiaires (Hald *et al.*, 2007, 2001; Rasmussen *et al.*, 2012, 2007; Sarnthein *et al.*, 1995; Ślubowska-Woldengen *et al.*, 2008, 2007; Zamelczyk *et al.*, 2014). Toutefois, seulement quelques études font état de reconstitutions des conditions dans les eaux de surface. Ces études portent principalement sur la couverture de glace de mer (Müller et Stein, 2014; Müller *et al.*, 2012) ou des températures durant le dernier

maximum glaciaire (Rosell-Melé et Comes, 1999) et l'Holocène (Risebrobakken *et al.*, 2011). L'information sur les conditions des eaux de surface reste donc limitée et incomplète dans l'est du Détroit de Fram, particulièrement en ce qui a trait aux changements de la salinité, qui ont pourtant un effet déterminant sur la circulation thermohaline.

Dans ce contexte, ce mémoire vise à reconstituer les conditions des eaux de surface dans l'est du Détroit de Fram depuis le dernier maximum glaciaire, afin d'être en mesure de mieux circonscrire l'influence des eaux nord-atlantiques à travers les différentes phases de la déglaciation et au cours de l'Holocène. Les reconstitutions des conditions des eaux de surface sont basées sur la technique des analogues modernes (*Modern Analogue Technique*; MAT; Guiot, 1990) utilisée avec les assemblages de kystes de dinoflagellés. Les dinoflagellés sont des protistes algaires autotrophes et/ou hétérotrophes dont certaines espèces forment un kyste (dinokyste) lors de leur cycle de reproduction sexuée. Ce kyste est le plus souvent composé de matière organique réfractaire. La distribution des différents assemblages de dinokystes varie en fonction de paramètres du milieu ambiant tels que la température, la salinité et les nutriments. Les reconstitutions portent ainsi sur les températures (°C) en été et en hiver, la salinité (psu) en été et en hiver, la couverture de glace de mer (mois/an) et la productivité primaire (gC/m<sup>2</sup>an). Les deux sites étudiés (MSM5/5-712-2, 78°54.94'N - 6°46.04'E; PS2863, 80°33.46'N - 10°17.96'E) sont respectivement situés à l'ouest et au nord-ouest du Svalbard. Les sites se trouvent ainsi dans la trajectoire des eaux nord-atlantiques qui circulent à l'est du Détroit de Fram par le courant ouest du Spitzberg (*West Spitsbergen Current*; WSC) (Figure 1.1). Il s'agit donc d'endroits clés pour évaluer la variation de l'intensité de l'advection de chaleur via le courant WSC dans le temps et dans l'espace.

## CHAPITRE I

# PALEOCEANOGRAPHY OF NORTHEASTERN FRAM STRAIT SINCE THE LAST GLACIAL MAXIMUM: PALYNOLOGICAL EVIDENCE OF LARGE AMPLITUDE CHANGES

Jade Falardeau<sup>1\*</sup>, Anne de Vernal<sup>1</sup>, Robert F. Spielhagen<sup>2,3</sup>

1. GEOTOP-UQAM CP 8888 Montréal, H3C 3P8, Canada

2. GEOMAR Helmholtz Centre for Ocean Research, 24148 Kiel, Germany

3. Academy of Sciences, Humanities and Literature, 55131 Mainz, Germany

\* Corresponding author

## ABSTRACT

Sea-surface conditions in northeastern Fram Strait since the last glacial maximum (LGM) have been reconstructed from the analyses of dinocyst assemblages in cores MSM5/5-712-2 and PS2863/1-2. During the LGM, eastern Fram Strait was occasionally sea ice-free and characterized by large seasonal contrasts of SSTs from freezing in winter to relatively mild summer conditions (up to 16°C). However, such sea-surface reconstructions are equivocal because of the weak analogue situation and the low dinocyst concentrations. Between 19 and 14.7 ka, sea ice up to 9 months/yr, low summers SSTs (~ 4.5°C), and abundant reworked palynomorphs suggest harsh conditions and intense glacial erosion, during an early stage of the deglaciation in western Svalbard. At 14.7-14.5 ka, an abrupt warming is recorded with summer SSTs reaching up to ~14°C. During most of the Bølling-Allerød, summer SSTs of about 12.5°C prevailed while SSSs < 31 psu indicate continuous freshwater inputs. At 12.6 ka, a change in sea-surface conditions marked by a 10°C cooling in summer and SSSs increase of ~2 psu would correspond to the regional onset of the Younger Dryas. On a regional scale, the 12.6-12 ka interval is an important transition marked by decreased meltwater inputs and the establishment of coastal fronts along the western and northern Svalbard margins. Modern-like oceanic conditions with relatively high salinity (> 33 psu) and low seasonal temperature contrasts (1.3°C – 4.3°C from winter to summer) developed at about 7.6 ka. Since then, a slight cooling trend of about 1.5°C has been recorded especially in winter.

**KEYWORDS:** Fram Strait, Last Glacial Maximum (LGM), Late and Post-Glacial, Holocene, temperature, salinity, sea ice, dinocysts

### 1.1 Introduction

The northernmost extension of the North Atlantic Drift (NAD) reaches the Arctic Ocean through the Fram Strait, which is the main gateway between the Atlantic and the Arctic oceans (Fahrbach et al., 2001; Maslowski et al., 2004; Schauer, 2004). Hence, the NAD acts as a major heat source in the Arctic Ocean and shapes the northern limit of the regional sea-ice margins, which in turn plays a determinant role for the energy budget. As the Atlantic Water (AW) flows northward in eastern Fram Strait, heat loss to the atmosphere accompanied with surface water cooling and increased density leads to convection, thus contributing to the formation of North Atlantic Deep Water (NADW) and to the strength of the Atlantic Meridional Overturning Circulation (AMOC). From this point of view, the oceanography of the Fram Strait is key not only for the climate in the Arctic realm but also for the thermohaline circulation of the ocean.

In this context, the objective of the present study is to document changes in sea-surface conditions in the northeastern Fram Strait since the last glacial maximum (LGM; 23–19 ka; cf. Kucera et al., 2005) in order to assess on the role of northward heat flux through the NAD on the regional deglaciation and climate variations during the postglacial.

Many studies investigated the changes in AW inflows in western Svalbard during the LGM and the deglaciation. Most of them are based on planktic and/or benthic foraminifer assemblages and stable isotope analyses of foraminifer shells (cf. Hebbeln et al., 1994; Sarnthein et al., 1995, 2003; Nørgaard-Pedersen et al., 2003; Hald et al., 2001, 2007; Ślubowska-Woldengen et al., 2007, 2008; Rasmussen et al., 2007, 2012; Werner et al., 2011, 2013, 2016; Aagaard-Sørensen et al., 2014a-b, Chauhan et al., 2014; Zamelczyk et al., 2014; Bartels et al., 2017). Other studies are based on sedimentological data (Andersen et al., 1996; Forwick and Vorren, 2009; Jessen et al., 2010). However, whereas these studies document paleoceanographical conditions in sub-surface and bottom waters, there is still little information on the surface waters at

regional scale. To date, the studies of past sea-surface conditions mostly document on sea-ice cover based on IP25 (Müller et al., 2012 Müller and Stein, 2014, Bartels et al., 2017) and temperature estimated from alkenones during the LGM (Rosell-Melé and Comes, 1999) and the Early Holocene (Risebrobakken et al., 2011). The data documenting the variation of sea-surface conditions including seasonal temperatures and salinity in the western Svalbard area since the LGM in western Svalbard remain rare.

Here, we present two new palynological data records covering the last 23,000 years focusing on dinoflagellate cyst populations, which permit to reconstruct simultaneously several sea-surface parameters, including winter and summer sea-surface temperatures (SSTs) and sea-surface salinities (SSSs), along with sea-ice cover extent (month/yr) and productivity ( $\text{gC/cm}^2/\text{yr}$ ). Hence, our data may provide clue on freshwater discharges and seasonal gradients of temperatures (Rochon et al., 1999; de Vernal et al., 2001, 2005, 2013; Grøsfjeld et al., 2009) which are key parameters in ice-ocean dynamics, especially during deglacial phases. The study sites MSM5/5-712-2 and PS2863 from the western and the northwestern continental slopes of Svalbard, respectively (Fig. 1.1; Table 1.1), provide suitable stratigraphic framework for the interval of interest (cf. Werner et al., 2013; Aagaard-Sørensen et al., 2014a; Zamelczyk et al., 2014). Moreover, previous work based on biomarkers and stable isotopes have illustrated that site MSM5/5-712-2 is a good location to document, at least qualitatively, the changes of the AW inflows and its impact on the sea-ice cover extent (Werner et al., 2011, 2013; Müller et al., 2012; Müller and Stein, 2014; Spielhagen et al., 2014; Zamelczyk et al., 2014). In addition to develop a more detailed portrait of the surface water processes from the LGM to present, the study of these two sites aims at contributing to a better understanding of the AW modifications along its pathway, from the relatively confined channel of the eastern Fram Strait to the open Arctic Ocean north of Svalbard, where strong ocean-atmosphere heat transfer occurs today.

## 1.2 Regional hydrography

There are two main currents in Fram Strait (Fig. 1.1; Fahrbach et al., 2001; Schauer, 2004; Rudels et al., 2005; Schauer et al., 2008). In the west, the East Greenland Current (EGC) flows southward and transports cold and fresh waters from the Arctic Ocean, thus playing a major role in icebergs and sea-ice export to the North Atlantic. In the east, the West Spitsbergen Current (WSC) circulates northward along the west continental slope of Svalbard and carries relatively warm and saline Atlantic waters towards the Arctic Ocean. The WSC thus constitutes the northernmost branch of the NAD. It originates from two distinct branches in the Nordic Seas: the Norwegian Atlantic Slope Current (NwASC) and the Norwegian Atlantic Current (NwAC), further named the WSC western branch. Part of the NwASC turns east at the surface into the shallow Barents Sea (Rudels et al., 1999), where it is responsible for a significant flux and heat transport (5.07 Sv; 106 TW; Maslowski et al., 2004), while the rest continues north as the WSC core. Parts of the WSC western branch bifurcate to the west following topographical features to finally turn south with the EGC (Gascard et al., 1995). The WSC western branch and the NwASC converge into the WSC core around 78°N due to the bottom topography (Walczowski and Piechura, 2007).

Because of the complex bathymetry of the Fram Strait, the WSC core splits further on into three branches (Manley, 1995). A western branch recirculates in Fram Strait as part of the Return Atlantic Current (RAC), without extending further than 80-81°N (Rudels et al., 2000). A central branch called the Yermak Branch (YB) flows north and reaches the Arctic Ocean along the western and northern shelf of the Yermak Plateau (YP). The third branch is the Svalbard Branch (SB) that flows east following the northern Svalbard shelf and continues by circulating south of the Yermak Plateau at depth reaching 600 m.

Arctic waters circulate southward through the East Spitsbergen Current (ESC) and follow the east Svalbard coast in the Barents Sea (Loeng, 1991). The ESC is renamed

as the South Cape Current (SCC) after passing the Storfjorden, in south Svalbard, and follows the western coast of Svalbard carrying freshwater from glaciers melt and rivers run off in summer (Skogseth et al., 2005). Storfjorden is an area of deep water formation as dense waters formed from brine rejection flow along the slope into the deeper Fram Strait (Rudels et al., 2005).

The WSC transports about 11.6 Sv at 78°50'N corresponding to 70.6 TW of heat (Walczowski et al., 2005). Previous studies from moored instruments obtained similar values with mean annual transport of  $9 \pm 2$  to  $10 \pm 1$  Sv (Schauer, 2004) and a monthly mean average over two years of  $9.5 \pm 1.4$  Sv (Fahrbach et al., 2001).

The regional sea-ice cover extent is mainly controlled by the advection of warm AW. Site MSM5/5-712 is located under the path of the WSC on the western continental slope of Svalbard and it is therefore largely influenced by the AW. Site PS2863 is located 200 km north of MSM5/5-712 downstream of the WSC. It is located close to the distal influence of the AW and close to the limit of mean sea-ice extent in summer, which corresponds to the Polar Front.

At site PS2863, the mean sea-surface temperature and salinity in summer are  $2.3 \pm 2.3^\circ\text{C}$  and  $33.3 \pm 0.9$  psu, respectively (1900-2001 data from the World Ocean Atlas 2001; Conkright et al., 2002; Table 1.1). The sea-ice cover is highly variable at the coring site since it is located at the vicinity of the sea-ice margin. Hence, the sea-ice cover with concentration > 50% varied between 0 and 11 months/yr from 1954 to 2003, with an average of  $3.7 \pm 3.2$  months/yr (data provided by the National Snow and Ice Data Center -NSIDC- in Boulder). At site MSM5/5-712, the mean-sea surface temperature and salinity in summer are  $4.9 \pm 1.40^\circ\text{C}$  and  $34.73 \pm 0.43$  psu, respectively (Conkright et al., 2002; Table 1.1). From 1954 to 2003, sea-ice cover with concentration > 50% varied between 0 and 6 months/yr with an average of  $1.2 \pm 1.7$  month/yr (data from NSIDC, 2003).

### 1.3 Methods

Gravity core PS2863-1 ( $80^{\circ}33.46'N$ ,  $10^{\circ}17.96'E$ ; water depth 808 m) was collected in 1997 during RV Polarstern expedition ARK-XIII/2 (Stein and Fahl, 1997). The core is 580 cm long. The uppermost 183 cm were subsampled at 4 cm intervals for palynological analyses. Box core PS2863-2 from the same location is 41 cm long. It was subsampled at 1 cm intervals (Table 1.1). Here we used a composite sequence referred to as PS2863 by combining the box core data for better time resolution in the upper part of the record and gravity core data below 39 cm.

Sediment core MSM5/5-712-2 ( $78^{\circ}54.94'N$ ,  $6^{\circ}46.04'E$ ; water depth 1487 m) was retrieved from RV Maria S. Merian in 2007 (Budéus, 2007). The kastenlot core has a total length of 950 cm. Palynological results from this core (hereafter MSM5-712) are presented at 4 cm intervals for the uppermost 283 cm and at 8 cm intervals down to 777 cm (Table 1.1).

Samples were prepared for palynological analyses in the micropaleontology laboratory of GEOTOP according to standard procedures (de Vernal et al., 2010). Briefly, approximately 5 cc of sediment were wet sieved at 10 and  $106\ \mu m$  after addition of one *Lycopodium clavatum* capsule with a known number of spores for further palynomorph concentration calculations (Matthews, 1969). Dinocyst and other palynomorph concentrations were calculated as follows:

$$N_p = (N_e \times n_p)/n_e$$

Where  $N_p$  is the total number of dinocysts in the sample,  $N_e$  is the known number of *Lycopodium clavatum* spores in the capsule added to the sample,  $n_p$  is the number of dinocysts counted and  $n_e$  is the number of *Lycopodium clavatum* counted. The concentrations lead to calculate dinocyst fluxes as follows:

$$\text{Flux (nb/cm}^2/\text{yr}) = \text{Sedimentation rate (cm/yr)} \times \text{Concentration (nb/cm}^3)$$

Where sedimentation rate corresponds to interpolated sedimentation according to the age vs. depth relationship established based on  $^{14}\text{C}$  dating and sedimentological correlations with other cores using the Bayesian software Bacon 2.2 developed by Blaauw and Christen (2011) (see Fig. 1.2). The 10-106  $\mu\text{m}$  fraction was treated with hydrochloric acid (HCl 10%) and hydrofluoric acid (HF 49%) in order to dissolve the carbonate and the silica particles, respectively. Residues were mounted between slides and cover slide in glycerin gel for microscopic analysis.

Analysis of the palynological content includes dinoflagellate cysts (or dinocysts), foraminiferal organic linings and reworked pre-Quaternary palynomorphs. Pollen grains, spores and other palynomorphs were also counted (see Falardeau 2017), but not used here. Dinocyst species were identified using the standardized taxonomy and nomenclature of Rochon et al. (1999). On average, 318 dinocysts were counted per sample, except in the LGM samples (110 specimens on average), which are characterized by very low concentrations.

Reworked palynomorphs, which result from the erosion of older sedimentary rocks and subsequent deposition (Strel and Bless, 1980), include pollen grains, spores, acritarchs as well as dinocysts. They were distinguished by a darker color and a flattened morphology owing to the longer preservation period in the sediment. A number of well-preserved palynomorphs identified at genus or family level to be stratigraphically older than Quaternary were also counted as reworked (cf. Williams and Brideaux, 1975). Quantitative reconstructions of sea-surface parameters were made using the Modern Analogue Technique (MAT; Guiot, 1990) applied on the dinocyst assemblages following the procedures described by de Vernal et al. (2013). We have calculated the most probable values from a set of 5 analogues identified in the reference dinocyst database which includes data from the Greenland margins (cf. Allan et al., in prep.) in addition to data from the  $n = 1492$  database (de Vernal et al., 2013) for a total of 1777 sites. The procedure used for reconstruction is the same as in de Vernal et al. (2013). It

consists in log-transformation of the 66 dinocyst taxa. The distance between modern and fossil spectra (sum of the differences in taxa occurrence expressed in log values) allows identifying the 5 best analogues. The most probable sea-surface values correspond to the average of the selected analogues, weighted inversely to the distance. Poor analogues having a distance larger than a threshold value of 1.2 are excluded from the reconstructions. The uncertainty of sea-surface reconstructions or the error of prediction are established at  $\pm 1.4^{\circ}\text{C}$  and  $\pm 2.0^{\circ}\text{C}$  for the sea-surface temperatures in winter and summer respectively,  $\pm 1.9$  psu for the salinity in summer and  $\pm 1.6$  month/yr for the sea-ice cover (cf. Allan et al., in prep.). The error of prediction is large for salinity due to the high variability in the low salinity domain. When considering only the  $> 30$  psu salinity range, the uncertainty is  $\pm 0.73$  psu.

#### 1.4 Chronology of the cores

The chronology of core MSM5-712 (Table 1.2; Figure 1.2) is based on 18 accelerator mass spectrometry (AMS)  $^{14}\text{C}$  dates obtained on *Neogloboquadrina pachyderma* and compiled by Müller et al. (2012) and Müller and Stein (2014). Additional age tie points were obtained from correlations with the total organic carbon content of PS2837-5 (Nørgaard-Pedersen et al., 2003) and the western Svalbard reference stratigraphy of Jessen et al. (2010) (for details see Müller and Stein, 2014). A distinct interval of rapid sedimentation rate is well represented in core MSM5-712 between 657 and 433 cm.

The chronology of core PS2863-1 is based on five AMS  $^{14}\text{C}$  dates on *N. pachyderma* (Table 1.2; Fig. 1.2). In addition, a sixth chronological tie point was obtained from stratigraphic correlation with the nearby core PS2837-5 ( $81^{\circ}13.99'\text{N}, 02^{\circ}22.85'\text{E}$ ) from the western slope of the Yermak Plateau (Nørgaard-Pedersen et al., 2003) based on a well identified IRD peak which was found at 106.5 cm in core PS2863-1 (Fig. 1.2). This peak has an age of  $14,202 \pm 285$  cal. years BP in core PS2837-5 according to our age model. Further, a very fine grained laminated layer at 133-120 cm in core PS2863-1 was associated with a regional sedimentary event recorded all along the northwestern

Barents Sea and the western Svalbard continental slopes up to the Yermak Plateau (Jessen et al., 2010; Lucchi et al., 2015). In Jessen et al. (2010), the interval started at  $13,140 \pm 150$   $^{14}\text{C}$  years BP and ended at  $12,840 \pm 150$   $^{14}\text{C}$  years BP, which corresponds to  $14,931 \pm 560$  and  $14,434 \pm 620$  cal. years BP, respectively. This sedimentological event may have been caused by the cold turbid meltwater originating from the retreat of the Barents Sea Ice Sheet during the early Bølling interstadial (Jessen et al., 2010; Lucchi et al., 2015). The rapidly deposited sediments in core MSM5-712 occurs within the limits of the unit described by Jessen et al. (2010) with a weighted mean age of 14,660-13,930 cal. years BP.

The age-depth relationship of cores PS2863-1, MSM5-712 and PS2837-5 was defined by the Bacon 2.2 software that uses Bayesian statistics with default probability intervals of 95% (2-sigma) (Blaauw and Christen, 2011). All the original and correlated AMS  $^{14}\text{C}$  ages were calibrated using the Marine13 calibration curve of Reimer et al. (2013) with an additional correction (delta R) of  $98 \pm 37$  years calculated from six values from the Svalbard area (Olsson, 1980; Mangerud, 1972; Mangerud and Gulliksen, 1975) in the Marine Reservoir Data Base of Calib 7.10 (<http://calib.org/marine/>). All the ages in this study are given as thousand calibrated years before present (ka), unless stated otherwise. We assumed that the surface of the cores was modern with an error of  $\pm 460$  years for core PS2863-1 and  $\pm 160$  years for core MSM5-712. The errors were determined considering the mean underlying sedimentation rates and mixing by bioturbation over the upper 3.5 centimeters. The average sedimentation rate of the rapidly deposited sediment layer found in both cores is calculated to about 43 cm/kyr in core PS2863-1 and 309 cm/kyr in core MSM5-712. With the exception of this layer, the mean sedimentation rate in core PS2863-1 is about 8 cm/kyr, which much less than in core MSM5-712 (27 cm/kyr).

## 1.5 Results

### 1.5.1 Palynological assemblages

Dinocysts largely dominate the palynological assemblages at both sites, MSM5-712 and PS2863, with concentrations recording similar positive trends towards present (Fig. 1.3). The lower part of the studied section, dated prior to 17 ka, contains low dinocyst concentrations (50-1000 cysts/g in PS2863 and 150-800 cysts/g in MSM5-712) while the last 8000 years are characterized by concentrations ranging  $10^4$ - $10^5$  cysts/g, with a maximum recorded in the upper part of the sequence representing the last 4000 years (Fig. 1.3). Core MSM5-712 records about twice higher concentrations than core PS2863. The concentrations led to calculated fluxes that are one order of magnitude higher in the late and postglacial sediments of core MSM5-712 (~800 cysts/cm<sup>2</sup>/yr on the average) than those of core PS2863 (~60 cysts/cm<sup>2</sup>/yr on the average). Beyond these general characteristics, a double concentration peak is recorded at ~14.8 and ~13.9 ka in core MSM5-712 (Fig. 1.3). Core PS2863 also recorded maximum concentrations centered at 13.7 and 13 ka. However, the peaks are less pronounced, possibly due to the effect of bioturbation in this core with a lower sedimentation rate.

The concentrations of benthic foraminifer linings are ranging from 100 to 2000 linings/g in sediments of the last 14 ka at site PS2863 (Fig. 1.3). In core MSM5-712, foraminifer lining concentrations continuously increased from 14 ka to present (2500 linings/g on the average) (Fig. 1.3), mirroring the trend in dinocyst concentrations, which suggests a higher primary productivity after 14 ka and high organic carbon fluxes especially during the Middle-to-Late Holocene. The concentrations of reworked palynomorphs vary from 500 to 2000/g, with highest values in the 20-12 ka interval (Fig. 1.3).

The dinocyst assemblages show high species diversity, with occurrences of both phototrophic and heterotrophic taxa at the two sites (Figs. 1.4, 1.5). Among the phototrophic taxa, *Operculodinium centrocarpum*, *Nematosphaeropsis labyrinthus*, *Bitectatodinium tepikiense*, *Spiniferites elongatus* and *Spiniferites ramosus* dominate

the assemblages, reaching more than 50% in some intervals. The accompanying taxa comprised the Cyst of *Pentapharsodinium dalei*, *Impagidinium pallidum* and *Spiniferites* spp. (5-20%). Heterotrophic species are represented by *Brigantedinium* spp. and *Islandinium minutum* with low abundance of *Islandinium cezare* and *Selenopemphix quanta* (< 5%). Dinocysts are present throughout the record, including heterotrophic taxa that are more sensitive to dissolution (cf. Kodrans-Nsiah et al., 2008), suggesting generally good preservation of organic-walled microfossils in the sediment.

The dinocyst record is characterized by large variations in assemblages since the last glacial maximum (LGM). The major transitions are generally synchronous in both cores and the assemblages are similar, which allowed us to recognize five distinct dinocyst assemblage zones at regional scale (Figs. 1.4, 1.5).

In Zone V (~23-19 ka), the dinocyst assemblages are distinguished by abundant *B. tepikiense* reaching up to 40% in PS2863 and 46% in MSM5-712 of the dinocyst assemblages. The occurrence of this species is a characteristic feature of the LGM interval in the northern North Atlantic (de Vernal et al., 2005). According to its modern distribution, *B. tepikiense* tolerates high amplitude variation of seasonal temperature and relatively low salinity in stratified surface waters (Rochon et al., 1999; de Vernal et al., 2001, 2005). The occurrence of *O. centrocarpum*, which is a cosmopolitan species, is also high with a relative abundance of about 30%. Three peaks of *Brigantedinium* spp. (33%, 53% and 20%) are observed, but only at site MSM5-712. The dinocyst assemblages in core MSM5-712 also holds low but significant concentrations of more temperate species such as *Spiniferites mirabilis* (< 3.5%) and *Lingulodinium machaerophorum* (< 5%).

Zone IV, which spans ~19 to 14.7 ka, is characterized by the dominance of *Brigantedinium* spp. with a relative abundance of 76-94% at site PS2863 and of 68-87% at site MSM5-712. The accompanying taxa include *I. minutum*, *S. elongatus* and

*O. centrocarpum* (0-10%). Such an assemblage reflects harsh conditions and dense sea-ice cover (cf. Rochon et al., 1999; de Vernal et al., 2001, 2013).

Zone III spans from 14.7 to 12.6 ka and thus covers most of the Bølling-Allerød interstadial (14.7-12.9 ka; Rasmussen et al., 2006). It also comprises the interval marked by very high sedimentation rates. This interval is distinguished by short-lived variations of high amplitude in the dinocyst assemblages, but also by discrepancies between the two records. At site PS2863, the dinocyst assemblages are mainly dominated by *Spiniferites* taxa, mostly *S. elongatus* from 14.7 to 13.7 ka, and *S. ramosus* from 13.7 to 12.6 ka. In this interval, the specimens of *S. ramosus* include wide ranges of morphologies with regard to body size and shape, the length of processes and the presence/absence of an apical boss. They also include specimens with processes joined by more or less complete trabecula network, ranging from a typical *S. ramosus* to a *Nematosphaeropsis*-like morphology (Fig. 1.6). At site MSM5-712, the interval is characterized by a very short peak of *B. tepikiense* particularly at 14.6-14.5 ka, but *Brigantedinium* spp. dominates the assemblages from 14.5 to 14.1 ka. It is progressively replaced by *O. centrocarpum*, *S. elongatus*, *S. ramosus*, the Cyst of *P. dalei* and *I. minutum*. At 13.2-12.6 ka, *O. centrocarpum* increases of about 10% at the expense of *S. ramosus*. Despite differences between the assemblages of the Zone III, the two sites are characterized by the significant occurrences of different morphotypes of *S. ramosus*.

Zone II covers the latest Pleistocene and the early Holocene (12.6-7.6 ka). It is characterized by a high relative abundance of *O. centrocarpum* and the first significant occurrence of *I. pallidum*. Beyond these general features, there are differences in the dinocyst assemblages of the two cores, probably due to the effect of local hydrographic conditions. While the dinocyst assemblages in core MSM5-712 contain abundant heterotrophic taxa, especially *I. minutum* (10-50%) and *Brigantedinium* spp. (5-30%),

the dinocyst assemblages at site PS2863 are almost entirely composed of phototrophic taxa such as *N. labyrinthus*, the Cyst of *P. dalei* and *O. centrocarpum*.

Finally, Zone I covers from 7.6 ka to present. It is characterized by the dominance of *O. centrocarpum*, which constitutes about 70% of the assemblages in both cores. *N. labyrinthus* and *I. minutum* are the main accompanying taxa while *I. pallidum* records about 3-9% in core PS2863, but does not exceed 2% in core MSM5-712.

### 1.5.2 Reconstructions of sea-surface conditions

Application of the MAT revealed close analogues for all samples. Hence, 5 analogues were used for the reconstruction in all samples with a distance never exceeding the threshold value of 1.2 for a suitable analogue (Figs. 1.7, 1.9). The distances are actually lower than 0.2 for most samples, which corresponds to very similar analogues. Therefore, the reconstructions appear as reliable as possible for most parts of the records. Largest distances from modern analogues, however, are recorded from ~23 to 19 ka (mean of 0.62 and of 0.61 for MSM5-712 and PS2863, respectively) and also at  $\pm$  14.5 ka (mean of 0.46) and at 10.7 ka (mean of 0.84) at site MSM5-712 and between 17.1 and 16.6 ka at site PS2863 (mean of 0.50). In these intervals, one must be more cautious with quantitative estimates.

The reconstruction of sea-surface conditions from the MAT is generally coherent at the two sites (Figs. 1.7-1.9). From 23 to 7.6 ka, high amplitude changes of all parameters are recorded with a distinct higher frequency between 14.7 and 13 ka, especially in core MSM5-712 (Figs. 1.8, 1.9), whereas the establishment of more stable conditions similar to the modern ones occurred after 7.6 ka.

In Zone V spanning ~23-19 ka, sea-surface conditions reconstructed from the MAT point to a strong seasonality with high temperatures in summer (13-16.5°C), but low temperatures in winter (1.7-1.9°C). Summer salinity was relatively low with a mean of 31.6 psu at site MSM5-712, but the mean was 1 psu higher at site PS2863. Such

conditions are compatible with estuarine and coastal environments, where modern analogues are characterized by *B. tepikiense*. However, the reconstructions indicate almost no sea-ice cover and a relatively high primary productivity, which can be challenged in the context of the LGM. Hence, intervals of low phytoplankton productivity (Rosell-Melé and Comes, 1999; Müller and Stein, 2014), as well as low dinocyst concentrations (de Vernal et al., 2005, 2006) were reported from the Nordic Seas during the LGM, which would be coherent with the low dinocyst fluxes at the study sites (Fig. 1.3).

The Zone IV, from ~19 to 14.7 ka, corresponds to the coldest conditions of the entire record with extensive sea-ice cover in winter (5-10 months/yr) and summer SSTs of about 4-5°C at both sites. During this interval, sea-surface salinity remained low, of about 31.1 and 31.7 psu in summer, at sites PS2863 and MSM5-712, respectively.

In Zone III, spanning 14.7-12.6 ka, the two sites yielded different results as could be expected from the discrepancies in the dinocyst assemblages. The sea-surface estimates from the composite core PS2863 indicate reduced sea-ice cover extent (mean of 2.4 months/yr) and warmer summer conditions up to 12.3°C, which corresponds to large seasonal contrast of temperature. They also point towards saltier surface waters with an increase of about 1 psu. The estimates from core MSM5-712 suggest warm sea-surface conditions reaching about 12°C in summer, similar as in PS2863, and relatively low SSSs in summer with an average of 31 psu except in the first 600 years of the interval. The high temporal resolution of analyses in core MSM5-712 permitted to identify two short-lived events at ~14.7-14.5 ka and at ~14.5-14.1 ka (Fig. 1.8). At 14.7 ka a warm pulse is marked by summer SSTs up to 14.4°C and by 2 months/yr decrease in the sea-ice cover extent. In the first 100 years, the SSSs in summer were low with an average of 30.7 psu, but they increased up to 33.4 psu between 14.6 and 14.5 ka. In the 14.5-14.1 ka interval, colder conditions prevailed with enhanced sea-ice cover reaching a maximum of 9 months/yr. The SSTs drastically decrease down to 0.8°C,

concomitantly with a drop in primary productivity. The SSSs remain relatively low with an average of 31.6 psu.

In Zone II, spanning 12.6 to 7.6 ka, summer SSTs decrease to a mean of 5.5-6°C at both sites, which resulted in reduced amplitude of seasonal temperature. The SSSs increased from 32.2 to 34.3 psu at site PS2863 and from 30.5 to 33.5 psu at site MSM5-712. The sea-ice cover increased to a maximum of 5 months/yr at 11.4 ka at site PS2863 and to an average of 7 months/yr at 11.9-10.7 ka at site MSM5-712, prior to a decrease down to 1-2 months/yr towards the end of the interval.

In the Zone I, corresponding to the last 7,600 years, summer SSTs remained relatively stable with values of about 4.5°C and 4.0°C at sites PS2863 and MSM5-712, respectively. However, a decrease of about 1.5-2°C in winter SSTs and an increase of 1-2 months/yr in sea-ice cover are recorded towards modern conditions. The estimated summer SSSs decrease by about 1 psu in core PS2863. A less pronounced decrease of SSSs is recorded in core MSM5-712.

## 1.6 Discussion

### 1.6.1 The LGM paradox

In the literature about the LGM in Nordic Seas, major discrepancies characterize the SST reconstructions depending upon the proxies (cf. de Vernal et al., 2006). On one side, alkenones, dinocysts and coccoliths provide evidence for conditions as warm as or even warmer than at present in the surface waters with SSTs as high as 9-15°C in summer (Rosell-Melé and Comes, 1999; de Vernal et al., 2000, 2005). On the other side, planktic foraminifers led to suggest significantly colder than modern conditions, with SSTs not exceeding 4°C in summer (Sarnthein et al., 1995, 2003; Weinelt et al., 1996, 2003; Nørgaard-Pedersen et al., 2003; Pflaumann et al., 2003).

Our results from sites PS2863 and MSM5-712 are in agreement with the previous study using dinocysts and suggest that the Nordic Seas and the eastern Fram Strait

experienced seasonally sea ice-free conditions during the LGM. This was previously inferred, not only from dinocysts (de Vernal et al., 2000, 2005) but also from coccoliths (Hebbeln and Wefer, 1997; de Vernal et al., 2000), alkenones (Rosell-Melé and Comes, 1999) IP25 biomarkers Müller and Stein, 2014; Xiao et al., 2015) and planktic foraminifers (Hebbeln et al., 1994; Sarnthein et al., 1995, 2003; Weinelt et al., 1996, 2003; Nørgaard-Pedersen et al., 2003; Pflaumann et al., 2003; Zamelczyk et al., 2014). Seasonal ice-free conditions may even have prevailed along the northern continental slope of Svalbard where high fluxes of planktic and benthic foraminifers were recorded (Chauhan et al., 2014, 2016).

Open waters, at least seasonally, in the Nordic Seas were probably an essential moisture source for the rapid growth of the Svalbard Barents Sea Ice Sheet (SBSIS) (Hebbeln et al., 1994). The low sea-level and the SBSIS at the LGM certainly influenced ocean circulation as the Barents Sea pathway for AW advection was blocked, implying that all the heat of AW was channelized along the western Barents Sea continental margin towards the Fram Strait. A sea-ice massif in the Arctic Ocean and a lower freshwater input from circum-Arctic rivers have been suggested to increase the influence of recirculating AW in the Fram Strait area in the LGM (Nørgaard-Pedersen et al., 2003). Mg/Ca data of Cronin et al. (2012) from Arctic Ocean ostracods also point to a strong inflow of AW, with a circulation pattern of this water mass similar to modern, at significantly greater depth, but even warmer than at present. Thus, there is ample evidence for a strong advection of AW to the Nordic Seas, the Fram Strait and northern Svalbard during the LGM, which is also in agreement with good calcium carbonate preservation (Zamelczyk et al., 2014) and regional  $\delta^{18}\text{O}$  signals of planktic foraminifers (Nørgaard-Pedersen et al., 2003; Sarnthein et al., 2003). However, a flow of AW at the surface and the conditions that actually prevailed in the uppermost water layer are more equivocal. The biogenic remains leading to the reconstructions of seasonally ice-free conditions might reflect fluxes during episodic phases of open waters representing the breakout of continuous sea-ice cover rather than being the result of recurrent seasonally

ice-free conditions throughout the LGM as proposed by Nørgaard-Pedersen et al. (2003) and Weinelt et al. (2003). Accordingly, the dinocyst assemblages would represent episodes of open waters marked by relatively warm conditions and high productivity alternating with intervals characterized by permanent sea-ice cover and nil dinocyst fluxes as in the modern Arctic Ocean. The low dinocyst concentrations during the LGM could therefore be the result of very low fluxes except during short-lived high productivity events. Such an assumption is compatible with the paleoceanographical record of MD95-2010 from the southern Norwegian Sea showing very large amplitude centennial variations of sea-surface conditions during the LGM with oscillations between 0 to 6 months/yr of sea-ice cover and evidence of episodic high SSTs (cf. Eynaud et al., 2004; de Vernal et al., 2006). The dinocyst fluxes recorded since 18.5 ka in core PS2863 are mostly constant ( $\sim 50$  cysts/cm $^2$ /yr) which differ from the very low fluxes of the LGM ( $\sim 1$  cyst/cm $^2$ /yr). Assuming uniform regional dinocyst fluxes during the summer season, we may calculate that sea ice-free conditions in northern Fram Strait occurred with an average frequency of one or two years per century during the LGM. Higher temporal resolution of analyses would be needed at our study sites for an unequivocal demonstration and to provide more information on the frequency or the duration of the AW pulses at the surface in eastern Fram Strait.

When providing quantitative estimates for LGM paleoenvironmental parameters in the NE Fram Strait, one should consider the weak analogue situation for the LGM (cf. de Vernal et al., 2005; de Vernal et al., 2006; Figs. 1.7, 1.9). During the LGM, the hydrographical conditions in the Nordic Seas were probably unique with no perfect equivalent today. For instance, the selected modern analogues of the LGM were obtained from the northeastern shore of the United States, the northern margin of Norway and the Gulf of St-Lawrence where high amplitude seasonal variations prevail today at the favor of estuarine type circulation. Such conditions do not exist in the open ocean settings such as Fram Strait. Hence, the quantitative reconstructions for the LGM must be interpreted with caution. In a context of low dinocyst concentrations, there is

also a risk of distortion of the signal due to distal input of reworked material from a southern source. However, this is unlikely here considering the similarity of assemblages at both sites MSM5-712 and PS2863 that are located 200 km apart from each other. Moreover, SST reconstructions from alkenones by Rosell-Melé and Comes (1999) show increasing sea-surface temperatures towards the northeast which would be inconsistent with a warm source originating from the south as well. Furthermore, even if some lateral transport of material occurred, warm sea-surface conditions must have prevailed in the source area.

One consistent feature in most LGM records from the northern North Atlantic and the Nordic Seas is the amplitude of variations that suggest unstable conditions in addition to high seasonality (de Vernal et al., 2000, 2005; Sarnthein et al., 2003; Müller and Stein, 2014). The reconstructions from dinocyst assemblages showing high SSTs, but still freezing sea-surface conditions in winter also support large seasonal amplitude of temperature (Figs. 1.7, 1.9). The inflows of AW in the context of a heavily glaciated environment might have led to large amounts of freshwater input causing stratification and low thermal inertia in the surface layers. The sea-surface warming in summer was probably amplified by intensive advection of AW, particularly since they were confined to the Fram Strait during the LGM. At that time, sea-surface conditions in the Nordic Seas including the Fram Strait were probably unstable, with an alternation of surface warming with strong northward AW fluxes and cold meltwater discharge events, as proposed by de Vernal et al. (2006).

### 1.6.2 Transition from the LGM to the postglacial

The occurrence of the heterotrophic taxa *Brigantedinium* spp. and *I. minutum* increased at 20 ka (Figs. 1.4, 1.5) and reached a maximum in Zone II, which corresponds to the establishment of pervasive cold conditions from 19 to 14.7 ka (Figs. 1.7, 1.9).

In the dinocyst records of both sides, a transition between 20 and 18.5 ka was accompanied by an increase of reworked palynomorphs (Fig. 1.3) pointing to intense

glacial erosion, which is consistent with an IRD signal recorded at  $20.5 \pm 0.5$  ka on the western Svalbard slope (Jessen et al., 2010). Other studies reconstructed cooling at about 19 ka. This was inferred from a decrease in the percentages of subpolar taxa in planktic foraminifer assemblages in eastern Fram Strait (Zamelczyk et al., 2014) and from biomarker data (Müller and Stein, 2014). The summer SST decrease and enhanced sea-ice cover extent were suggested to result from reduced AW inflows towards the end of the LGM (Rasmussen et al., 2007), which could be associated with a near shut down of the AMOC at 18-17.5 ka (McManus et al., 2004; Hall et al., 2006; Stanford et al., 2011). Actually, the cooling recorded after ~19 ka may have occurred in an early phase of the deglaciation, as recorded at about 19.2 ka on the southern Yermak Plateau from low  $\delta^{18}\text{O}$  in planktic foraminifers (Chauhan et al., 2014) or at about 18.5-17 ka in the Fram Strait based on various evidences (Hebbeln et al., 1994; Andersen et al., 1996; Nørgaard-Pedersen et al., 2003; Rasmussen et al., 2007). A weakening of the AMOC may well have been linked to large freshwater and iceberg discharges from the SBSIS, leading to cold and buoyant waters at the sea-surface. Major inputs of meltwaters near the onset of the deglaciation are coherent with the low  $\delta^{18}\text{O}$  of planktic foraminifers from 18.5 to 17.5 ka from the Nordic Seas (Jones and Keigwin, 1988; Lehman et al., 1991; Hebbeln et al., 1994; Bauch et al., 2001; Nørgaard-Pedersen et al., 2003; Rasmussen et al., 2007). They are also consistent with the sustained low SSSs in our two core records (< 32 psu; Figs. 1.7, 1.9) and roughly corresponds to the onset of Heinrich event I (H1; Heinrich, 1988; Bond et al., 1993), spanning from 17.9 to 15.7 ka as defined in Gibb et al. (2014). The high dinocyst flux recorded after 17 ka (Fig. 1.3) is synchronous with increased primary productivity as deduced from biomarkers in core MSM5-712 (Müller and Stein, 2014) and planktic foraminifers in the Yermak Plateau (Chauhan et al., 2014), which suggest a transition from harsh and unstable conditions of the earliest phase of the deglaciation to more favorable pelagic conditions.

At the beginning of Zone III, there was a short pulse of high SSTs accompanied by reduced sea-ice cover lasting about 200 years (Figs. 1.8, 1.9). This short interval probably resulted from enhanced AW contribution, which led to warming and strong meltwater inputs during a short-lived interval of about 100 years. Afterwards, the SSSs increased, but remained relatively low (< 32 psu). This warm event is only observed in core MSM5-712, probably due to the very high temporal resolution of the core that permits to identify short-lived events. It occurred shortly after the resumption of the AMOC at about 14.6 ka, coincident with the Bølling warming (McManus et al., 2004; Stanford et al., 2011). It also corresponds to a change in the benthic foraminifer assemblages indicating a shift from polar to subarctic conditions along the western Svalbard margin (Ślubowska-Woldengen et al., 2007, 2008).

After the warm pulse, from 14.5 to 14.1 ka, the sea-surface reconstructions indicate completely opposite trends, with the setting of extremely cold conditions and extended sea-ice cover (Figs. 1.8, 1.9). This cold event covers the larger part of the rapidly deposited layer, which has an age of 14,660 to 13,930 cal. years BP in core MSM5-712.

The sediment of this layer would originate from the scouring of the northwestern Barents Sea continental shelf in relation with Meltwater Pulse 1a (Lucchi et al., 2015). In the upper continental slope of the Storfjorden, Lucchi et al. (2015) identified a thick rapidly deposited sediment layer, which presented sedimentological features similar to the deposit described by Jessen et al. (2010) from the western Svalbard and the Yermak Plateau continental slopes. The stratification of surface waters would have led to enhanced sediment dispersal at regional scale of a meltwater plume resulting from major ice sheet collapse (Lucchi et al., 2015). Such a collapse might well be have been triggered by the AW influence and short warming as documented above, together with eustatic sea level rise. The palynological content of the rapidly deposited layer of both sites is characterized by a maximum peak in reworked palynomorphs, implying

erosional processes on the shelves and subsequent outwash deposition. The dinocyst assemblages are dominated by *Brigantedinium* spp. which is today highly abundant in sites affected by glacier meltwater discharge from Novaya Zemlya (Voronina et al., 2001) in the eastern Barents Sea. Our data thus support the interpretation that this layer was formed from the erosion and subsequent deposition of sediments originating from the northwestern Barents Sea continental shelf.

The low dinocyst concentrations (mean of 390 cysts/g) in sediments accumulated from 14.6 to 14.3 ka (Fig. 1.3) likely result from dilution with deposits from the sediment-laden meltwater plume. Nevertheless, the calculated fluxes are about 140 cysts/cm<sup>2</sup>/yr during this interval, which corresponds to relatively high fluxes and productivity.

From 14.1 ka until the top of Zone III, recurring high SSTs possibly relate to enhanced AW heat advection. However, while subpolar conditions are recorded in bottom waters around Svalbard (Bartels et al., 2017), particularly between 14.5-13.5 ka (Ślubowska-Woldengen et al., 2007), the planktic foraminifer assemblages rather indicate polar conditions during the Bølling-Allerød interstadial (Rasmussen et al., 2007; Aagaard-Sørensen et al., 2014b; Chauhan et al., 2014), probably linked to heat loss to the atmosphere and/or outpouring of cold waters as suggested by Rasmussen et al. (2007).

At the study sites, the SSTs are also marked by high seasonal amplitude from winter to summer (Figs. 1.7, 1.9). Strong inflow of AW during the deglaciation probably initiated atmospheric warming at the margin of the SBSIS and enhanced meltwater discharge, leading to low salinities and a strong stratification of surface water. Enhanced ice calving and meltwater inflows during the Allerød are indicated by coarse sediment and low  $\delta^{18}\text{O}$  from foraminifer shells (Andersen et al., 1996; Hald et al., 2001; Jessen et al., 2010; Zamelczyk et al., 2012; Aagaard-Sørensen et al., 2014b, Bartels et al., 2017). Moreover, low  $\delta^{13}\text{C}$  of *N. Pachyderma* in core MSM5-712 throughout the Bølling-Allerød suggests stratification in the water column (Aagaard-Sørensen et al., 2014b). Hence, the high SSTs in summer can be ascribed to a low thermal inertia of the surface

water layer together with heat advection by AW. Such conditions would explain the opposite relationship between the SSS and the  $\delta^{18}\text{O}$  NGRIP record during the Allerød period.

In situations of low SSTs in summer, notably in Zone IV and the cold event of 14.5–14.1 ka, the sea-surface conditions were associated with low seasonal amplitude of temperatures. This could be an effect of a weakened inflow of AW, reducing the meltwater inputs and the stratification of the surface water layer. It could also reflect a vertical mixing of water masses. Therefore, contrarily to intervals of high summer SSTs and large seasonal contrasts, the low summer SST phases were not associated with pronounced SSS decreases during the deglaciation.

#### 1.6.2.1 The *Spiniferites ramosus* morphotypes

The dinocyst assemblages of the Allerød interval are characterized by abundant specimens of *Spiniferites* including the cosmopolitan species *S. ramosus* (Figs. 1.4, 1.5), and by the presence of a large variety of morphotypes, ranging from typical *S. ramosus* to *Nematosphaeropsis*-like morphologies (Fig. 1.6). This is particularly the case at ~13.4 ka where the highest concentrations of *Spiniferites* are recorded, but other atypical specimens were observed from 14.3 to 11.4 ka. The two dinocyst species *S. ramosus* and *N. labyrinthus* are related to the same motile dinoflagellate species *Gonyaulax spinifera* (Dodge, 1989). From culture experiments, Rochon et al. (2009) proposed that they could be the two endmembers of the same genotype or at least related species. According to Rochon et al. (2009), the different phenotypes only occur in salinities between 25 and 30 psu, whereas typical *S. ramosus* and *N. labyrinthus* are usually more abundant in saltier water of 32–36 psu and 31–37 psu, respectively (Rochon et al., 1999; Marret and Zonneveld, 2003). Ellegaard (2000) also found unusual cyst morphotypes more abundant during low salinity events in the last 2000 years in the Limfjorden, northern Denmark. Other morphological disparities seem to be a response to salinity constraints, like the processes length of *O. centrocarpum*

(Mertens et al., 2012) or the development of cross shaped cysts in the Black Sea during the Late Pleistocene (Rochon et al., 2002). From 14 to 12.6 ka, the analogues selected for the MAT reconstructions are mainly from the Gulf of St-Lawrence. However, analogues were also obtained from northern Norway in the Barents Sea and the northeast shore of the United States. While all these analogues are associated with warm summers ( $> 8^{\circ}\text{C}$ ), they relate to variable salinities ranging from  $< 31$  psu in the Gulf of St-Lawrence to oceanic conditions at some other analogue locations. In our cores, the morphotypes occurred mostly in intervals of low reconstructed SSSs, with the exception of a few high salinities excursions, notably at 13 ka (33.9 psu) at site PS2863 and at 13.2 ka (32.4 psu) at site MSM5-712. Hence, the interval from 14 to 12.6 ka was apparently characterized by unstable conditions with high amplitude variations of SSSs and large seasonal contrasts of temperatures, as it is often the case in nearshore environments. The episode of strongly reduced SSSs in core MSM5-712 at 14-12.6 ka coincides with accelerated glacial retreat around Svalbard (e.g., Andersen et al., 1996; Hald et al., 2001). Therefore, morphological variations of processes during the cyst formation may well result from reduced salinities as proposed by Rochon et al. (2009), but highly variable conditions and/or turbulent environment could also have impacted the cyst morphology.

#### 1.6.2.2 The Younger Dryas

At the studied sites, the Younger Dryas interval (YD, 12.9-11.7 ka), as defined by Rasmussen et al. (2006), corresponds to a transition from large regional meltwater discharges with salinity  $< 32$  (Zone III) to modern-like conditions with regard to thermohaline properties in surface waters (Zone II; Figs. 1.7, 1.9). The first clear occurrence of *I. pallidum* at 12.5 ka marked this transition in the dinocyst assemblages of both cores, especially PS2863. It is of note that the occurrence of *I. pallidum* also characterized core PS1295 from central Fram Strait at about 12.9 ka (see Fig. 1.1; Matthiessen and Baumann, 1997). This taxon is a typical component of the modern assemblages from the Nordic Seas and indicates cold ocean conditions (Matthiessen,

1995; Rochon et al., 1999; Grøsfjeld et al., 2009; Bonnet et al., 2010). Hence, the occurrence of *I. pallidum* by 12.6 ka suggests a change towards cold but saline surface waters possibly under the influence of the AW. The dinocyst assemblages also indicate low stratification of the upper water masses, which his is compatible with the multi proxy data from northern Svalbard (cf. Bartels et al., 2017).

A change in the benthic fauna around Svalbard at 12.5 ka indicates the recurrence of cold bottom waters (Ślubowska-Woldengen et al., 2007, 2008). During YD, the planktic foraminifer assemblages that remained unchanged from the Bølling-Allerød still indicate cold conditions (Rasmussen, 2007; Aagaard-Sørensen et al., 2014b). In surface waters, our data indicate a strong cooling with SSTs decrease by about 10°C in summer. The cooling was accompanied by an increase in SSSs from 31 to 33 psu (Figs. 1.7, 1.9), which likely relates to reduced meltwater discharges during a slowdown of the ice sheet retreat as indicated by a stabilization of the sea level (Landvik et al., 1987). Hence, the benthic and planktic foraminifer data together with dinocyst data suggest cold surface to bottom water conditions during the YD and a weak stratification of water masses throughout the water column, which can be associated with the AW, then characterized chilled and low saline properties in the subpolar North Atlantic (e.g., Rasmussen, 2007; Carlson, 2013; Aagaard-Sørensen et al., 2014b). Therefore, higher thermal inertia inhibited an enhanced surface warming in summer. The decrease in summer SSTs was then probably an effect of lowered seasonal amplitudes and a shallower thermocline together with generally weakened AW heat advection.

Beyond the general cooling of the YD, the timing and the regional pattern of the climate signal in the Nordic Seas and the Svalbard area are not yet fully elucidate. Unlike in the Fennoscandian areas (Stroeve et al., 2016), there is no evidence that local glaciers of western (Mangerud and Landvik, 2007) and northern Svalbard (Bartels et al., 2017) experienced any re-advance during the YD.  $^{10}\text{Be}$  data even revealed that the Linnébreen glacier of western central Svalbard even underwent a glacial retreat at that time

(Reusche et al., 2014) whereas extensive sea-ice cover likely prevailed in eastern Svalbard, the Storfjorden and the western fjords of Svalbard (Forwick and Vorren, 2009; Kristensen et al., 2013; Rasmussen and Thomsen, 2014). Hence, the apparent offset between southern vs. northern glacier advances during the YD can be due to particularly cold and dry climate which limited snow accumulation and prevented glaciers growth in the Svalbard area (cf. Mangerud and Landvik, 2007).

Dinocyst assemblages of Zone II, from 12.6 to about 7.6 ka, are distinguished by abundant *I. minutum* in MSM5-712 and by maximum occurrence of the Cyst of *P. dalei* at site PS2863 (Figs. 1.4, 1.5). This interval would correspond to the development of the Arctic Coastal Front and the Polar Front in western and northern Svalbard, respectively. The Cyst of *P. dalei* has previously been associated with the Polar Front (Voronina et al., 2001), together with high productivity (Voronina et al., 2001; Grøsfjeld et al., 2009). *I. minutum*, which is typical of sea-ice environment and often associated with high productive polynya (Hamel et al., 2002), characterizes the present day surface arctic waters around Svalbard (Grøsfjeld et al., 2009). Therefore, from 12.6 to 7.6 ka, the study sites were probably lying in high productivity zones close to the sea-ice margin. This is compatible with the development of the coastal fronts that was suggested to have occurred at 12.6 ka from the high concentration of the benthic foraminifer *Nonionellina labradorica* in cores JM02-440 and NP94-51 (see Fig. 1.1; Koç et al., 2002; Ślubowska et al., 2005; Ślubowska-Woldengen et al., 2007). Increased *N. Labradorica* was also recorded at 12.7 ka in the northern margin of Svalbard (Bartels et al., 2017). However, the presence of the Polar Front was reported earlier at 14.4-11.5 ka in the southern Yermak Plateau near site PS2863 from high relative abundance of *N. labradorica* as well (Chauhan et al., 2014). It coincides with an increase of the Cyst of *P. dalei* at site PS2863 prior to its maximum abundance during Zone II. Hence, the the Polar Front might have oscillated in a position close to site PS2863 in norhtwestern Svalbard, from 14.5-12.6 ka, before it stabilized in a position similar to the present day one (Fig. 1.1). The establishment of the Arctic coastal front actually implies

strengthened ESC and SCC, which carry Arctic waters around the southern tip of Svalbard. The influence of cold Arctic waters on the Svalbard continental shelves is consistent with the dense sea-ice cover as suggested from *I. minutum* in our records and from sedimentological evidences in other coastal cores (Forwick and Vorren, 2009; Kristensen et al., 2013; Rasmussen and Thomsen, 2014). It is also coherent with the near-synchronous opening of the northeastern shelf of Svalbard at about 12.6 ka (Koç et al., 2002). Open waters around Svalbard necessarily fostered oceanic flow and enhanced Arctic waters circulation through the SCC and the ESC. At about the same time an increase in the strength of the EGC with enhanced southward flow of Arctic water/ice through Fram Strait was also inferred based on low  $\delta^{18}\text{O}$  in planktic foraminifers (Bauch et al., 2001; Zamelczyk et al., 2012) and the radiogenic signature in sediments from core MC16 (see Fig. 1.1; cf. Hillaire-Marcel et al., 2013).

Regardless the issues of the precise timing of events, very important changes in the sea-surface circulation in Fram Strait occurred during the YD, which have to be related to a major reorganization of the ocean circulation in the Arctic and subarctic Atlantic. With the possible initiation of an early Transpolar Drift as proposed by England and Furze (2008), the export of freshwater and icebergs from the Arctic Ocean may have triggered the YD cooling event and the decline of AMOC strength (Tarasov and Peltier, 2005; Condron and Winsor, 2012), which occurring at about 12.7 ka (McManus et al., 2004). In this hypothesis, the opening of the Bering Strait could well have led to enhanced southward export of sea ice through Fram Strait and to the weakening of the AMOC as simulated by Hu et al. (2015) from Community Climate System Model (CCSM) experiments.

### 1.6.3 The setting of full “interglacial” conditions

The Holocene was climatically more stable than the deglaciation. However, many studies point to significant variations of sea-surface conditions at regional scale, especially during the early Holocene, which was marked by delayed establishment of

optimal conditions (Solignac et al., 2004; de Vernal and Hillaire-Marcel, 2006; Bonnet et al., 2010; Werner et al., 2011, 2013, 2016; de Vernal et al., 2013; Van Nieuwenhove et al., 2016; Zumaque et al., 2017).

In the eastern Fram Strait, our results show that the transition towards modern-like conditions took place in surface water, from the end of the YD to about 7.6 ka. It was mostly marked by the pervasive increase in SSSs, likely in relation with the diminution of meltwater discharges. This transition was also characterized decreasing stratification of the upper water mass accompanied by decreased seasonal gradient of SSTs. It also corresponds to the recovery of the AMOC after 11.7 ka and lasting up to about 8 ka (cf. McManus, 2004) according to  $^{231}\text{Pa}$  data (see Fig. 1.10). The establishment of a strong Transpolar Drift together with enhanced penetration of AW into the Arctic Ocean might have altered the stratification in Fram Strait.

In our records, there is a tenuous SST optimum in summer from 10.5 to 8.5 ka. It is characterized by low, but significant occurrence of temperate taxa *Spiniferites mirabilis* at site MSM5-712 (Fig. 1.4) and *Impagidinium sphaericum* at site PS2863 (Fig. 5), which lead to reconstruct mean summer SSTs about  $2.5^{\circ}\text{C}$  higher than those of the late Holocene at site MSM5-712 (Fig. 1.7) and a minimum sea-ice cover extent at site PS2863 (Fig. 1.9). In core MSM5-712, high amplitude variations in summer SSTs and salinity suggest unstable conditions possibly due to freshwater supply.

In subsurface waters, foraminifer data indicate that temperatures started increasing by about 11 ka highlighting enhanced northward heat fluxes through the AW with maximum values reached at about 10 ka (Hald et al., 2007; Risebrobakken et al., 2011; Werner et al., 2016). However, the alkenone-based surface temperatures reached their maximum values later, between 9 and 6 ka south of Svalbard (Risebrobakken et al., 2011). The postglacial sea-surface warming was delayed to about 8.5 ka in the southeastern Norwegian Sea and at various locations of the northern North Atlantic according to diatoms (Koç and Jansen, 1992; Andersen et al., 2004a) and alkenones

(Calvo et al., 2002). The difference of timing in the establishment of optimum conditions might be due, at least in part, to seasonal biases depending upon proxy (e.g., Sejrup et al., 2016). Nevertheless, all proxies tend to indicate that the early Holocene was marked by regional changes in ocean conditions.

An important transition in dinocyst assemblages occurred at ca. 7.6 ka when *O. centrocarpum* became dominant and the relative abundances of the main taxa reached close to modern values, thus leading to define Zone I (Figs. 1.4, 1.5). The shift in dinocyst assemblages at about 8-7.5 ka, which corresponds to an abrupt decrease in *N. labyrinthus* at the benefit of *O. centrocarpum*, has been noticed from the study of many other cores from the southern Norwegian Sea and the Fram Strait (Baumann and Matthiessen, 1992; Matthiessen and Baumann, 1997; Van Nieuwenhove et al., 2016). A transition occurring at about the same time if not slightly later is also recorded in coccolith assemblages of the Nordic Seas (Baumann and Matthiessen, 1992) and by the onset of maximum  $\delta^{13}\text{C}$  values in both planktic and benthic foraminifers from the deep Greenland Sea, pointing to maximum deep water renewal (Telesiński et al., 2014).

The dinocysts of the Mid to Late Holocene interval show low amplitude variations, which permit to depict a cooling throughout the noise as illustrated by a decrease in winter SSTs of about 1.5°C and an increase in sea-ice cover of 1-2 months/yr at both study sites. The surface cooling is coherent with the subsurface temperature cooling recorded after 7.9 ka from planktic foraminifer data (Werner et al., 2013, 2016; Aagaard-Sørensen et al., 2014a) particularly at 5 ka with the establishment of the modern sea-ice factory (cf. Werner et al., 2013, 2016).

### 1.7 Conclusion

The dinocyst assemblages permit to document important shifts in the sea-surface conditions at two sites from the northeastern Fram Strait over the last 23,000 years. In particular, they permit the documenting of seasonal SSTs, SSSs and sea-ice cover. Hence, our records provide insights into the interrelation between the meltwater inputs

and the AW inflows throughout the deglaciation, as the approach permits to disentangle the salinity and the temperature signals as well as the SSTs from winter to summer. The records also point to major changes in the sea-surface circulation of northeastern Fram Strait during the deglaciation and the early Holocene.

In the Nordic Seas, the LGM was characterized by hydrographic conditions having no perfect modern analogue and which remain equivocal as reconstructions range from cold to relatively warm conditions depending upon the proxy (cf. de Vernal et al., 2006). During the LGM, there was most probably AW heat advection, but the low dinocyst fluxes led us to hypothesize that the inflows might have been episodic, causing short-lived events of open waters and high productivity throughout generally harsh conditions. A high temporal resolution of sedimentary records would be needed to validate our hypothesis.

The deglaciation started between 19 and 18 ka in the northeastern Fram Strait, which remained under the influence of important meltwater discharge resulting in low salinity until about 12.6 ka. During the course of the deglaciation, a warm episode likely related to strong AW inflows was recorded between 14.7 and 12.6 ka. It was interrupted by a cooling event dated of 14.5-14.1 ka at site MSM5-712, which probably related to the enhanced calving of the Barents Sea Ice Sheet. This event followed a surge associated with a well-known rapidly deposited sediment layer in the northwestern Barents Sea and the western Svalbard continental slopes (Jessen et al., 2010; Lucchi et al., 2015). The ice surge and subsequent cooling could have been triggered by the influence of warm AW inflows, the advection of heat being responsible for accelerated melting of the SBSIS.

During the YD, particularly from 12.6 to 12 ka, there was a major change towards colder but more saline conditions, suggesting reduced meltwater inputs. The YD was also a transition marked by the establishment of coastal fronts in the western and northern margins of Svalbard as the result of enhanced contribution of arctic waters

around Svalbard together with northward flow of AW at the surface through Fram Strait.

The transition towards full interglacial conditions was marked by increasing salinity until about 7.6 ka. During the Mid to Late Holocene, small amplitude variations are recorded but a general cooling trend was detected mostly from a decrease in winter SSTs.

This study combining SST and SSS records permitted to identify important climate parameters like meltwater discharges and stratification of the surface water layer. The major transitions in sea-surface condition, notably shortly after the Bølling-Allerød and the YD, seemed closely related to shifts in the AMOC strength as reconstructed from mid latitude North Atlantic geochemical data of McManus et al. (2004). This relation points to the high sensitivity of eastern Fram Strait to record AW inflows intensity, but also its critical role in the ocean circulation.

### 1.8 Acknowledgements

This study was supported by the *Fonds Québécois de la Recherche sur la Nature et les Technologies* (FQRNT) and the Natural Sciences and Engineering Research Council of Canada (NSERC). The laboratory analyses have been possible thanks to the GEOTOP facilities. The sediment samples from cores PS2863-1 and PS2832-2BC were made available through the ARK-XIII/2 expedition of the RV Polarstern and through the MSM05/5b expedition of the RV Maria S. Merian for core MSM5/5-712-2. A  $^{14}\text{C}$  age was operated by the NOSAMS facility at the Woods Hole Oceanographic Institution with National Science Foundation sponsorship (OCE-1239667). Special thanks go to Maryse Henry and Sophie Bonnet for the palynological analysis of the first 315 cm of the MSM5/5-712-2 core. We are grateful to Simon Van Bellen for his help in developing the age models from the Bacon software.

### 1.9 References

- Aagaard-Sørensen, S., Husum, K., Hald, M., Marchitto, T., Godtliebsen, F., 2014a. Sub sea surface temperatures in the Polar North Atlantic during the Holocene: Planktic foraminiferal Mg/Ca temperature reconstructions. *The Holocene* 24, 93-103.
- Aagaard-Sørensen, S., Husum, K., Werner, K., Spielhagen, R.F., Hald, M., Marchitto, T.M., 2014b. A Late Glacial–Early Holocene multiproxy record from the eastern Fram Strait, Polar North Atlantic. *Marine Geology* 355, 15-26.
- Allan, E., de Vernal, A., Henry, M., Knudsen, M. F., Moros, M., Ouellet-Bernier, M. M., Ribeiro, S. (in preparation). Centennial scale variations of sea-surface conditions in the Disko Bugt, west Greenland.
- Andersen, E.S., Dokken, T.M., Elverhøi, A., Solheim, A., Fossen, I., 1996. Late Quaternary sedimentation and glacial history of the western Svalbard continental margin. *Marine Geology* 133, 123-156.
- Andersen, C., Koç, N., Moros, M., 2004a. A highly unstable Holocene climate in the subpolar North Atlantic: evidence from diatoms. *Quaternary Science Reviews* 23, 2155-2166.
- Andersen, K.K., Azuma, N., Barnola, J.-M., Bigler, M., Biscaye, P., Caillon, N., Chappellaz, J., Clausen, H.B., Dahl-Jensen, D., Fischer, H., 2004b. High-resolution record of Northern Hemisphere climate extending into the last interglacial period. *Nature* 431, 147-151.
- Bartels, M., Titschack, J., Fahl, K., Stein, R., Seidenkrantz, M.-S., Hillaire-Marcel, C., Hebbeln, D., 2017. Atlantic Water advection vs glacier dynamics in northern Spitsbergen since early deglaciation. *Climate of the Past Discussions*, 1-53
- Bauch, H.A., Erlenkeuser, H., Spielhagen, R.F., Struck, U., Matthiessen, J., Thiede, J., Heinemeier, J., 2001. A multiproxy reconstruction of the evolution of deep and surface

waters in the subarctic Nordic seas over the last 30,000 yr. Quaternary Science Reviews 20, 659-678.

Baumann, K.-H., Matthiessen, J., 1992. Variations in surface water mass conditions in the Norwegian Sea: evidence from Holocene coccolith and dinoflagellate cyst assemblages. Marine Micropaleontology 20, 129-146.

Blaauw, M., Christen, J.A., 2011. Flexible paleoclimate age-depth models using an autoregressive gamma process. Bayesian Analysis 6, 457-474.

Bond, G., Broecker, W., Johnsen, S., McManus, J., Labeyrie, L., Jouzel, J., Bonani, G., 1993. Correlations between climate records from North Atlantic sediments and Greenland ice. Nature 365, 143-147.

Bonnet, S., de Vernal, A., Hillaire-Marcel, C., Radi, T., Husum, K., 2010. Variability of sea-surface temperature and sea-ice cover in the Fram Strait over the last two millennia. Marine Micropaleontology 74, 59-74.

Budéus, G., 2007. Short Cruise Report RV Maria S. Merian Cruise MSM05/5. University of Hamburg, Institute of Oceanography.

Calvo, E., Grimalt, J., Jansen, E., 2002. High resolution U 37 K sea surface temperature reconstruction in the Norwegian Sea during the Holocene. Quaternary Science Reviews 21, 1385-1394.

Carlson, A.E., 2013. The Younger Dryas Climate Event. In: Elias, S.A. and Mock, C.J. (eds.), Encyclopedia of Quaternary Science (Second Edition). Elsevier, Amsterdam, 126-134.

Chauhan, T., Rasmussen, T., Noormets, R., Jakobsson, M., Hogan, K., 2014. Glacial history and paleoceanography of the southern Yermak Plateau since 132 ka BP. Quaternary Science Reviews 92, 155-169.

- Chauhan, T., Rasmussen, T.L., Noormets, R., 2016. Palaeoceanography of the Barents Sea continental margin, north of Nordaustlandet, Svalbard, during the last 74 ka. *Boreas* 45, 76-99.
- Condron, A., Winsor, P., 2012. Meltwater routing and the Younger Dryas. *Proceedings of the National Academy of Sciences* 109, 19928-19933.
- Conkright, M.E., Locarnini, R.A., Garcia, H.E., O'Brien, T.D., Boyer, T.P., Stephens, C., Antonov, J.I., 2002. World Ocean Atlas 2001: Objective analyses, data statistics, and figures: CD-ROM documentation. US Department of Commerce, National Oceanic and Atmospheric Administration, National Oceanographic Data Center, Ocean Climate Laboratory.
- Cronin, T.M., Dwyer, G.S., Farmer, J., Bauch, H.A., Spielhagen, R.F., Jakobsson, M., Nilsson, J., Briggs Jr, W., Stepanova, A., 2012. Deep Arctic Ocean warming during the last glacial cycle. *Nature Geoscience* 5, 631-634.
- de Vernal, A., Hillaire-Marcel, C., Turon, J., Matthiessen, J., Rochon, A., Vallières, S., Levesque, L., 2000. Sea-surface conditions in middle to high latitudes of the North Atlantic during the last glacial maximum (LGM): the cold paradigm revisited. *Canadian Journal of Earth Sciences* 37, 725-750.
- de Vernal, A., Henry, M., Matthiessen, J., Mudie, P.J., Rochon, A., Boessenkool, K.P., Eynaud, F., Grøsfjeld, K., Guiot, J., Hamel, D., Harland, R., Head, M.J., Kunz-Pirring, M., Levac, E., Loucheur, V., Peyron, O., Pospelova, V., Radi, T., Turon, J.-L., Voronina, E., 2001. Dinoflagellate cyst assemblages as tracers of sea-surface conditions in the northern North Atlantic, Arctic and sub-Arctic seas: the new 'n= 677' data base and its application for quantitative palaeoceanographic reconstruction. *Journal of Quaternary Science* 16, 681-698.

- de Vernal, A., Eynaud, F., Henry, M., Hillaire-Marcel, C., Londeix, L., Mangin, S., Matthiessen, J., Marret, F., Radi, T., Rochon, A., Solignac, S., Turon, J.L., 2005. Reconstruction of sea-surface conditions at middle to high latitudes of the Northern Hemisphere during the Last Glacial Maximum (LGM) based on dinoflagellate cyst assemblages. *Quaternary Science Reviews* 24, 897-924.
- de Vernal, A., Hillaire-Marcel, C., 2006. Provincialism in trends and high frequency changes in the northwest North Atlantic during the Holocene. *Global and Planetary Change* 54, 263-290.
- de Vernal, A., Rosell-Melé, A., Kucera, M., Hillaire-Marcel, C., Eynaud, F., Weinelt, M., Dokken, T., Kageyama, M., 2006. Comparing proxies for the reconstruction of LGM sea-surface conditions in the northern North Atlantic. *Quaternary Science Reviews* 25, 2820-2834.
- de Vernal, A., Bilodeau, G., Henry, M., 2010. Micropaleontological preparation techniques and analyses. *Cahier du Geotop*.
- de Vernal, A., Hillaire-Marcel, C., Rochon, A., Fréchette, B., Henry, M., Solignac, S., Bonnet, S., 2013. Dinocyst-based reconstructions of sea ice cover concentration during the Holocene in the Arctic Ocean, the northern North Atlantic Ocean and its adjacent seas. *Quaternary Science Reviews* 79, 111-121.
- Dodge, J., 1989. Some revisions of the family Gonyaulacaceae (Dinophyceae) based on a scanning electron microscope study. *Botanica marina* 32, 275-298.
- Ellegaard, M., 2000. Variations in dinoflagellate cyst morphology under conditions of changing salinity during the last 2000 years in the Limfjord, Denmark. *Review of Palaeobotany and Palynology* 109, 65-81.

- England, J.H., Furze, M.F.A., 2008. New evidence from the western Canadian Arctic Archipelago for the resubmergence of Bering Strait. *Quaternary Research* 70, 60-67.
- Eynaud, F., Duprat, J., Turon, J.-L., Zaragosi, S., 2004. Paleohydrological evidence of a two step evolution of the Last Glacial Maximum (LGM) along the western European margins. Eighth International Conference on Paleoceanography, Biarritz, September, Programme and abstracts, B1-153.
- Fahrbach, E., Meincke, J., Østerhus, S., Rohardt, G., Schauer, U., Tverberg, V., Verduin, J., 2001. Direct measurements of volume transports through Fram Strait. *Polar Research* 20, 217-224.
- Fetterer, F., Knowles, K., Meier, W., Savoie, M., 2016. Sea Ice Index, Version 2. National Snow and Ice Data Center, Boulder, CO, USA. Digital Media, updated daily.
- Forwick, M., Vorren, T.O., 2009. Late Weichselian and Holocene sedimentary environments and ice rafting in Isfjorden, Spitsbergen. *Palaeogeography, Palaeoclimatology, Palaeoecology* 280, 258-274.
- Gascard, J.-C., Richez, C., Rouault, C., 1995. New insights on large-scale oceanography in Fram Strait: The West Spitsbergen Current. *49*, 131-182.
- Gibb, O.T., Hillaire-Marcel, C., de Vernal, A., 2014. Oceanographic regimes in the northwest Labrador Sea since Marine Isotope Stage 3 based on dinocyst and stable isotope proxy records. *Quaternary Science Reviews* 92, 269-279.
- Giraudeau, J., (in preparation). EPOC (University Bordeaux 1/CNRS) within the framework of an ongoing IFM-GEOMAR. EPOC collaboration.
- Grøsfjeld, K., Harland, R., Howe, J., 2009. Dinoflagellate cyst assemblages inshore and offshore Svalbard reflecting their modern hydrography and climate. *Norwegian Journal of Geology* 89, 121-134.

- Guiot, J., 1990. Methodology of the last climatic cycle reconstruction in France from pollen data. *Palaeogeography, Palaeoclimatology, Palaeoecology* 80, 49-69.
- Hald, M., Dokken, T., Mikalsen, G., 2001. Abrupt climatic change during the last interglacial–glacial cycle in the polar North Atlantic. *Marine Geology* 176, 121-137.
- Hald, M., Andersson, C., Ebbesen, H., Jansen, E., Klitgaard-Kristensen, D., Risebrobakken, B., Salomonsen, G.R., Sarnthein, M., Sejrup, H.P., Telford, R.J., 2007. Variations in temperature and extent of Atlantic Water in the northern North Atlantic during the Holocene. *Quaternary Science Reviews* 26, 3423-3440.
- Hall, I.R., Moran, S., Zahn, R., Knutz, P.C., Shen, C.C., Edwards, R., 2006. Accelerated drawdown of meridional overturning in the late-glacial Atlantic triggered by transient pre-H event freshwater perturbation. *Geophysical Research Letters* 33.
- Hamel, D., de Vernal, A., Gosselin, M., Hillaire-Marcel, C., 2002. Organic-walled microfossils and geochemical tracers: sedimentary indicators of productivity changes in the North Water and northern Baffin Bay during the last centuries. *Deep Sea Research Part II: Topical Studies in Oceanography* 49, 5277-5295.
- Hebbeln, D., Dokken, T., Andersen, E.S., Hald, M., Elverhøi, A., 1994. Moisture supply for northern ice-sheet growth during the Last Glacial Maximum.
- Hebbeln, D., Wefer, G., 1997. Late Quaternary paleoceanography in the Fram Strait. *Paleoceanography* 12, 65-78.
- Heinrich, H., 1988. Origin and consequences of cyclic ice rafting in the Northeast Atlantic Ocean during the past 130,000 years. *Quaternary Research* 29, 142-152.
- Hillaire-Marcel, C., Maccalli, J., Not, C., Poirier, A., 2013. Geochemical and isotopic tracers of Arctic sea ice sources and export with special attention to the Younger Dryas interval. *Quaternary Science Reviews* 79, 184-190.

- Hu, A., Meehl, G.A., Han, W., Otto-Bliestner, B., Abe-Ouchi, A., Rosenbloom, N., 2015. Effects of the Bering Strait closure on AMOC and global climate under different background climates. *Progress in Oceanography* 132, 174-196.
- Jessen, S.P., Rasmussen, T.L., Nielsen, T., Solheim, A., 2010. A new Late Weichselian and Holocene marine chronology for the western Svalbard slope 30,000–0 cal years BP. *Quaternary Science Reviews* 29, 1301-1312.
- Jones, G.A., Keigwin, L.D., 1988. Evidence from Fram Strait (78 N) for early deglaciation. *Nature* 336, 56-59.
- Knies, J., Vogt, C., Stein, R., 1998. Late Quaternary growth and decay of the Svalbard/Barents Sea ice sheet and paleoceanographic evolution in the adjacent Arctic Ocean. *Geo-Marine Letters* 18, 195-202.
- Koç, N., Jansen, E., Haflidason, H., 1993. Paleoceanographic reconstructions of surface ocean conditions in the Greenland, Iceland and Norwegian seas through the last 14 ka based on diatoms. *Quaternary Science Reviews* 12, 115-140.
- Koç, N., Klitgaard-Kristensen, D., Hasle, K., Forsberg, C.F., Solheim, A., 2002. Late glacial palaeoceanography of Hinlopen Strait, northern Svalbard. *Polar Research* 21, 307-314.
- Kodrans-Nsiah, M., de Lange, G.J., Zonneveld, K.A.F., 2008. A natural exposure experiment on short-term species-selective aerobic degradation of dinoflagellate cysts. *Review of Palaeobotany and Palynology* 152, 32-39.
- Kucera, M., Rosell-Melé, A., Schneider, R., Waelbroeck, C., Weinelt, M., 2005. Multiproxy approach for the reconstruction of the glacial ocean surface (MARGO). *Quaternary Science Reviews* 24, 813-819.

- Kristensen, D.K., Rasmussen, T.L., Koç, N., 2013. Palaeoceanographic changes in the northern Barents Sea during the last 16 000 years—new constraints on the last deglaciation of the Svalbard–Barents Sea Ice Sheet. *Boreas* 42, 798–813.
- Landvik, J.Y., Mangerud, J., Salvigsen, O., 1987. The Late Weichselian and Holocene shoreline displacement on the west-central coast of Svalbard. *Polar Research* 5, 29–44.
- Lehman, S., Jones, G., Keigwin, L., Andersen, E., Butenkoi, G., Østmo, S., 1991. Initiation of Fennoscandian ice-sheet retreat during the last deglaciation.
- Loeng, H., 1991. Features of the physical oceanographic conditions of the Barents Sea. *Polar research* 10, 5–18.
- Lucchi, R.G., Sagnotti, L., Camerlenghi, A., Macrì, P., Rebesco, M., Pedrosa, M.T., Giorgetti, G., 2015. Marine sedimentary record of Meltwater Pulse 1a along the NW Barents Sea continental margin. *arktos* 1, 7.
- Mangerud, J., 1972. Radiocarbon dating of marine shells, including a discussion of apparent age of recent shells from Norway. *Boreas* 1, 143–172.
- Mangerud, J., Gulliksen, S., 1975. Apparent radiocarbon ages of recent marine shells from Norway, Spitsbergen, and Arctic Canada. *Quaternary Research* 5, 263–273.
- Mangerud, J., Landvik, J.Y., 2007. Younger Dryas cirque glaciers in western Spitsbergen: smaller than during the Little Ice Age. *Boreas* 36, 278–285.
- Manley, T., 1995. Branching of Atlantic Water within the Greenland–Spitsbergen Passage: An estimate of recirculation. *Journal of Geophysical Research: Oceans* 100, 20627–20634.
- Marret, F., Zonneveld, K.A., 2003. Atlas of modern organic-walled dinoflagellate cyst distribution. *Review of Palaeobotany and Palynology* 125, 1–200.

- Maslowski, W., Marble, D., Walczowski, W., Schauer, U., Clement, J.L., Semtner, A.J., 2004. On climatological mass, heat, and salt transports through the Barents Sea and Fram Strait from a pan-Arctic coupled ice-ocean model simulation. *Journal of Geophysical Research: Oceans* 109.
- Matthews, J., 1969. The assessment of a method for the determination of absolute pollen frequencies. *New Phytologist* 68, 161-166.
- Matthiessen, J., 1995. Distribution patterns of dinoflagellate cysts and other organic-walled microfossils in recent Norwegian-Greenland Sea sediments. *Marine Micropaleontology* 24, 307-334.
- Matthiessen, J., Baumann, A., 1997. Dinoflagellate cyst records from the East Greenland continental margin during the last 15,000 years: implications for paleoceanographic reconstructions, in: Hass, H.C. & Kaminski, M.A. (Eds.), Contributions to the Micropaleontology and Paleoceanography of the Northern North Atlantic. Gryzbowski Foundation Special Publication, pp. 149-165.
- McManus, J.F., Francois, R., Gherardi, J.-M., Keigwin, L.D., Brown-Leger, S., 2004. Collapse and rapid resumption of Atlantic meridional circulation linked to deglacial climate changes. *Nature* 428, 834-837.
- Mertens, K.N., Bringué, M., Van Nieuwenhove, N., Takano, Y., Pospelova, V., Rochon, A., De Vernal, A., Radi, T., Dale, B., Patterson, R.T., Weckström, K., Andrén, E., Louwye, S., Matsuoka, K., 2012. Process length variation of the cyst of the dinoflagellate *Protoceratium reticulatum* in the North Pacific and Baltic-Skagerrak region: calibration as an annual density proxy and first evidence of pseudo-cryptic speciation. *Journal of Quaternary Science* 27, 734-744.
- Müller, J., Werner, K., Stein, R., Fahl, K., Moros, M., Jansen, E., 2012. Holocene cooling culminates in sea ice oscillations in Fram Strait. *Quaternary Science Reviews* 47, 1-14.

- Müller, J., Stein, R., 2014. High-resolution record of late glacial and deglacial sea ice changes in Fram Strait corroborates ice–ocean interactions during abrupt climate shifts. *Earth and Planetary Science Letters* 403, 446–455.
- Nørgaard-Pedersen, N., Spielhagen, R.F., Erlenkeuser, H., Grootes, P.M., Heinemeier, J., Knies, J., 2003. Arctic Ocean during the Last Glacial Maximum: Atlantic and polar domains of surface water mass distribution and ice cover. *Paleoceanography* 18 (3), 1063.
- National Snow and Ice Data Center (NSIDC), 2003. Brightness temperature and ice concentrations grids for the polar regions. Boulder, CO: NSIDC Distributed Active Archive Center.
- Olsson, I.U., 1980. Content of  $^{14}\text{C}$  in marine mammals from northern Europe. *Radiocarbon* 22, 662–675.
- Pflaumann, U., Sarnthein, M., Chapman, M., d'Abreu, L., Funnell, B., Huels, M., Kiefer, T., Maslin, M., Schulz, H., Swallow, J., van Kreveld, S., Vautravers, M., Vogelsang, E., Weinelt, M., 2003. Glacial North Atlantic: Sea-surface conditions reconstructed by GLAMAP 2000. *Paleoceanography* 18 (3), 1065.
- Rasmussen, S.O., Andersen, K.K., Svensson, A.M., Steffensen, J.P., Vinther, B.M., Clausen, H.B., Siggaard-Andersen, M.L., Johnsen, S.J., Larsen, L.B., Dahl-Jensen, D., Bigler, M., Röhlisberger, R., Fischer, H., Goto-Azuma, K., Hansson, M.E., Ruth, U., 2006. A new Greenland ice core chronology for the last glacial termination. *Journal of Geophysical Research* 111.
- Rasmussen, T.L., Thomsen, E., Ślubowska, M.A., Jessen, S., Solheim, A., Koç, N., 2007. Paleoceanographic evolution of the SW Svalbard margin ( $76^\circ\text{N}$ ) since 20,000  $^{14}\text{C}$  yr BP. *Quaternary Research* 67, 100–114.

- Rasmussen, T.L., Forwick, M., Mackensen, A., 2012. Reconstruction of inflow of Atlantic Water to Isfjorden, Svalbard during the Holocene: Correlation to climate and seasonality. *Marine Micropaleontology* 94-95, 80-90.
- Rasmussen, T., Thomsen, E., 2014. Brine formation in relation to climate changes and ice retreat during the last 15,000 years in Storfjorden, Svalbard, 76–78°N. *Paleoceanography* 29, 911-929.
- Reimer, P.J., Bard, E., Bayliss, A., Beck, J.W., Blackwell, P.G., Bronk Ramsey, C., Buck, C.E., Cheng, H., Edwards, R.L., Friedrich, M., 2013. IntCal13 and Marine13 radiocarbon age calibration curves 0-50,000 years cal BP.
- Reusche, M., Winsor, K., Carlson, A.E., Marcott, S.A., Rood, D.H., Novak, A., Roof, S., Retelle, M., Werner, A., Caffee, M., 2014. <sup>10</sup>Be surface exposure ages on the late-Pleistocene and Holocene history of Linnébreen on Svalbard. *Quaternary Science Reviews* 89, 5-12.
- Risebrobakken, B., Dokken, T., Smedsrød, L.H., Andersson, C., Jansen, E., Moros, M., Ivanova, E.V., 2011. Early Holocene temperature variability in the Nordic Seas: The role of oceanic heat advection versus changes in orbital forcing. *Paleoceanography* 26.
- Rochon, A., Vernal, A.d., Turon, J.-L., Matthiessen, J., Head, M., 1999. Distribution of recent dinoflagellate cysts in surface sediments from the North Atlantic Ocean and adjacent seas in relation to sea-surface parameters. *American Association of Stratigraphic Palynologists Contribution Series* 35, 1-146.
- Rochon, A., Mudie, P.J., Aksu, A.E., Gillespie, H., 2002. *Pterocystagen. nov.: A new dinoflagellate cyst from pleistocene glacial-stage sediments of the black and Marmara Seas. Palynology* 26, 95-105.

- Rochon, A., Lewis, J., Ellegaard, M., Harding, I.C., 2009. The *Gonyaulax spinifera* (Dinophyceae) “complex”: Perpetuating the paradox? Review of Palaeobotany and Palynology 155, 52-60.
- Rosell-Melé, A., Comes, P., 1999. Evidence for a Warm Last Glacial Maximum in the Nordic Seas or an example of shortcomings in UK37'and UK37to estimate low sea surface temperature? Paleoceanography 14, 770-776.
- Rudels, B., Friedrich, H.J., Quadfasel, D., 1999. The Arctic circumpolar boundary current. Deep Sea Research Part II: Topical Studies in Oceanography 46, 1023-1062.
- Rudels, B., Meyer, R., Fahrbach, E., Ivanov, V., Østerhus, S., Quadfasel, D., Schauer, U., Tverberg, V., Woodgate, R., 2000. Water mass distribution in Fram Strait and over the Yermak Plateau in summer 1997, *Annales Geophysicae*. Springer, pp. 687-705.
- Rudels, B., Björk, G., Nilsson, J., Winsor, P., Lake, I., Nohr, C., 2005. The interaction between waters from the Arctic Ocean and the Nordic Seas north of Fram Strait and along the East Greenland Current: results from the Arctic Ocean-02 Oden expedition. Journal of Marine Systems 55, 1-30.
- Sarnthein, M., Jansen, E., Weinelt, M., Arnold, M., Duplessy, J.C., Erlenkeuser, H., Flatøy, A., Johannessen, G., Johannessen, T., Jung, S., 1995. Variations in Atlantic surface ocean paleoceanography, 50°-80° N: A time-slice record of the last 30,000 years. Paleoceanography 10, 1063-1094.
- Sarnthein, M., Pflaumann, U., Weinelt, M., 2003. Past extent of sea ice in the northern North Atlantic inferred from foraminiferal paleotemperature estimates. Paleoceanography 18 (2), 1047.
- Schauer, U., 2004. Arctic warming through the Fram Strait: Oceanic heat transport from 3 years of measurements. Journal of Geophysical Research 109.

- Schauer, U., Beszczynska-Möller, A., Walczowski, W., Fahrbach, E., Piechura, J., Hansen, E., 2008. Variation of measured heat flow through the Fram Strait between 1997 and 2006, Arctic–Subarctic Ocean Fluxes. Springer, pp. 65-85.
- Sejrup, H.P., Seppä, H., McKay, N.P., Kaufman, D.S., Geirsdóttir, Á., de Vernal, A., Renssen, H., Husum, K., Jennings, A., Andrews, J.T., 2016. North Atlantic-Fennoscandian Holocene climate trends and mechanisms. Quaternary Science Reviews 147, 365-378.
- Skogseth, R., Haugan, P.M., Jakobsson, M., 2005. Watermass transformations in Storfjorden. Continental Shelf Research 25, 667-695.
- Ślubowska, M.A., Koç, N., Rasmussen, T.L., Klitgaard-Kristensen, D., 2005. Changes in the flow of Atlantic water into the Arctic Ocean since the last deglaciation: Evidence from the northern Svalbard continental margin, 80°N. Paleoceanography 20, PA4014.
- Ślubowska-Woldengen, M., Rasmussen, T.L., Koç, N., Klitgaard-Kristensen, D., Nilsen, F., Solheim, A., 2007. Advection of Atlantic Water to the western and northern Svalbard shelf since 17,500 cal. yr BP. Quaternary Science Reviews 26, 463-478.
- Ślubowska-Woldengen, M., Koç, N., Rasmussen, T.L., Klitgaard-Kristensen, D., Hald, M., Jennings, A.E., 2008. Time-slice reconstructions of ocean circulation changes on the continental shelf in the Nordic and Barents Seas during the last 16,000 cal. yr BP. Quaternary Science Reviews 27, 1476-1492.
- Solignac, S., de Vernal, A., Hillaire-Marcel, C., 2004. Holocene sea-surface conditions in the North Atlantic—contrasted trends and regimes in the western and eastern sectors (Labrador Sea vs. Iceland Basin). Quaternary Science Reviews 23, 319-334.
- Spielhagen, R.F., Müller, J., Wagner, A., Werner, K., Lohmann, G., Prange, M., Stein, R., 2014. Holocene Environmental Variability in the Arctic Gateway. In: Schulz, M. and

Paul, A. (eds.), Integrated Analysis of Interglacial Climate Dynamics, Springer Briefs, Springer-Verlag, Berlin, 37-41.

Stanford, J., Rohling, E.J., Bacon, S., Roberts, A., Grousset, F., Bolshaw, M., 2011. A new concept for the paleoceanographic evolution of Heinrich event 1 in the North Atlantic. *Quaternary Science Reviews* 30, 1047-1066.

Stein, R., Fahl, K., 1997. Scientific cruise report of the Arctic expedition ARK-XIII/2 of RV "Polarstern" in 1997= Wissenschaftlicher Fahrbericht über die Arktis-Expedition ARK-XIII/2 von 1997 mit FS "Polarstern". Berichte zur Polarforschung (Reports on Polar Research) 255.

Strel, M., Bless, M., 1980. Occurrence and significance of reworked palynomorphs. *Mededelingen-Rijks Geologische Dienst* 32, 69-80.

Stroeven, A.P., Hättestrand, C., Kleman, J., Heyman, J., Fabel, D., Fredin, O., Goodfellow, B.W., Harbor, J.M., Jansen, J.D., Olsen, L., 2016. Deglaciation of Fennoscandia. *Quaternary Science Reviews* 147, 91-121.

Tarasov, L., Peltier, W.R., 2005. Arctic freshwater forcing of the Younger Dryas cold reversal. *Nature* 435, 662-665.

Telesiński, M.M., Spielhagen, R.F., Bauch, H.A., 2014. Water mass evolution of the Greenland Sea since lateglacial times. *Clim. Past* 10, 123–136.

Van Nieuwenhove, N., Baumann, A., Matthiessen, J., Bonnet, S., de Vernal, A., 2016. Sea surface conditions in the southern Nordic Seas during the Holocene based on dinoflagellate cyst assemblages. *The Holocene* 26, 722-735.

Voronina, E., Polyak, L., Vernal, A.D., Peyron, O., 2001. Holocene variations of sea-surface conditions in the southeastern Barents Sea, reconstructed from dinoflagellate cyst assemblages. *Journal of Quaternary Science* 16, 717-726.

- Walczowski, W., Piechura, J., Osinski, R., Wieczorek, P., 2005. The West Spitsbergen Current volume and heat transport from synoptic observations in summer. Deep Sea Research Part I: Oceanographic Research Papers 52, 1374-1391.
- Walczowski, W., Piechura, J., 2007. Pathways of the Greenland Sea warming. Geophysical Research Letters 34.
- Walker, M.J.C., Berkelhammer, M., Björck, S., Cwynar, L.C., Fisher, D.A., Long, A.J., Lowe, J.J., Newnham, R.M., Rasmussen, S.O., Weiss, H., 2012. Formal subdivision of the Holocene Series/Epoch: a Discussion Paper by a Working Group of INTIMATE (Integration of ice-core, marine and terrestrial records) and the Subcommission on Quaternary Stratigraphy (International Commission on Stratigraphy). Journal of Quaternary Science 27, 649-659.
- Weinelt, M., Sarnthein, M., Pflaumann, U., Schulz, H., Jung, S., Erlenkeuser, H., 1996. Ice-free Nordic seas during the last glacial maximum. Potential sites of deepwater formation. Paleoclimates 1, 283-309.
- Weinelt, M., Vogelsang, E., Kucera, M., Pflaumann, U., Sarnthein, M., Voelker, A., Erlenkeuser, H., Malmgren, B.A., 2003. Variability of North Atlantic heat transfer during MIS 2. Paleoceanography 18 (3), 1071.
- Werner, K., Spielhagen, R.F., Bauch, D., Hass, H.C., Kandiano, E., Zamelczyk, K., 2011. Atlantic Water advection to the eastern Fram Strait — Multiproxy evidence for late Holocene variability. Palaeogeography, Palaeoclimatology, Palaeoecology 308, 264-276.
- Werner, K., Spielhagen, R.F., Bauch, D., Hass, H.C., Kandiano, E., 2013. Atlantic Water advection versus sea-ice advances in the eastern Fram Strait during the last 9 ka: Multiproxy evidence for a two-phase Holocene. Paleoceanography 28, 283-295.

Werner, K., Müller, J., Husum, K., Spielhagen, R.F., Kandiano, E.S., Polyak, L., 2016. Holocene sea subsurface and surface water masses in the Fram Strait – Comparisons of temperature and sea-ice reconstructions. *Quat. Sci. Rev.* 147, 194-209. doi:10.1016/j.quascirev.2015.09.007

Williams, G.L., Brideaux, W.W., 1975. Palynologic analyses of Upper Mesozoic and Cenozoic rocks of the Grand Banks, Atlantic continental margin. Department of Energy, Mines and Resources: available from Information Canada.

Xiao, X., Fahl, K., Müller, J., Stein, R., 2015. Sea-ice distribution in the modern Arctic Ocean: biomarker records from trans-Arctic Ocean surface sediments. *Geochimica et Cosmochimica Acta* 155, 16-29.

Zamelczyk, K., Rasmussen, T.L., Husum, K., Haflidason, H., de Vernal, A., Ravna, E.K., Hald, M., Hillaire-Marcel, C., 2012. Paleoceanographic changes and calcium carbonate dissolution in the central Fram Strait during the last 20ka. *Quaternary Research* 78, 405-416.

Zamelczyk, K., Rasmussen, T.L., Husum, K., Godtliebsen, F., Hald, M., 2014. Surface water conditions and calcium carbonate preservation in the Fram Strait during marine isotope stage 2, 28.8-15.4 kyr. *Paleoceanography* 29, 1-12.

Zumaque, J., Eynaud, F., de Vernal, A., 2017. Holocene paleoceanography of the Bay of Biscay: Evidence for west-east linkages in the North Atlantic based on dinocyst data. *Palaeogeography, Palaeoclimatology, Palaeoecology* 468, 403-413.

**Tableau 1.1** Information on cores

Core name	Abbreviation used in text	Core location	Latitude	Longitude	Water depth (m)	Core length (cm)	Modern sea-surface conditions			Core sampling	
							SST in summer (°C)	SSS in summer (psu)	Sea-ice cover (month/yr)	Length (cm)	Interval (cm)
MSM5/5-712-2	MSM5-712	Western Svalbard margin	78°54.937'N	06°46.036'E	1,487	950	4.94±1.40	34.73±0.43	1.2±1.7	10-283	4
PS2863-1	PS2863	NW Svalbard margin	80°33.46'N	10°17.96'E	808	580	2.3±2.3	33.3±0.9	9.32±2.0	41-184	4
PS2863-2			80°33.47'N	10°17.93'E	807	41				0-39	1

Core location, water depth (m) and recovery (cm); present day sea-surface conditions at the core sites (Conkright et al., 2002) and sea-ice cover from NSIDC. Sections and subsampling intervals (cm) are indicated.

**Tableau 1.2** Radiocarbon chronology of cores MSM5/5-712-2, PS2863-1 and PS2837-5

Core	Depth (cm)	Conventional $^{14}\text{C}$ age ( $^{14}\text{C}$ years BP)	Calibrated age (cal. years BP)	Minimum age	Maximum age	Lab n°	Reference
MSM5/5-712-2	10-12	$815 \pm 25$	381.7	218	471.4	KIA 45217	Werner et al., 2013
MSM5/5-712-2	20-22	$1,570 \pm 25$	1,018.7	884	1,161.2	KIA 41024	Werner et al., 2013
MSM5/5-712-2	27-29	$1,985 \pm 25$	1,432.2	1,299.7	1,568.6	KIA 45218	Werner et al., 2013
MSM5/5-712-2	40-42	$2,565 \pm 25$	2,114.1	1,935.9	2,284	KIA 45219	Werner et al., 2013
MSM5/5-712-2	60.5	$3,365 \pm 30$	3,093.8	2,896	3,295.1	SacA 19113	Giraudeau (in preparation)
MSM5/5-712-2	94.5	$4,915 \pm 30$	5,077.5	4,861.2	5,264.5	SacA 19114	Giraudeau (in preparation)
MSM5/5-712-2	139	$6,440 \pm 30$	6,796.2	6,622.9	6,960.5	SacA 19115	Giraudeau (in preparation)
MSM5/5-712-2	169	$7,305 \pm 35$	7,669.5	7,530.1	7,809.3	KIA 38080	Werner et al., 2013
MSM5/5-712-2	192	$7,815 \pm 45$	8,194.9	8,029.8	8,342.9	KIA 41025	Werner et al., 2013
MSM5/5-712-2	214.5	$8,362 \pm 50$	8,730.4	8,526.8	8,937.4	Poz-30723	Aagaard-Sørensen et al., 2014a
MSM5/5-712-2	280.5	$9,220 \pm 50$	9,895.3	9,640.2	10,137.6	KIA 37423	Aagaard-Sørensen et al., 2014a
MSM5/5-712-2	322.5	$9,580 \pm 47$	10,699.2	10,324.1	11,203.5	Poz-30725	Aagaard-Sørensen et al., 2014a
MSM5/5-712-2	350	$10,940 \pm 50^*$	12,047.8	11,375.4	12,443.1	KIA 7571	Nørgaard-Pedersen et al., 2003
MSM5/5-712-2	428-431	$12,358 \pm 63$	13,920.4	13,737.9	14,137.5	Poz-30726	Aagaard-Sørensen et al., 2014a
MSM5/5-712-2	480	$12,655 \pm 60^*$	14,077.5	13,892.8	14,296.8	KIA 7572	Nørgaard-Pedersen et al., 2003
MSM5/5-712-2	660	$12,9400 \pm 70^*$	14,792.5	14,450	15,620	KIA 10864	Nørgaard-Pedersen et al., 2003
MSM5/5-712-2	687.5	$14,650 \pm 75$	17,052.9	16,555.4	17,465.1	Poz-30727	Zamelczyk et al., 2014
MSM5/5-712-2	716.25	$17,200 \pm 120$	19,912.5	19,337.2	20,379.1	Poz-38427	Zamelczyk et al., 2014
MSM5/5-712-2	762.25	$19,300 \pm 140$	22,444.5	21,856.3	22,841.4	Poz-30728	Zamelczyk et al., 2014
MSM5/5-712-2	801	$20,150 \pm 130^{**}$	23,669.9	23,237	24,059.6	-	Jessen et al., 2010

MSM5/5-712-2	842	$20,580 \pm 130^{**}$	24,972.2	24,285.4	25,628.1	-	Jessen et al., 2010
MSM5/5-712-2	876	$23,340 \pm 200^{**}$	27,068.9	26,339.5	27,562	-	Jessen et al., 2010
MSM5/5-712-2	882.75	$24,480 \pm 190$	27,521.8	26,659.1	27,944.5	Poz-30729	Zamelczyk et al., 2014
PS2863-1	36-39	$7,150 \pm 35$	7,537.3	7,319	7,7717.3	OS-122305	This study
PS2863-1	52-54	$9,336 \pm 40$	10,156.1	9,841.2	10,508.4	KIA-50537	This study
PS2863-1	120	$12,840 \pm 150^{**}$	14,700.4	14,250.5	15,122.9	-	Jessen et al., 2010
PS2863-1	133	$13,140 \pm 150^{**}$	14,985.6	14,521.4	15,397.6	-	Jessen et al., 2010
PS2863-1	162.5	$15,660 \pm 80$	18,387.8	17,883.2	18,814.8	KIA-50401	This study
PS2863-1	168.5	$17,700 \pm 100$	19,669.8	18,896.3	20,522.2	KIA-50402	This study
PS2863-1	199.5	$19,140 \pm 120$	22,643.5	22,074.2	23,223.2	KIA-50403	This study
PS2837-6	10.5	$535 \pm 25$	1,46.7	11.1	270.4	KIA 7570	Nørgaard-Pedersen et al., 2003
PS2837-5	50.5	$2,130 \pm 40$	1,639.3	1,451.7	1,847.8	KIA 4652	Nørgaard-Pedersen et al., 2003
PS2837-5	76.5	$3,340 \pm 35$	3,059.3	2,858.5	3,268.7	KIA 8927	Nørgaard-Pedersen et al., 2003
PS2837-5	111.5	$4,965 \pm 45$	5,153.4	4,908.1	5,392.3	KIA 8928	Nørgaard-Pedersen et al., 2003
PS2837-5	153.5	$7,405 \pm 45$	7,709	7,483.3	7,874.6	KIA 8929	Nørgaard-Pedersen et al., 2003
PS2837-5	182.5	$8,070 \pm 60$	8,506.1	8,322.7	8,780	KIA 4653	Nørgaard-Pedersen et al., 2003
PS2837-5	225.5	$9,290 \pm 60$	10,0095.9	9,823.6	10,499.3	KIA 8930	Nørgaard-Pedersen et al., 2003
PS2837-5	253.5	$10,940 \pm 50$	12,243.5	11,886	12,354.8	KIA 7571	Nørgaard-Pedersen et al., 2003
PS2837-5	274.5	$12,155 \pm 60$	13,411	13,151.6	13,620	KIA 10863	Nørgaard-Pedersen et al., 2003
PS2837-5	300.5	$12,+655 \pm 60$	14,195.7	13,972.5	14,541.8	KIA 7572	Nørgaard-Pedersen et al., 2003
PS2837-5	359.5	$12,940 \pm 70$	14,746	14,466.5	15,080.7	KIA 10864	Nørgaard-Pedersen et al., 2003
PS2837-5	382.5	$16,040 \pm 80$	18,593.1	18,001.1	19,025.9	KIA 10865	Nørgaard-Pedersen et al., 2003
PS2837-5	389.5	$17,440 \pm 110$	20,123.8	19,543.2	20,639.3	KIA 4654	Nørgaard-Pedersen et al., 2003
PS2837-5	415.5	$24,230 \pm 180$	27,504.8	26,553.3	28,243.1	KIA 7573	Nørgaard-Pedersen et al., 2003

All  $^{14}\text{C}$  dates are from *Neogloboquadrina pachyderma* (sinistral). The calibrated ages correspond to the modelled weighted mean age obtained after 8000 iterations executed with the Bacon 2.2 software (see text section 1.4).

\* Ages obtained from a correlation with core PS2837-5

\*\* Ages obtained from a correlation with the western Svalbard MS stack

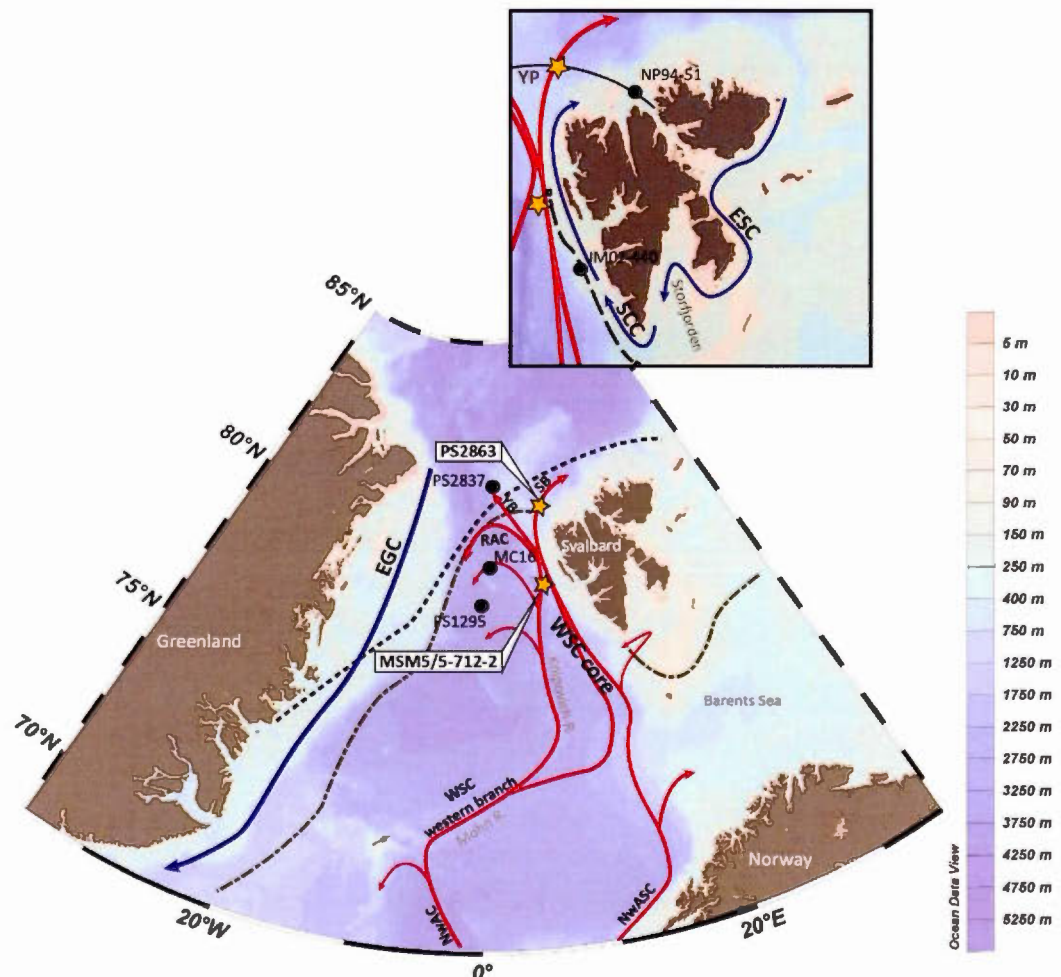


**Figure 1.1** Map of the main surface currents in Fram Strait and around Svalbard and location of the study sites MSM5/5-712-2 and PS2863 (yellow stars). Limits of minimum (September) and maximum (March) median sea-ice cover extent from 1979 to 2016 are represented by blue and gray dotted lines, respectively, from the Sea Ice Index (Fetterer et al., 2016). Red arrows indicate the warmer Atlantic waters derived from the North Atlantic Drift and were reproduced with respect to Walczowski et al. (2005). Blue arrows indicate cold surface water currents. In the Svalbard close up, the Arctic Coastal Front and the Polar Front are depicted, shown by a dotted and a uniform black line, respectively. The locations of other cores discussed in the text are indicated by

black dots. Main features of the sea-floor such as the Yermak Plateau (YP), the Storfjorden and the Mohn and Knipovich Ridges are also indicated on the map. EGC: East Greenland Current, WSC: West Spitsbergen Current, NwASC: Norwegian Atlantic Slope Current, NwAC: Norwegian Atlantic Current, ESC: East Spitsbergen Current, SCC: South Cape Current, RAC: Return Atlantic Current, SB: Svalbard Branch, YB: Yermak Branch

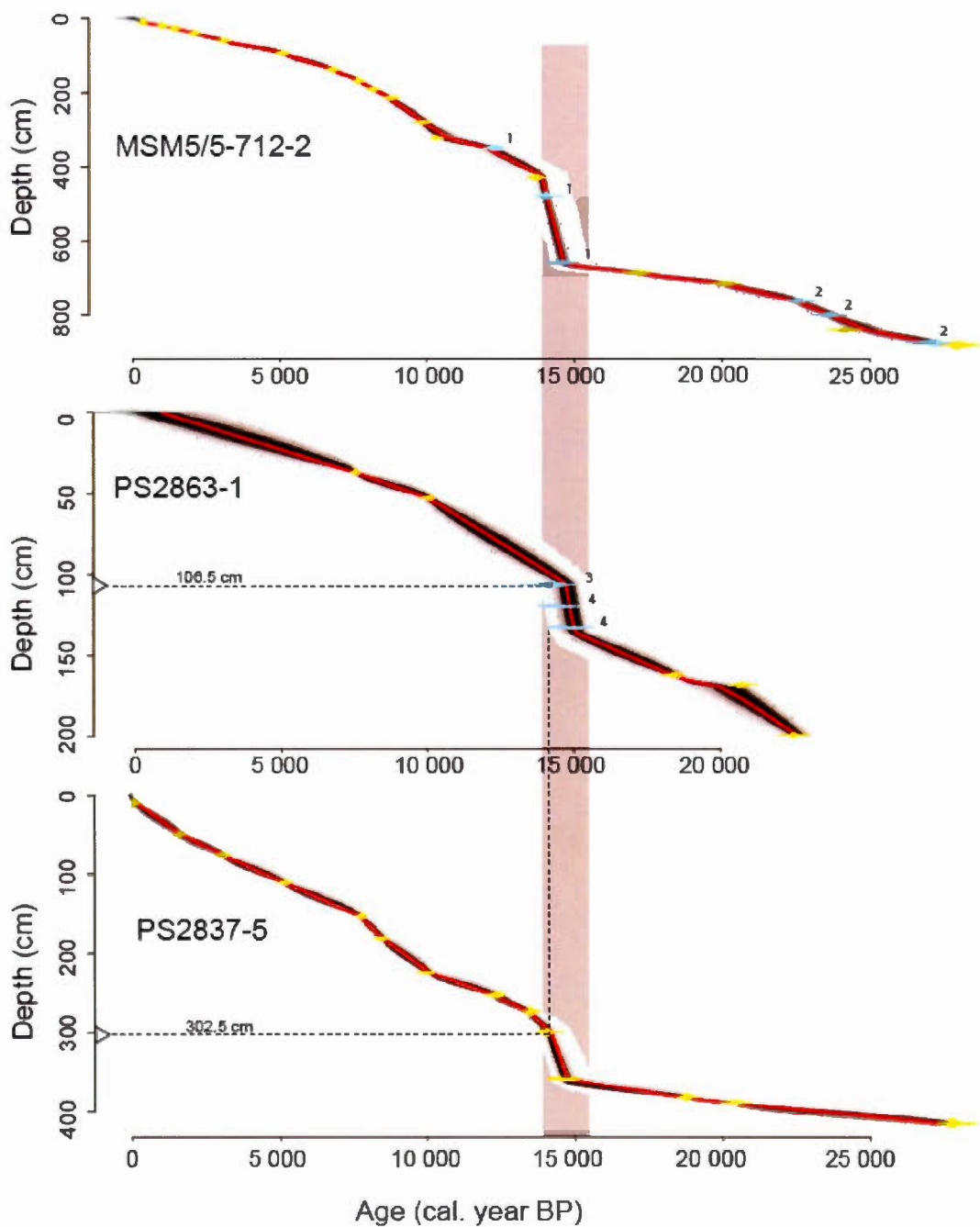


**Figure 1.2** Age model for cores MSM5/5-712-2, PS2863-1 and PS2837-5 (see Table 1.2 for data and text section 1.4). The red line corresponds to the weighted

average. The darker gray areas show the most probable ages. The dates are indicated yellow and the correlated tie points are indicated in blue, with numbering as follows : (1) correlations with core PS2837-5 based on total organic carbon (cf. Müller and Stein, 2014), (2) correlations with the western Svalbard magnetic susceptibility stack of Jessen et al. (2010) from Müller and Stein (2014), (3) sedimentological correlation with core PS2837-5 based on IRD (this study; see triangle and dotted lines), (4) correlation of a fine-grained layer in core PS2863-1 with the rapidly deposited layer in the western Svalbard (Jessen et al., 2010). The vertical shaded zone corresponds to the interval of the rapidly deposited sediment layer defined by Jessen et al. (2010) including its 95% probability. Since the rapid sedimentation rate interval is a well-documented regional event (Jessen et al., 2010; Lucchi et al., 2015), we added hiatuses at the depths of the first and last age of the event so the model would interpret the accumulation rate of this interval separately.

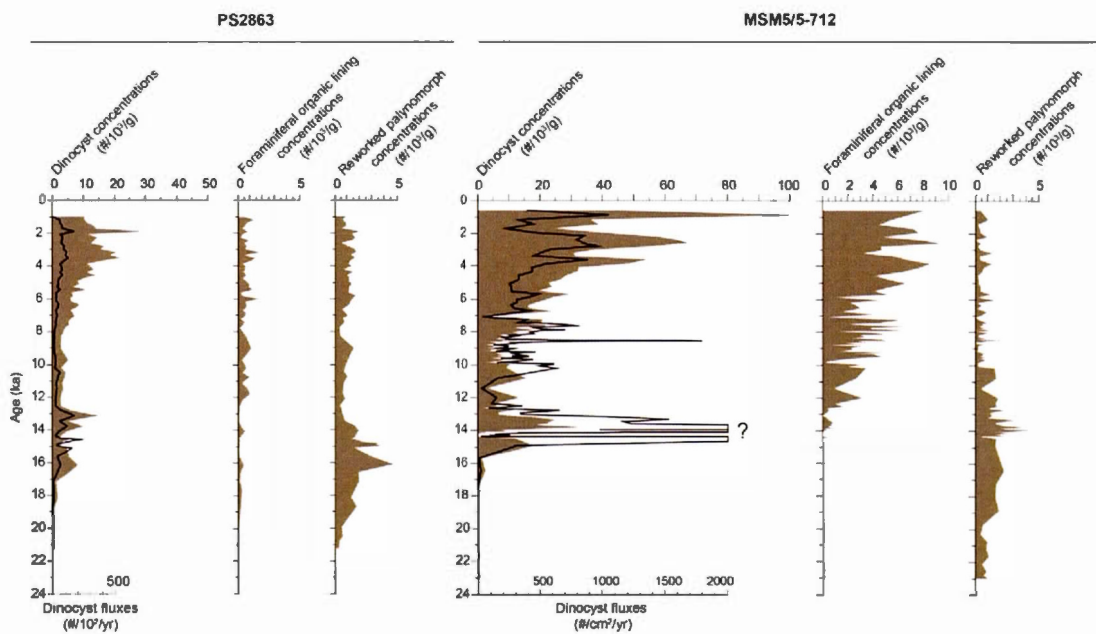


**Figure 1.3** Palynomorph concentrations at sites PS2863 and MSM5/5-712-2. Dinocyst fluxes are represented by a thick line.

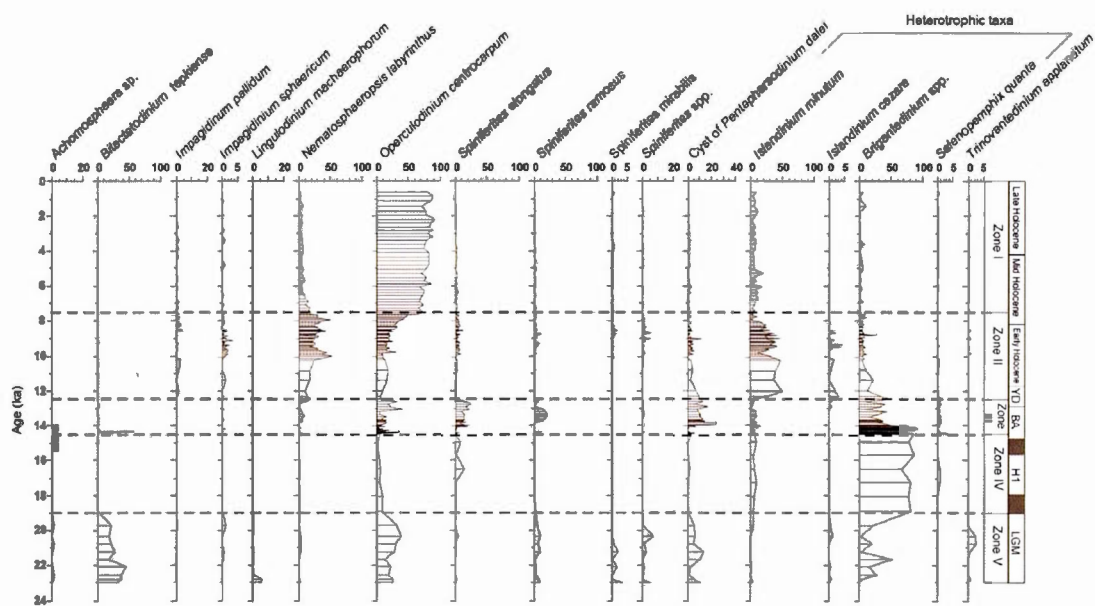


**Figure 1.4** Percentages of dinocyst taxa at site MSM5/5-712-2. Zones described in the text are delimited by dotted lines. The age of the LGM is established according to the MARGO working group (Kucera et al., 2005). The age of the Heinrich event 1 (H1), is determined according to Gibb et al. (2014). Limits of the Bølling-Allerød (BA) and the Younger Dryas (YD) intervals are set according to Rasmussen et al. (2006); the divisions between Early, Mid- and Late Holocene follow suggestions by Walker et al. (2012). On the calibrated age axis, the black bar indicates the interval of the rapidly deposited sediment layer described by Jessen et al. (2010), including its 95% probability while the gray bar represents the rapidly deposited sediment layer at the site.

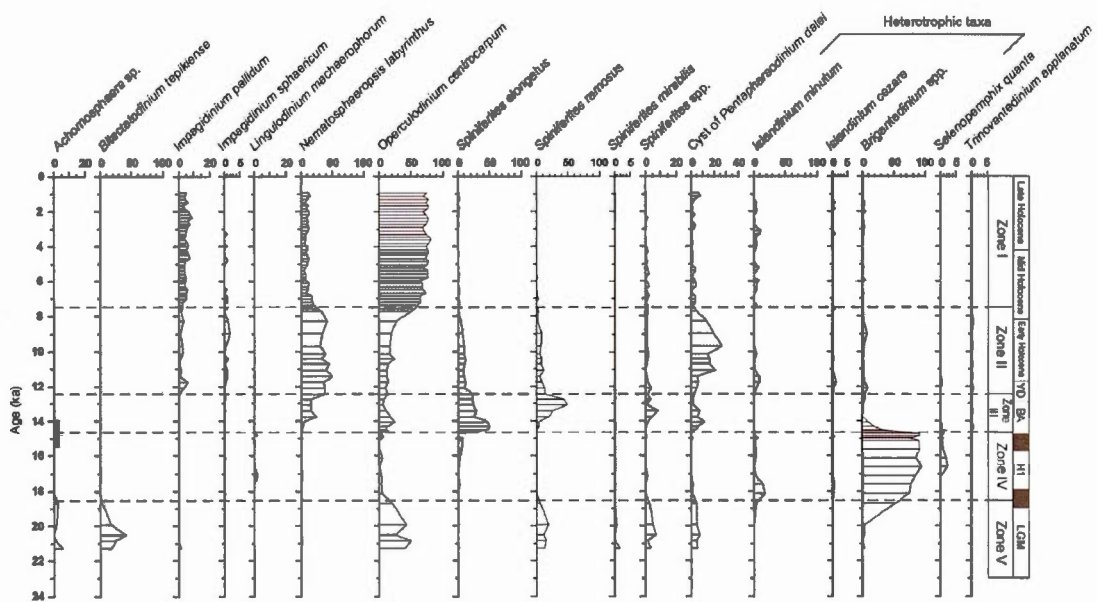


**Figure 1.5** Percentages of dinocyst taxa at site PS2863. For explanations see Fig.

1.4

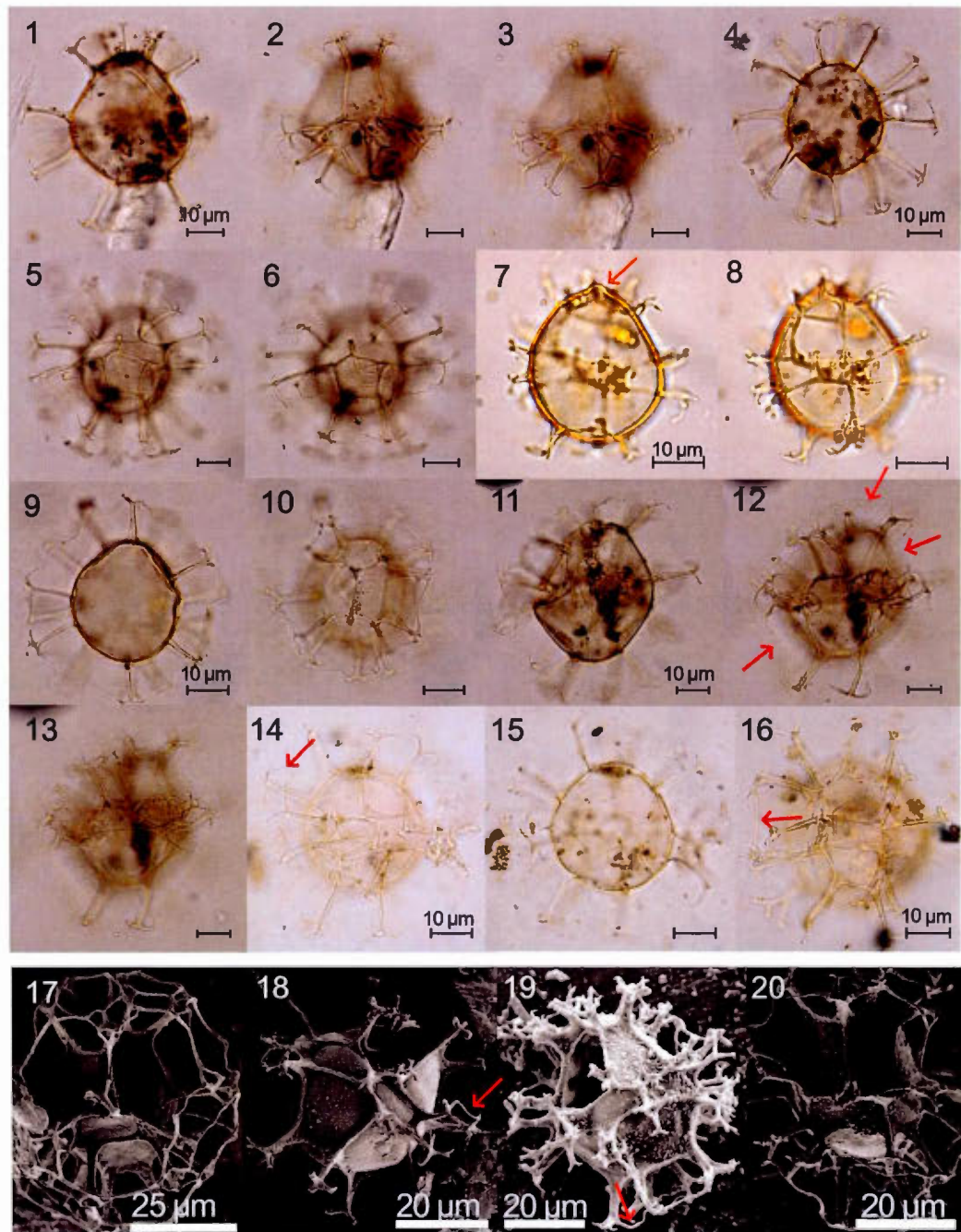


**Figure 1.6** Light micrographs and SEM photographs of the morphological variations of *Spiniferites ramosus* and *Nematospaeropsis labyrinthus* during the 14.3–11.4 ka interval in cores PS2863-1 and MSM5/5-712-2.

**1-3:** Core PS2863-1, slide 3145-6E, 93-94 cm (EF G24/2). *Spiniferites ramosus* with an ovoid to a pear-shaped body. The gonal processes are shorter at the apex than at the antapex.

**4-6:** Core PS2863-1, slide 3145-6E, 93-94 cm (EF K20/2). *Spiniferites ramosus* with a spherical central body and long radial processes which have an equivalent length all around the cyst body. The specimen exposes long trifurcations and bifurcate tips.

**7-8:** Core PS2863-1, side 3145-6C, 93-94 cm (EF L16/1). A small specimen of *Spiniferites ramosus* having aberrant morphologic characteristics like the development of an apical boss and a microgranular surface body. The processes are short and the processes' tips are irregular.

**9-10:** Core PS2863-1, slide 3145-6E, 93-94 cm (EF G23/4). *Nematosphaeropsis labyrinthus* with a spherical body and solid processes. The cyst shows a particularly clear paratabulation.

**11-13:** Core PS2863-1, slide 3145-6E; 93-94 cm (EF G24/2). A large ovoid specimen of *Spiniferites ramosus* which developed a partial trabecular network.

**14-15:** Core MSM5/5-712-2, slide 2799-6; 410-411 cm (EF H22/1). Specimen of *Spiniferites ramosus* with a spherical body and relatively long trifurcations exposing at least one clear trabecula joining the distal ends of two adjacent processes.

**16:** Core MSM5/5-712-2, slide 2799-6; 410-411 cm (EF H17/3). Another specimen of *Spiniferites ramosus* exposing at least one clear trabecula.

**17:** Core PS2863-1, sample 3145-5, 89-90 cm. SEM photograph of a *Nematosphaeropsis labyrinthus* specimen with a particularly well-developed paratabulation with large sutural ridges and solid processes.

**18-19:** Core PS2863-1, sample 3145-5, 89-90 cm. SEM photographs of two different specimens of *Spiniferites ramosus* exposing random processes being connected by a single trabecular liaison, at the cingulum (18) and at the antapex (19).

**20:** Core PS2863-1, sample 3145-5, 89-90 cm. SEM photograph of a *Spiniferites ramosus* specimen with an almost complete trabecular network.

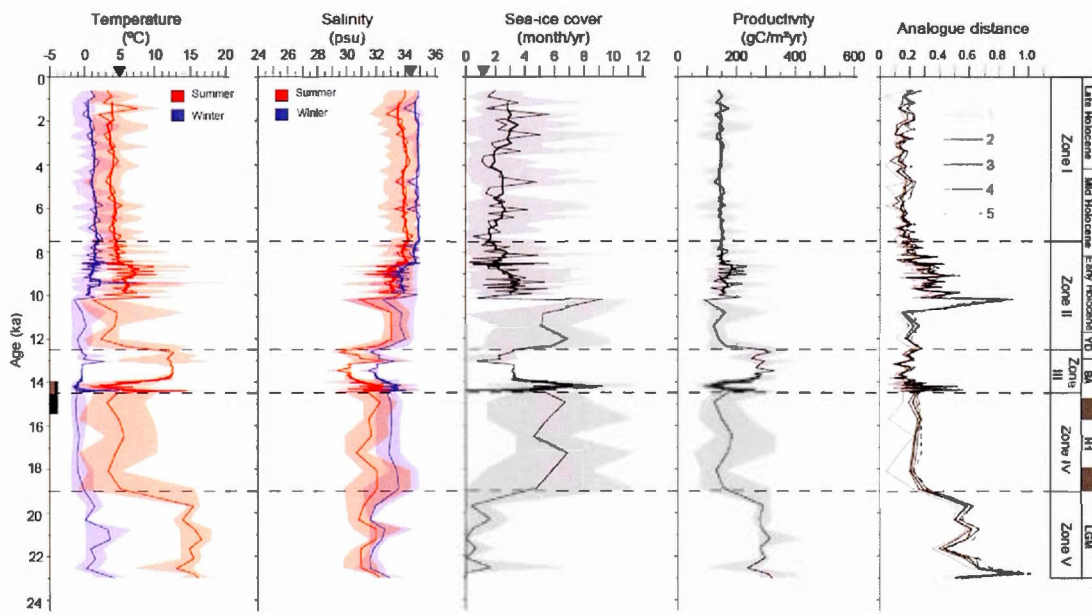


**Figure 1.7** Reconstructions of sea-surface conditions at site MSM5/5-712-2 including summer and winter SSTs in red and blue, respectively, summer and winter SSSs in red and blue, respectively, sea-ice cover duration, and productivity. Mean values are represented by a thin line, the thick line shows a five-point running average. Maximum and minimum values are represented in brighter shading. At the right is the distance of the five closest analogues. The calculated threshold value for poor analogue is 1.2. Black triangles indicate modern values at the core site (SSTs and SSSs in summer) from the World Ocean Atlas 2001 (Conkright et al., 2002) and the average sea-ice cover extent from NSIDC data. Zones as described in the text are divided by horizontal black dotted lines. On the calibrated age axis, the black bar indicates the interval of the rapidly deposited sediment layer as defined by Jessen et al. (2010), including its 95% probability while the gray bar represents the rapidly deposited sediment layer at the site.

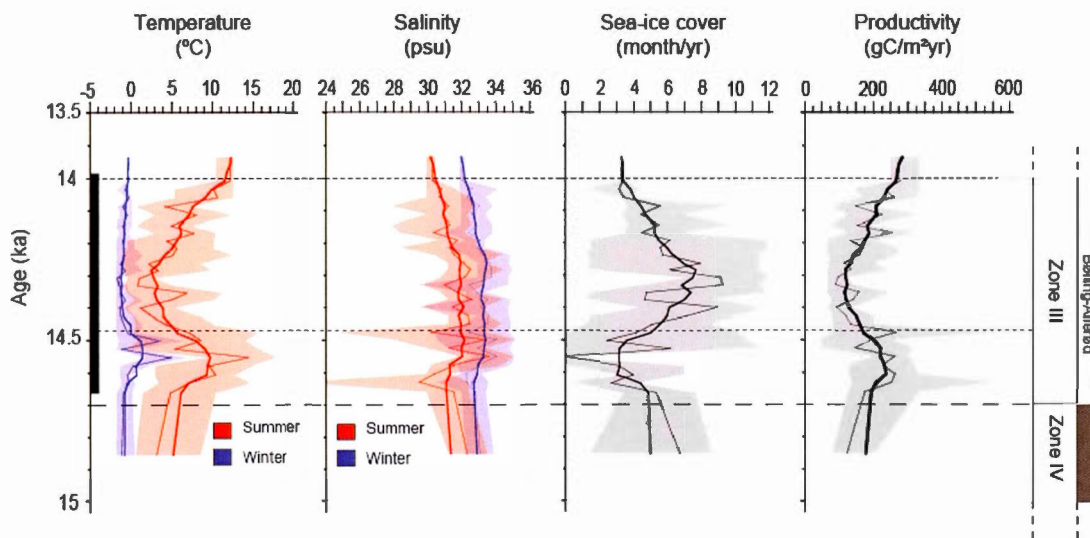


**Figure 1.8** Close-up of sea-surface conditions at site MSM5/5-712-2 during the Bølling-Allerød interstadial. The two finer dotted lines indicate the limits of a cooling event. For explanations see Fig. 1.7 and text section 1.6.2.

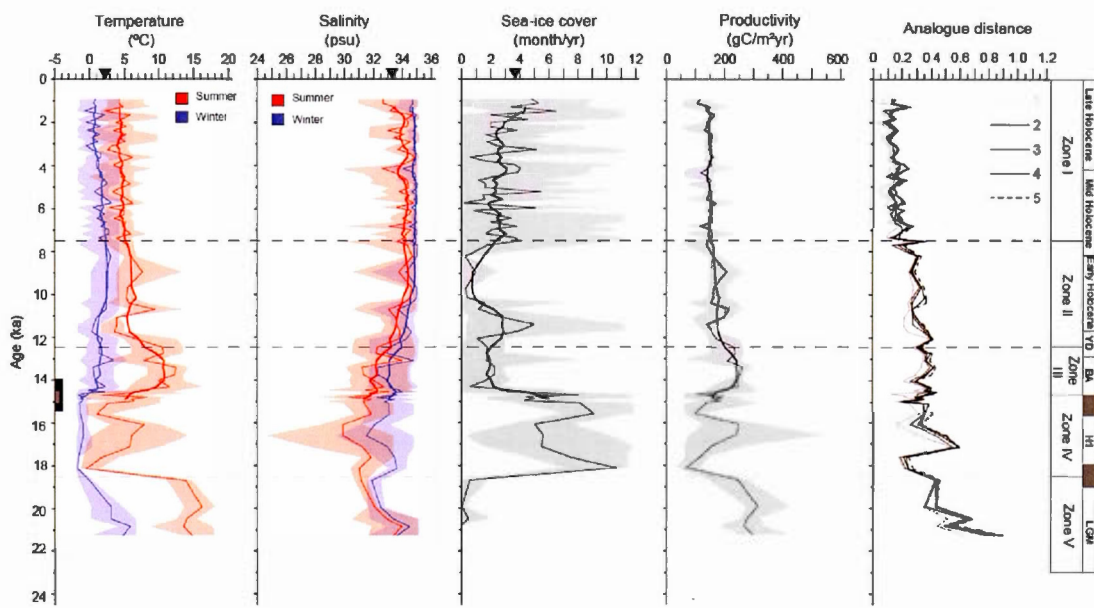


**Figure 1.9** Reconstructions of the sea-surface conditions at site PS2863 including summer and winter SSTs in red and blue, respectively, summer and winter SSSs in red and blue, respectively, sea-ice cover duration, and productivity. For explanations see Fig. 1.7.

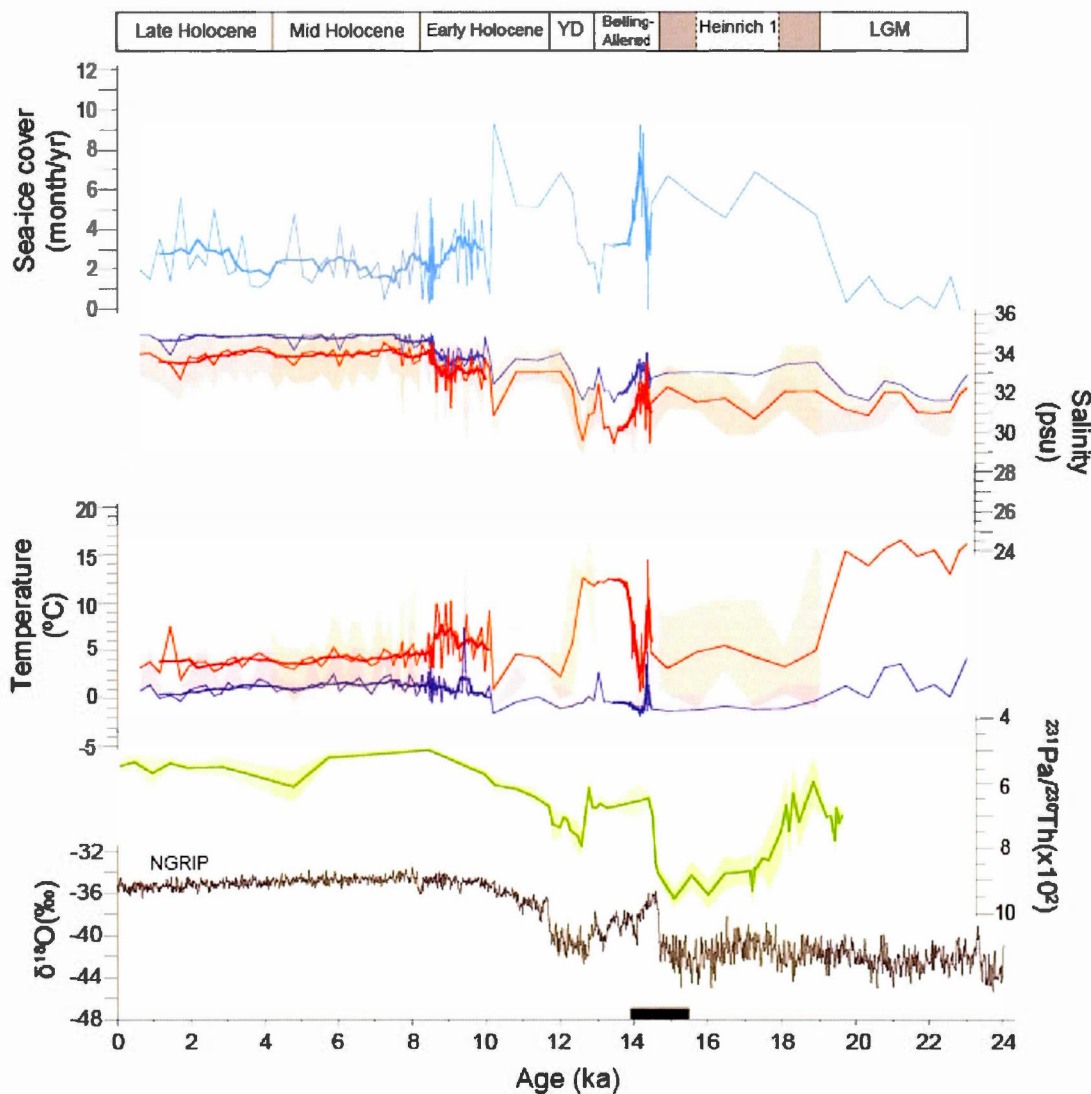


**Figure 1.10** Sea-surface reconstructions at site MSM5/5-712-2 including sea-ice cover seasonal duration, SSTs in summer (red) and winter (blue), SSSs in summer (red) and winter (blue) in correlation with the  $^{231}\text{Pa}/^{230}\text{Th}$  record (green) as a proxy of AMOC strength (McManus et al., 2004), and  $\delta^{18}\text{O}$  data (gray) from the NGRIP ice core (Andersen et al., 2004b). On the calibrated age axis, the black bar indicates the interval of the rapidly deposited sediment layer defined by Jessen et al. (2010), including its 95% probability.

## CONCLUSION

Les analyses de kystes de dinoflagellés ont mené à l'élaboration de deux enregistrements paléocéanographiques complets qui couvrent de 23 000 ans cal. BP à aujourd'hui, avec une résolution séculaire. Dans la mesure où il a été possible de dissocier les changements de température et de salinité des eaux de surface, en plus des écarts saisonniers de températures, cette étude a permis de retracer des paramètres clés de l'évolution des conditions des eaux de surface depuis le dernier maximum glaciaire, particulièrement en ce qui a trait à la circulation thermohaline globale. La relation entre les eaux de fonte et les eaux nord-atlantiques à travers différentes phases de la déglaciation a notamment pu être définie. Les deux enregistrements ont permis d'identifier des variations de grande amplitude dans les eaux de surface depuis le dernier maximum glaciaire et la composition taxonomique des assemblages de dinokystes a également permis de distinguer l'origine de courants de surface, en plus de la position de fronts océaniques.

Durant le dernier maximum glaciaire, enregistré de 23 000 à ~19 000 ans cal. BP, l'est du Détriot de Fram a connu des épisodes libres de glace de mer, et ce jusqu'à 80°N, malgré un climat généralement froid dans l'hémisphère nord (*e.g.*, Rosell-Melé *et al.*, 2004). L'advection de chaleur se produisait donc durant le dernier maximum glaciaire, sans doute à la faveur d'une physiographie rendant compte d'une canalisation des eaux nord-atlantiques via le Détriot de Fram, puisque la calotte glaciaire de la mer de Barents bloquait toute bifurcation du courant nord-atlantique vers l'est comme c'est le cas actuellement (Figure 1.1). Les masses d'eau de surface étaient probablement stratifiées, tel qu'en témoignent l'amplitude des variations saisonnières de température ainsi que les faibles salinités. Le paradoxe qui existe entre les reconstitutions enregistrant des

conditions relativement chaudes et productives à travers le dernier maximum glaciaire et les flux de dinokystes qui sont extrêmement faibles de l'ordre de 1 à 10 kystes/cm<sup>2</sup>/an suggèrent que les dinokystes observés dans le sédiment seraient probablement issus d'événements brefs plutôt que d'une productivité continue. La circulation d'eaux nord-atlantiques en surface aurait donc été occasionnelle et les signaux qui en découlent seraient dilués à travers des conditions générales très froides accompagnées d'un dense couvert de glace empêchant la production des dinoflagellés. Une meilleure résolution analytique serait nécessaire pour étayer ces interprétations et mieux définir la récurrence et la durée des épisodes de ces poussées d'eaux nord-atlantiques.

De ~19 000 à 14 700 ans cal. BP, de basses températures de surface en été et un couvert de glace de mer particulièrement étendu indiqueraient des apports atténués d'eaux nord-atlantiques au début de la déglaciation. Cet intervalle est caractérisé également par des concentrations maximales de palynomorphes remaniés, suggérant l'apport de sédiments issus de l'érosion glaciaire.

La région a ensuite été influencée par une advection accrue d'eaux nord-atlantiques, de 14 700 à 12 600 ans cal. BP. La présence des eaux nord-atlantiques se traduit par des températures estivales élevées. Toutefois, de grands écarts entre les températures hivernales et estivales indiqueraient la stratification des masses d'eau de surface qui se réchauffent davantage en été en raison de la faible inertie thermique. Ainsi, durant la déglaciation, une augmentation des flux d'eaux nord-atlantiques se serait accompagnée d'une accélération de la fonte de la calotte glaciaire et des apports d'eaux douces. Les températures estivales ont diminué entre 14 500 et 14 100 ans cal. BP, sans doute en relation avec un vêlage accéléré de la calotte glaciaire de la mer de Barents à la suite duquel une coulée de débris se serait déposée le long du talus continental de l'ouest du Svalbard (Jessen *et al.*, 2010, Lucchi *et al.*, 2015). Cet événement est représenté par un assemblage presque mono-spécifique de *Brigantedinium* spp.

Lors du Dryas Récent, les conditions de surface jusqu’alors influencées par des apports d’eaux de fonte importants enregistrent une transition vers des conditions plutôt océaniques. Un refroidissement dans le nord-est du Détroit de Fram marquerait également cet événement. À partir d’environ 12 600 ans cal. BP, les sites d’étude auraient été sous l’influence d’un régime océanographique régional se manifestant par l’installation du Front Arctique à l’ouest et du Front Polaire au nord du Svalbard tel que l’indique l’augmentation singulière d’*Islandinium minutum* au site MSM5-712 et de *Pentapharsodinium dalei* au site PS2863. La formation de ces fronts impliquerait une intensification des courants qui transportent des eaux arctiques autour du Svalbard (Figure 1.1). Une telle réorganisation de la circulation le long des marges du Svalbard est enregistrée de façon quasi-synchrone avec une intensification du courant est groenlandais (*East Greenland Current; EGC*) (Bauch *et al.*, 2001; Hillaire-Marcel *et al.*, 2013; Zamelczyk *et al.*, 2012) et probablement du WSC dans le Détroit de Fram en réponse au développement initial de la dérive transpolaire dans l’Océan Arctique suite à la déglaciation.

Après le Dryas Récent, la salinité de surface a continué d’augmenter et l’écart saisonnier des températures diminue graduellement jusqu’à 7 600 ans cal. BP. Contrairement à la situation de l’intervalle précédent le Dryas Récent, la présence des eaux nord-atlantiques se traduit dès lors par une salinité plus élevée (> 32 psu) démontrant une diminution des apports d’eaux de fonte après la déglaciation, ainsi qu’une stratification moindre des eaux de surface. À 7 600 ans cal. BP, un changement dans les assemblages de dinokystes, avec le remplacement de *Nematosphaeropsis labyrinthus* à *Operculodinium centrocarpum* comme espèce dominante, marque l’instauration des conditions océaniques modernes (Baumann et Matthiessen, 1992; Matthiessen et Baumann, 1997; Van Nieuwenhove *et al.*, 2016). De l’Holocène moyen à tardif, les conditions des eaux de surface se sont caractérisées par un léger refroidissement, soit une diminution des températures de surface hivernales.

Finalement, il est important de noter que deux des transitions majeures qui ont marquées les eaux de surface, la première au commencement du Bølling et la seconde lors du Dryas Récent, démontrent une certaine cohérence avec des changements dans la vigueur de la circulation méridienne de retournement de l'Atlantique (*Atlantic Meridional Overturning Circulation; AMOC*) telle que reconstituée par McManus *et al.* (2004). La cohérence des données obtenues indépendamment souligne l'importance du Détroit de Fram en ce qui concerne les flux nord-atlantiques vers le nord et met en évidence le rôle des conditions de surface à l'échelle régionale sur la circulation thermohaline.

## APPENDICE A

### DÉNOMBREMENT ET CONCENTRATIONS DES PALYNOmorphes

**Tableau A1** : Dénombrement des palynomorphes de la carotte MSM5/5-712-2

**Tableau A2** : Dénombrement des palynomorphes de la carotte PS2863-2BC

**Tableau A3** : Dénombrement des palynomorphes de la carotte PS2863-1

**Tableau A4** : Dénombrement des dinokystes de la carotte MSM5/5-712-2

**Tableau A5** : Dénombrement des dinokystes de la carotte PS2863-2BC

**Tableau A6** : Dénombrement des dinokystes de la carotte PS2863-1

**Tableau A7** : Concentration des palynomorphes de la carotte MSM5/5-712-2

**Tableau A8** : Concentration des palynomorphes de la carotte PS2863-2BC

**Tableau A9** : Concentration des palynomorphes de la carotte PS2863-1

**Tableau A.1** Dénombrement des palynomorphes de la carotte MSM5/5-712-2

Profondeur (cm)	10	14	18	22	26	30	34	38	42	46	50	54	58	62	66	70	74	78	82	86	90	94	98	102	
<i>Abies</i>	0	0	0	0	0	0	0	0	0	0	0	0	0	0	0	0	0	0	0	0	0	0	0	0	
<i>Picea</i>	0	0	0	0	0	0	2	0	0	1	2	1	0	0	3	1	2	0	0	1	0	0	4	2	3
<i>Pinus</i>	1	6	2	6	4	3	3	4	2	9	9	6	10	10	18	7	16	10	16	10	13	10	11	6	
<i>Tsuga</i>	0	0	0	0	0	0	0	0	0	0	0	0	0	0	0	0	0	0	0	0	0	0	0	0	
<i>Acer</i>	0	0	0	0	0	0	0	0	0	0	0	0	0	0	0	0	0	0	0	0	0	0	0	0	
<i>Betula</i>	4	0	1	0	2	1	1	0	1	1	3	1	1	3	1	1	2	0	0	0	1	0	1	0	
<i>Corya</i>	0	0	0	0	0	0	0	0	0	0	0	0	0	0	0	0	0	0	0	0	0	0	0	0	
<i>Corylus</i>	0	0	0	0	0	0	0	0	0	0	0	0	0	0	0	0	0	0	0	0	0	0	0	0	
<i>Fraxinus</i>	0	0	0	0	0	0	0	0	0	0	0	0	0	0	0	0	0	0	0	0	0	0	0	0	
<i>Quercus</i>	0	0	0	0	0	0	0	0	0	0	0	0	0	0	0	0	0	0	0	0	0	0	0	1	
<i>Tilia</i>	0	0	0	0	0	0	0	0	0	0	0	0	0	0	0	0	0	0	0	0	0	0	0	0	
<i>Alnus</i>	0	0	0	0	0	1	0	0	0	1	0	1	0	0	0	0	1	1	0	0	0	0	0	1	
Ericaceae	0	0	0	0	0	0	0	0	0	0	0	0	0	0	0	0	0	0	0	0	0	0	0	0	
<i>Ilex</i>	0	0	0	0	0	0	0	0	0	0	0	0	0	0	0	0	0	0	0	0	0	0	0	0	
<i>Salix</i>	0	0	0	0	0	0	0	0	0	0	0	0	0	0	0	0	0	0	0	0	0	0	0	0	
Type <i>Ambrosia</i>	0	0	0	0	0	0	0	0	0	0	0	0	0	0	0	0	0	0	0	0	0	0	0	0	
<i>Artemisia</i>	1	0	0	0	0	0	0	1	0	0	0	0	0	0	0	0	0	0	0	0	0	0	0	0	
<i>Liguliflorae</i>	0	0	0	0	0	0	0	0	0	0	0	0	0	0	0	0	0	0	0	0	0	0	0	0	
<i>Tubuliflorae</i>	0	0	0	0	0	0	0	0	0	0	0	0	0	0	0	0	0	0	0	0	0	0	0	0	
Brassicaceae	0	0	0	0	0	0	0	0	0	0	0	0	0	0	0	0	0	0	0	0	0	0	0	0	
Chenopodiaceae	0	0	0	0	0	0	0	0	0	0	0	0	0	0	0	0	0	0	0	0	0	0	0	0	
Cyperaceae	0	0	0	0	0	0	0	0	0	1	0	0	0	0	0	0	0	0	0	0	0	1	0	0	
Poaceae	0	0	0	0	0	0	0	0	0	0	0	0	0	0	0	0	0	0	0	0	0	0	0	0	
Polygonaceae	0	0	0	0	0	0	0	0	0	0	0	0	0	0	0	0	0	0	0	0	0	0	0	0	
Autre pollen	0	0	0	0	0	0	0	0	0	0	0	1	0	1	0	0	0	0	0	0	0	0	0	0	
<b>Somme des pollens</b>	6	5	3	6	7	5	4	4	6	12	15	7	18	17	20	10	19	11	17	10	15	14	16	10	
<i>Lycopodium</i>	0	1	0	1	0	4	0	0	0	0	1	2	0	0	1	0	0	2	0	0	0	4	0	1	
<i>Sphagnum</i>	2	0	2	2	0	2	1	0	1	0	2	1	1	0	0	0	2	1	4	0	1	0	1	2	
Spores monolètes	0	1	1	1	5	1	3	1	4	0	5	0	6	3	4	0	4	0	3	1	6	0	2	2	
Spores trilètes	0	0	1	0	3	0	0	1	0	1	1	2	2	0	3	0	2	2	0	1	1	2	0	3	
<b>Somme des spores</b>	2	2	4	4	8	7	4	2	5	1	9	5	9	3	8	0	8	5	7	2	8	6	3	8	
Grains de pollen d'angiospermes remaniés	0	0	0	0	0	0	0	0	0	0	0	1	0	0	0	0	0	0	0	0	0	0	0	0	
Grains de pollen de gymnospermes remaniés	0	1	0	2	1	3	2	0	1	2	0	8	3	0	4	4	3	1	0	5	1	4	2	1	
Spores remaniées	3	0	6	0	3	0	4	0	2	0	5	8	2	1	9	0	5	0	3	0	5	0	8	0	
Acritharches	0	1	0	0	0	0	0	0	0	0	0	1	0	0	0	0	0	2	0	0	1	0	0	0	
Dinokystes remaniés	0	3	0	2	0	1	0	0	0	0	0	1	0	2	0	8	0	0	1	0	0	7	5	2	
<b>Somme des palynomorphes remaniés</b>	3	5	6	4	4	4	6	0	3	2	5	19	5	3	13	12	8	3	4	6	7	11	15	3	
Réseaux organiques de foraminifères	54	43	31	77	77	71	30	59	62	43	54	44	73	58	87	134	90	55	75	123	82	104	63	18	
<i>Pediasium</i>	0	0	0	1	0	0	0	0	0	0	0	0	0	0	1	0	0	0	0	0	1	0	0		
<i>Halodinium</i>	2	5	0	6	2	4	2	3	4	4	3	4	4	3	6	5	0	1	0	4	2	3	1	1	

Profondeur (cm)	106	110	114	118	122	126	130	134	138	142	146	150	154	158	162	165	170	174	178	182	186	190	194	198
<i>Abies</i>	0	0	0	0	0	0	0	0	0	0	0	0	0	0	0	0	0	0	0	0	0	0	0	0
<i>Picea</i>	2	3	2	2	2	2	0	2	0	0	0	4	0	3	0	1	2	3	9	5	2	7	1	7
<i>Pinus</i>	8	11	11	19	25	15	13	13	10	14	22	13	8	33	25	22	41	27	24	19	11	36	11	26
<i>Tsuga</i>	0	0	0	0	0	0	0	0	0	0	0	0	0	0	0	0	0	0	0	0	0	0	0	0
<i>Acer</i>	0	0	0	0	0	0	0	0	0	0	0	0	0	0	0	0	0	0	0	0	0	0	0	0
<i>Betula</i>	0	6	1	2	2	1	2	5	1	4	5	5	0	2	1	1	5	16	6	2	5	5	1	2
<i>Carya</i>	0	0	0	0	0	0	0	0	0	0	0	0	0	0	0	0	0	0	0	0	0	0	0	0
<i>Carylus</i>	0	0	0	0	0	0	0	0	0	0	0	0	0	0	0	0	0	0	1	0	0	0	0	0
<i>Fraxinus</i>	0	0	0	0	0	0	0	0	0	0	0	0	0	0	0	0	0	0	0	0	0	0	0	0
<i>Quercus</i>	0	0	0	0	0	0	0	0	0	0	0	0	0	0	0	0	0	0	1	0	0	0	0	0
<i>Tilia</i>	0	0	0	0	0	0	0	0	0	0	0	0	0	0	0	0	0	0	0	0	0	0	0	0
<i>Alnus</i>	3	1	1	0	0	0	0	7	0	1	3	0	0	1	3	5	1	0	6	0	0	1	0	1
<i>Ericaceae</i>	0	0	0	0	0	0	1	0	0	0	0	0	0	0	0	0	0	0	0	0	0	1	0	0
<i>Ilex</i>	0	0	0	0	0	0	0	0	0	0	0	0	0	0	0	0	0	0	0	0	0	0	0	0
<i>Solix</i>	0	0	0	0	0	0	0	0	0	0	1	0	0	0	0	0	0	0	0	0	0	0	0	0
Type <i>Ambrasia</i>	0	0	0	0	0	0	0	0	0	0	0	0	0	0	0	0	0	0	0	0	0	0	0	0
<i>Artemisia</i>	0	1	0	0	0	0	0	0	1	0	0	0	0	0	0	0	0	0	0	0	0	0	0	0
<i>Liguliflorae</i>	0	0	0	0	0	0	0	0	0	0	0	0	0	0	0	0	0	0	0	0	0	0	0	0
<i>Tubuliflorae</i>	0	0	0	0	0	0	0	0	0	0	0	0	0	0	1	0	0	0	0	0	0	1	0	0
<i>Brassicaceae</i>	0	0	0	0	0	0	0	0	0	0	0	0	0	0	0	0	0	0	0	0	0	0	0	0
<i>Chenopodiaceae</i>	0	0	0	0	0	0	0	0	0	0	0	0	0	0	0	0	0	0	0	0	0	0	0	0
<i>Cyperaceae</i>	0	0	0	0	0	0	0	0	0	0	0	0	0	0	0	0	0	0	0	0	0	0	0	0
<i>Poaceae</i>	0	0	0	0	0	0	0	0	0	0	0	0	0	0	0	0	0	0	0	0	0	0	0	0
<i>Polygonaceae</i>	0	0	0	0	0	0	0	0	0	0	0	0	0	0	0	0	0	0	0	0	0	0	0	0
Autre pollen	1	0	0	0	1	0	0	0	0	0	0	0	0	0	0	0	0	1	0	0	0	0	0	0
<b>Somme des pollens</b>	14	22	15	23	30	19	22	21	12	23	27	22	9	42	31	25	49	53	40	26	20	39	14	36
<i>Lycopodium</i>	1	3	2	2	1	1	0	3	0	1	1	4	4	6	2	0	4	8	3	3	3	6	3	4
<i>Sphagnum</i>	2	3	0	0	0	2	0	0	2	1	2	1	1	2	0	2	0	2	1	3	3	5	0	3
Spores monolètes	12	9	5	1	10	2	6	1	7	13	8	5	10	5	7	6	22	18	3	3	12	5	2	5
Spores trilètes	4	1	1	1	0	2	0	1	1	0	4	0	2	2	0	0	6	3	6	3	2	12	2	2
<b>Somme des spores</b>	19	16	8	4	11	7	6	5	10	15	12	11	15	15	11	8	32	31	13	12	20	28	7	14
Grains de pollen d'angiospermes remaniés	0	0	0	0	0	1	0	0	0	0	1	0	0	0	2	0	0	1	0	0	0	1	0	0
Grains de pollen de gymnospermes remaniés	12	1	4	2	8	10	10	3	11	5	5	4	4	1	8	0	17	2	6	7	12	8	9	3
Spores remaniées	10	2	3	0	8	4	4	2	6	4	4	0	10	6	9	2	14	7	5	3	13	3	10	5
Acritharches	0	0	1	0	0	3	1	0	0	0	0	1	0	2	0	0	0	0	0	0	1	0	0	
Dinokystes remaniés	2	1	4	2	5	4	1	1	0	4	2	1	0	1	0	0	2	4	4	1	1	2	4	
<b>Somme des palynomorphes remaniés</b>	24	4	12	4	21	22	16	6	17	13	12	5	15	8	21	2	33	14	15	11	26	15	23	12
Réseaux organiques de foraminifères	69	43	63	86	37	133	56	135	76	51	76	115	74	104	110	31	119	139	144	148	75	289	44	172
<i>Pedialstrum</i>	0	0	0	0	0	0	0	0	0	0	0	0	0	0	0	0	1	2	0	2	0	0	0	
<i>Halodinium</i>	6	3	4	3	9	5	8	7	1	3	2	4	2	10	4	1	11	7	9	21	3	12	6	18

Profondeur (cm)	202	206	210	214	218	222	226	230	234	238	242	246	250	254	258	262	266	270	274	278	282	290	298	306
<i>Abies</i>	0	0	0	0	0	0	0	0	0	0	0	0	0	0	0	0	0	0	0	0	0	0	0	0
<i>Picea</i>	3	12	0	13	1	17	2	10	1	4	1	16	1	7	1	13	1	14	5	9	3	2	5	1
<i>Pinus</i>	6	23	17	39	10	19	10	51	73	29	19	51	16	62	29	26	10	31	34	27	27	2	15	15
<i>Tsuga</i>	0	0	0	0	0	0	0	0	0	0	0	0	0	0	0	0	0	0	0	0	0	0	0	0
<i>Acer</i>	0	0	0	0	0	0	0	0	0	0	0	0	0	0	0	0	0	0	0	0	0	0	0	0
<i>Betula</i>	1	4	1	7	1	4	3	4	8	2	2	1	10	6	8	4	6	9	3	3	4	1	3	4
<i>Carya</i>	0	0	0	0	0	0	0	0	0	0	0	0	0	0	0	0	0	0	0	0	0	0	0	0
<i>Corylus</i>	0	1	0	0	0	0	0	0	0	0	0	1	0	2	0	3	0	2	3	1	0	0	0	2
<i>Fraxinus</i>	0	0	0	0	0	0	0	0	0	0	0	0	0	0	0	0	0	0	0	0	0	0	0	0
<i>Quercus</i>	0	0	0	0	0	0	0	0	0	0	0	0	0	0	0	1	0	1	0	0	0	0	0	0
<i>Tilia</i>	0	0	0	0	0	0	0	0	0	0	0	0	0	0	0	0	0	0	0	0	0	0	0	0
<i>Alnus</i>	1	0	0	2	1	0	0	0	1	0	1	1	0	0	2	0	0	0	1	0	1	0	0	0
Ericaceae	0	0	0	0	0	0	0	0	1	0	0	1	0	0	0	0	0	0	0	0	0	0	0	0
<i>Ilex</i>	0	0	0	0	0	0	0	0	0	0	0	0	0	0	0	0	0	0	0	0	0	0	0	0
<i>Salix</i>	0	0	0	0	0	0	0	0	0	0	0	0	0	0	0	0	0	0	0	1	0	0	0	0
Type <i>Ambrosia</i>	0	0	0	0	0	0	0	0	0	0	0	0	0	0	0	0	0	0	0	0	0	0	0	0
<i>Artemisia</i>	0	0	0	0	1	0	0	0	0	0	0	0	0	0	0	0	0	0	0	0	0	0	0	0
Liguliflorae	0	0	0	0	1	0	0	0	1	0	0	0	0	0	0	0	0	0	0	0	0	0	0	0
Tubuliflorae	0	0	0	0	0	0	0	0	0	0	0	0	0	0	0	0	0	0	0	0	0	0	0	0
Brassicaceae	0	0	0	0	0	0	0	0	0	0	0	0	0	0	0	0	0	0	0	0	0	0	0	0
Chenopodiaceae	0	0	0	0	0	0	0	0	0	0	0	0	0	0	0	0	0	0	0	0	0	0	0	0
Cyperaceae	0	0	0	0	0	0	0	0	0	0	0	0	0	0	0	3	0	0	0	0	0	0	0	0
Poaceae	0	0	0	0	0	0	0	0	0	0	0	0	0	0	0	0	0	0	0	0	0	0	0	0
Polygonaceae	0	0	0	0	0	0	0	0	0	0	0	0	0	0	0	0	0	0	1	0	0	0	0	0
Autre pollen	0	0	0	0	0	0	0	0	0	1	0	1	0	0	0	0	0	0	0	1	0	0	0	0
<b>Somme des pollens</b>	<b>11</b>	<b>40</b>	<b>18</b>	<b>62</b>	<b>14</b>	<b>40</b>	<b>15</b>	<b>68</b>	<b>83</b>	<b>35</b>	<b>26</b>	<b>70</b>	<b>28</b>	<b>88</b>	<b>43</b>	<b>46</b>	<b>21</b>	<b>56</b>	<b>46</b>	<b>40</b>	<b>37</b>	<b>5</b>	<b>23</b>	<b>22</b>
<i>Lycopodium</i>	7	9	3	17	3	7	2	9	15	15	3	7	1	8	6	15	2	12	7	12	6	2	7	6
<i>Sphagnum</i>	1	2	0	4	2	3	1	5	2	7	1	3	4	0	1	7	1	5	5	7	1	0	2	4
Spores monolètes	12	3	6	7	5	9	3	10	24	7	5	8	13	8	18	15	5	8	13	9	13	7	9	8
Spores trilètes	1	10	0	12	2	7	0	9	2	13	0	4	3	6	1	13	1	21	5	15	0	2	0	3
<b>Somme des spores</b>	<b>21</b>	<b>24</b>	<b>9</b>	<b>40</b>	<b>12</b>	<b>26</b>	<b>6</b>	<b>33</b>	<b>43</b>	<b>42</b>	<b>9</b>	<b>22</b>	<b>21</b>	<b>22</b>	<b>26</b>	<b>50</b>	<b>9</b>	<b>46</b>	<b>30</b>	<b>43</b>	<b>20</b>	<b>11</b>	<b>18</b>	<b>21</b>
Grains de pollen d'angiospermes remaniés	1	0	2	0	0	0	0	0	0	0	0	0	0	0	0	0	1	0	0	0	2	0	0	0
Grains de pollen de gymnospermes remaniés	3	11	4	3	0	19	4	8	0	10	0	8	1	6	5	16	1	10	14	17	1	0	0	4
Spores remaniées	7	1	10	7	1	5	2	7	8	5	0	6	3	6	18	7	6	5	5	7	16	5	6	0
Acritharches	2	1	0	1	0	6	1	2	0	0	0	0	1	0	2	3	0	5	0	0	0	0	1	
Dinokystes remaniés	1	5	4	3	1	7	0	2	3	1	3	3	2	4	7	5	0	3	7	5	3	1	0	3
<b>Somme des palynomorphes remaniés</b>	<b>14</b>	<b>18</b>	<b>20</b>	<b>14</b>	<b>2</b>	<b>37</b>	<b>7</b>	<b>19</b>	<b>11</b>	<b>16</b>	<b>3</b>	<b>17</b>	<b>6</b>	<b>17</b>	<b>30</b>	<b>30</b>	<b>11</b>	<b>18</b>	<b>33</b>	<b>29</b>	<b>22</b>	<b>6</b>	<b>6</b>	<b>8</b>
Réseaux organiques de foraminifères	78	136	56	317	31	166	12	236	116	194	34	162	46	204	83	205	75	253	157	161	40	6	8	104
<i>Pediastrum</i>	0	1	0	1	0	0	0	2	0	1	1	0	0	1	0	3	0	0	2	0	0	0	0	0
<i>Haladinium</i>	4	22	5	35	2	26	6	35	18	45	2	58	5	39	14	48	17	70	34	66	21	1	11	17

Profondeur (cm)	314	322	330	338	346	354	362	370	378	386	394	402	410	418	426	434	442	450	458	466	474	482	490	500
<i>Abies</i>	0	0	0	0	0	2	0	0	0	1	1	0	0	0	0	0	0	0	0	0	0	1	0	0
<i>Picea</i>	4	0	0	3	0	2	1	2	0	1	3	1	1	0	0	0	0	0	0	0	0	0	0	0
<i>Pinus</i>	5	0	2	8	5	6	3	4	0	4	3	0	1	0	1	0	0	0	1	1	0	0	1	1
<i>Tsuga</i>	0	0	1	0	0	0	0	2	0	0	0	0	0	0	0	0	1	0	0	0	0	0	0	0
<i>Acer</i>	0	0	0	0	0	0	0	0	0	0	0	0	0	0	0	0	0	0	0	0	0	0	0	0
<i>Betula</i>	4	0	4	6	4	1	5	0	0	1	2	1	0	0	1	0	0	0	0	0	0	0	0	0
<i>Carya</i>	0	0	0	0	0	0	0	0	0	0	0	0	0	0	0	0	0	0	0	0	0	0	0	0
<i>Corylus</i>	0	0	0	0	0	0	0	0	0	0	0	0	0	0	0	0	0	0	0	0	0	0	0	0
<i>Fraxinus</i>	0	0	0	0	0	0	0	0	3	0	0	0	0	0	0	0	0	0	0	0	0	0	0	0
<i>Quercus</i>	0	0	0	0	1	0	0	0	0	0	0	2	0	0	0	0	1	0	2	0	0	0	1	1
<i>Tilia</i>	0	0	0	0	0	0	0	0	0	0	0	0	0	0	0	0	0	0	0	0	0	0	0	0
<i>Alnus</i>	0	0	0	0	0	0	0	0	0	0	0	0	0	0	0	0	0	0	0	0	0	0	0	0
Ericaceae	0	0	0	0	0	1	0	0	0	0	0	0	0	0	0	0	0	0	0	0	0	0	0	0
<i>Ilex</i>	0	0	0	0	0	0	0	0	0	1	0	0	0	0	0	0	0	1	0	0	0	0	0	0
<i>Salix</i>	1	0	0	0	0	2	3	0	0	0	0	0	0	0	0	0	0	1	1	0	0	0	1	0
Type <i>Ambrasia</i>	0	0	0	0	0	0	0	0	0	0	0	0	0	0	0	0	0	0	1	0	0	0	0	0
<i>Artemisia</i>	0	0	0	0	0	0	0	0	0	0	0	0	0	0	0	0	0	0	0	0	0	0	0	0
Liguliflorae	0	0	0	0	0	0	0	0	0	0	0	0	0	0	0	0	0	0	0	0	0	0	0	0
Tubuliflorae	0	0	0	0	0	0	0	0	0	0	0	0	0	0	0	0	0	0	0	0	0	0	0	0
Brassicaceae	0	0	0	0	0	3	3	5	0	4	2	0	1	1	1	0	0	2	1	0	1	3	2	0
Chenopodiaceae	0	0	0	0	0	1	2	0	0	0	1	0	1	0	1	1	2	0	0	0	0	0	0	0
Cyperaceae	0	0	0	0	0	0	0	0	0	0	0	0	0	0	0	0	0	0	0	0	0	0	0	0
Poaceae	0	0	0	0	1	0	0	1	0	0	0	0	0	0	0	0	0	0	0	0	0	0	0	0
Polygonaceae	2	0	0	0	0	0	0	0	0	0	0	0	0	0	0	0	0	0	0	0	0	0	0	0
Autre pollen	1	1	0	0	1	0	2	2	0	1	0	0	0	0	0	0	0	1	0	0	0	0	0	0
<b>Somme des pollens</b>	<b>17</b>	<b>1</b>	<b>7</b>	<b>17</b>	<b>12</b>	<b>16</b>	<b>21</b>	<b>17</b>	<b>0</b>	<b>12</b>	<b>13</b>	<b>2</b>	<b>4</b>	<b>1</b>	<b>3</b>	<b>2</b>	<b>3</b>	<b>5</b>	<b>8</b>	<b>1</b>	<b>1</b>	<b>6</b>	<b>3</b>	<b>3</b>
<i>Lycopodium</i>	4	1	1	0	2	1	1	0	1	0	0	0	0	0	0	0	0	0	0	0	0	0	0	1
<i>Sphagnum</i>	4	1	2	5	2	3	0	1	1	2	6	4	3	0	0	0	0	0	2	0	2	0	1	1
Spores monolètes	7	5	7	6	9	3	0	2	1	2	4	0	1	0	0	0	1	0	1	0	0	0	0	0
Spores trilètes	2	0	1	3	2	0	0	0	1	2	0	0	0	1	0	0	0	0	0	0	2	0	0	0
<b>Somme des spores</b>	<b>17</b>	<b>7</b>	<b>11</b>	<b>14</b>	<b>15</b>	<b>7</b>	<b>1</b>	<b>3</b>	<b>4</b>	<b>6</b>	<b>10</b>	<b>4</b>	<b>4</b>	<b>1</b>	<b>0</b>	<b>0</b>	<b>1</b>	<b>0</b>	<b>1</b>	<b>2</b>	<b>0</b>	<b>4</b>	<b>0</b>	<b>2</b>
Grains de pollen d'angiospermes remaniés	2	10	4	0	8	10	8	95	5	5	6	3	3	4	1	5	5	5	2	3	5	7	7	5
Grains de pollen de gymnospermes remaniés	0	8	6	7	5	16	17	28	24	13	16	3	7	3	4	10	10	4	4	3	19	41	14	19
Spores remaniées	4	20	20	11	14	45	36	21	19	19	26	9	19	10	10	16	14	13	5	20	43	90	77	42
Acritharches	0	9	3	1	6	13	6	9	4	4	8	1	3	4	6	4	2	5	6	5	20	19	16	14
Dinokystes remaniés	1	5	2	0	11	8	19	25	11	13	9	2	9	5	3	5	6	9	3	6	14	31	19	12
<b>Somme des palynomorphes remaniés</b>	<b>7</b>	<b>52</b>	<b>35</b>	<b>19</b>	<b>44</b>	<b>92</b>	<b>86</b>	<b>178</b>	<b>63</b>	<b>54</b>	<b>65</b>	<b>18</b>	<b>41</b>	<b>26</b>	<b>24</b>	<b>40</b>	<b>37</b>	<b>36</b>	<b>20</b>	<b>37</b>	<b>101</b>	<b>188</b>	<b>133</b>	<b>92</b>
Réseaux organiques de foraminifères	55	115	57	45	76	56	82	73	13	20	3	6	7	14	10	13	7	5	10	3	8	6	8	0
<i>Pediastrum</i>	0	0	0	0	3	1	0	4	2	0	1	0	1	1	1	0	1	0	0	2	0	1	1	1
<i>Halodinium</i>	10	26	19	7	13	11	12	0	2	4	0	1	4	1	1	3	2	1	3	1	1	1	2	1

Profondeur (cm)	507	514	521	528	536	542	549	556	563	570	577	585	593	601	608	616	624	632	640	648	656	664	672	680
<i>Abies</i>	0	0	0	0	0	0	0	0	0	0	0	0	0	0	0	0	0	0	0	0	0	0	0	
<i>Picea</i>	0	0	0	0	0	2	0	0	0	0	0	1	0	0	0	0	3	0	0	0	0	0	0	
<i>Pinus</i>	0	0	0	0	0	1	0	0	0	0	0	0	0	0	1	2	4	0	0	0	0	0	1	
<i>Tsuga</i>	0	0	0	0	0	0	0	0	0	0	0	0	0	0	0	0	0	0	0	0	0	0	0	
<i>Acer</i>	0	0	0	0	0	0	0	0	0	0	0	0	0	0	0	0	0	0	0	0	0	0	0	
<i>Betula</i>	0	0	0	0	0	0	0	0	0	0	0	0	0	0	0	0	0	0	0	0	0	0	0	
<i>Carya</i>	0	0	0	0	0	0	0	0	0	0	0	0	0	0	0	0	0	0	0	0	0	0	0	
<i>Corylus</i>	0	0	0	0	0	0	0	0	0	0	0	0	0	0	0	0	0	0	0	0	0	0	0	
<i>Fraxinus</i>	0	0	0	0	0	0	0	0	0	0	0	0	0	0	0	0	0	0	0	0	0	0	0	
<i>Quercus</i>	0	0	0	0	1	2	0	3	0	2	1	0	0	0	0	0	0	0	0	0	0	0	0	
<i>Tilia</i>	0	0	0	0	0	0	0	0	0	0	0	0	0	0	0	0	0	0	0	0	0	0	0	
<i>Alnus</i>	0	0	0	0	0	0	0	0	0	0	0	0	0	0	0	0	1	0	0	0	0	0	0	
Ericaceae	0	0	0	0	0	0	0	0	0	0	0	0	0	0	0	0	0	0	0	0	0	0	0	
<i>Ilex</i>	0	0	0	0	0	0	0	0	0	0	0	0	0	0	0	1	0	0	0	0	0	0	0	
<i>Salix</i>	0	0	0	0	0	0	0	0	0	0	0	0	0	0	0	0	0	0	0	0	0	0	0	
Type <i>Ambrosia</i>	0	0	0	0	0	0	0	0	0	0	0	0	0	0	0	0	0	0	0	0	0	0	0	
<i>Artemisia</i>	1	0	0	0	0	0	0	0	0	0	0	0	0	0	0	0	0	0	0	0	0	0	0	
<i>Liguliflorae</i>	0	0	0	0	0	0	0	0	0	0	0	0	0	0	0	0	0	0	0	0	0	0	0	
<i>Tubuliflorae</i>	0	0	0	0	0	0	0	0	0	0	0	0	0	0	0	0	0	0	0	0	0	0	0	
Brassicaceae	0	0	3	3	1	5	3	7	3	0	2	1	1	0	2	0	1	0	0	0	0	2	1	
Chenopodiaceae	0	0	0	1	0	0	1	0	0	0	0	0	1	0	0	0	0	0	0	0	0	0	0	
Cyperaceae	0	0	0	0	0	0	0	0	0	0	0	0	0	0	0	0	0	0	0	0	0	0	0	
Poaceae	0	0	0	0	0	0	0	0	0	0	0	0	0	0	0	0	0	0	0	0	0	0	0	
Polygonaceae	0	0	0	0	0	0	0	0	0	0	0	0	0	0	0	0	0	0	0	0	0	0	0	
Autre pollen	1	0	0	0	0	0	1	0	0	0	0	0	0	0	0	0	0	0	0	0	0	0	0	
<b>Somme des pollens</b>	2	0	3	4	2	10	5	10	3	2	3	2	1	1	3	3	9	0	0	0	0	0	2	
<i>Lycopodium</i>	0	0	1	0	0	1	1	0	2	0	0	1	0	0	0	0	0	0	0	0	0	0	0	
<i>Sphagnum</i>	0	0	1	1	1	0	0	0	0	2	0	0	0	0	3	0	1	1	0	0	0	0	1	
Spores monolètes	0	0	1	0	1	1	0	0	1	0	0	0	2	0	0	0	1	0	0	0	0	0	0	
Spores trilètes	0	0	0	0	0	0	0	0	0	0	0	0	0	0	0	0	0	0	0	0	0	0	1	
<b>Somme des spores</b>	0	0	3	1	2	2	1	0	3	2	0	1	2	0	3	0	2	1	0	0	0	0	2	
Grains de pollen d'angiospermes remaniés	0	1	3	9	9	8	3	4	8	14	3	3	6	3	18	9	8	11	6	5	1	0	3	5
Grains de pollen de gymnospermes remaniés	13	16	24	36	45	123	128	118	160	123	89	118	133	133	168	58	145	21	23	25	13	4	109	63
Spores remaniées	56	29	132	139	154	438	302	469	494	434	291	325	430	535	145	126	78	49	33	29	27	21	262	134
Acritharches	12	3	13	15	16	19	8	17	12	18	7	14	14	20	3	6	4	6	6	2	3	3	9	17
Dinokystes remaniés	19	11	26	41	24	73	61	37	73	89	41	52	49	68	30	22	40	7	3	10	0	0	29	61
<b>Somme des palynomorphes remaniés</b>	100	60	198	240	248	661	502	645	747	678	431	512	632	759	364	221	275	94	71	71	44	28	412	280
Réseaux organiques de foraminifères	6	2	6	10	4	3	0	0	8	2	2	5	4	2	13	160	0	47	30	19	0	1	2	7
<i>Pediastrum</i>	0	0	0	1	0	1	0	1	1	0	1	0	0	1	2	1	1	0	0	1	0	0	0	
<i>Haladinium</i>	1	4	5	7	4	5	4	4	1	2	3	4	5	8	0	0	0	4	2	4	0	0	3	2

<b>Profondeur (cm)</b>	688	696	704	712	720	728	736	744	752	760	768	776
<i>Abies</i>	0	1	0	0	6	1	0	0	4	4	3	0
<i>Picea</i>	0	1	0	1	9	0	0	0	2	6	9	0
<i>Pinus</i>	3	1	0	6	14	1	1	0	11	16	22	2
<i>Tsuga</i>	0	0	0	0	0	2	7	1	0	0	0	1
<i>Acer</i>	0	0	0	0	0	0	0	0	0	0	0	1
<i>Betula</i>	0	0	0	2	4	3	2	3	0	0	0	0
<i>Carya</i>	0	0	0	2	2	0	1	0	0	0	0	0
<i>Corylus</i>	0	0	0	1	2	0	0	1	1	0	1	0
<i>Fraxinus</i>	0	0	0	0	0	8	2	1	3	4	0	0
<i>Quercus</i>	0	0	0	1	0	3	2	1	1	0	0	0
<i>Tilia</i>	0	0	0	0	0	1	0	0	0	0	0	0
<i>Alnus</i>	0	0	0	0	1	0	0	1	0	1	6	0
Ericaceae	0	0	0	3	0	0	1	0	0	0	0	1
<i>Ilex</i>	0	0	0	0	0	3	2	3	0	0	0	0
<i>Salix</i>	0	0	0	2	0	2	3	0	0	0	0	0
Type <i>Ambrasia</i>	1	0	0	0	0	0	0	0	0	0	0	0
<i>Artemisia</i>	0	0	0	0	0	0	0	0	2	0	2	0
Liguliflorae	0	0	0	0	0	0	0	0	0	0	0	0
Tubuliflorae	0	0	0	0	0	0	0	0	0	0	0	0
Brassicaceae	3	4	4	6	0	5	3	9	0	0	0	1
Chenopodiaceae	3	2	3	3	0	3	2	3	0	0	0	2
Cyperaceae	0	0	0	0	0	0	0	0	0	0	0	0
Poaceae	0	0	0	0	0	0	0	0	0	0	0	0
Polygonaceae	0	0	0	0	0	0	0	0	0	0	0	0
Autre pollen	0	0	0	1	1	6	8	2	1	2	0	1
<b>Somme des pollens</b>	<b>10</b>	<b>9</b>	<b>7</b>	<b>28</b>	<b>39</b>	<b>38</b>	<b>34</b>	<b>25</b>	<b>25</b>	<b>33</b>	<b>43</b>	<b>9</b>
<i>Lycopodium</i>	0	1	0	0	3	0	0	3	0	1	0	1
<i>Sphagnum</i>	0	1	1	9	3	13	4	16	9	2	2	1
Spores monolètes	0	0	0	1	2	0	1	0	2	1	1	2
Spores trilètes	0	0	0	0	2	1	2	1	0	2	2	0
<b>Somme des spores</b>	<b>0</b>	<b>2</b>	<b>1</b>	<b>10</b>	<b>10</b>	<b>14</b>	<b>7</b>	<b>20</b>	<b>11</b>	<b>6</b>	<b>6</b>	<b>4</b>
Grains de pollen d'angiospermes remaniés	8	3	5	25	15	41	41	60	24	18	4	9
Grains de pollen de gymnospermes remaniés	123	88	51	64	55	92	87	45	149	115	83	84
Spores remaniées	415	196	175	76	161	95	63	104	254	298	114	67
Acritharches	15	6	11	11	3	11	6	17	0	1	3	6
Dinokystes remaniés	55	28	22	27	49	99	36	17	51	35	56	100
<b>Somme des palynomorphes remaniés</b>	<b>616</b>	<b>321</b>	<b>264</b>	<b>203</b>	<b>283</b>	<b>338</b>	<b>233</b>	<b>243</b>	<b>478</b>	<b>467</b>	<b>260</b>	<b>266</b>
Réseaux organiques de foraminifères	4	9	8	97	64	81	29	39	77	89	0	55
<i>Pediostrum</i>	0	3	0	29	5	3	13	18	2	2	0	3
<i>Halodinium</i>	5	3	3	6	3	1	4	2	1	3	0	0

**Tableau A.2** Dénombrement des palynomorphes de la carotte PS2863-2BC

Profondeur (cm)	0	1	2	3	4	5	6	7	8	9	10	11	12	13	14	15	16	17	18	19
<i>Picea</i>	4	6	7	3	9	2	6	3	0	4	0	1	5	4	0	2	2	1	4	2
<i>Pinus</i>	1	5	1	3	0	1	1	4	1	1	6	11	1	0	1	1	1	3	3	4
<i>Tsuga</i>	1	1	0	2	0	0	0	0	0	0	1	1	0	2	0	0	1	1	0	0
<i>Betula</i>	0	2	0	0	2	0	0	4	0	0	1	3	2	2	4	3	1	2	1	0
<i>Carya</i>	0	0	0	0	0	0	0	0	0	0	0	0	0	0	0	0	0	0	0	0
<i>Corylus</i>	0	0	0	0	0	0	0	0	0	0	0	0	0	0	0	0	0	0	0	0
<i>Fagus</i>	0	0	0	0	0	0	0	0	0	0	0	0	0	0	0	0	0	0	0	0
<i>Fraxinus</i>	0	0	0	0	0	0	0	0	0	0	0	0	0	0	0	0	0	0	0	0
<i>Quercus</i>	0	0	0	0	0	0	0	0	0	0	0	0	0	0	0	0	0	0	0	0
<i>Tilia</i>	0	0	0	0	0	0	0	0	0	0	0	0	0	0	0	0	0	0	0	0
<i>Alnus</i>	0	0	1	0	0	0	1	0	0	0	0	0	0	0	0	0	0	0	0	1
Ericaceae	0	0	0	0	0	0	0	0	0	0	0	0	0	0	0	0	0	0	0	0
<i>Salix</i>	0	0	0	0	0	0	0	0	0	0	0	1	0	0	0	0	0	0	0	0
Liguliflorae	0	0	0	0	0	0	0	0	0	0	0	0	0	0	0	0	0	0	0	0
Tubuliflorae	0	0	0	0	0	0	1	0	0	0	0	0	0	0	0	0	1	0	0	0
Chenopodiaceae	0	0	0	0	0	0	0	0	0	0	0	0	0	0	0	0	0	0	0	0
Poacea	0	0	0	0	0	0	0	0	0	0	0	0	0	0	0	0	0	0	0	0
Autre pollen	0	0	0	0	1	0	0	3	0	0	0	1	0	0	1	0	0	0	0	0
<b>Somme des pollens</b>	<b>6</b>	<b>14</b>	<b>9</b>	<b>8</b>	<b>12</b>	<b>3</b>	<b>9</b>	<b>14</b>	<b>1</b>	<b>5</b>	<b>8</b>	<b>18</b>	<b>8</b>	<b>8</b>	<b>6</b>	<b>6</b>	<b>6</b>	<b>7</b>	<b>8</b>	<b>7</b>
<i>Lycopodium</i>	1	3	1	1	1	0	0	0	1	2	2	3	0	1	1	0	2	0	0	1
<i>Sphagnum</i>	3	5	3	3	1	0	0	3	0	1	3	5	0	2	0	2	3	1	0	0
Spores monolètes	1	1	1	1	1	0	1	3	0	1	1	1	0	0	1	0	0	0	0	3
Spores trilètes	1	1	5	6	1	0	2	6	0	2	1	2	3	2	2	1	0	0	0	1
<b>Somme des spores</b>	<b>6</b>	<b>10</b>	<b>10</b>	<b>11</b>	<b>4</b>	<b>0</b>	<b>3</b>	<b>12</b>	<b>1</b>	<b>6</b>	<b>7</b>	<b>11</b>	<b>3</b>	<b>4</b>	<b>4</b>	<b>3</b>	<b>5</b>	<b>1</b>	<b>0</b>	<b>5</b>
Grains de pollen d'angiospermes remaniés	1	1	2	0	1	0	1	0	1	0	1	0	0	1	1	0	0	0	0	0
Grains de pollen de gymnospermes remaniés	3	4	3	4	3	1	6	11	7	3	7	11	6	12	3	3	5	6	7	10
Spores remaniées	14	7	11	7	11	12	19	30	14	7	14	25	13	7	16	10	21	21	9	16
Acritarches	6	3	5	3	3	4	4	4	7	4	4	5	10	5	6	5	5	8	6	12
Dinokystes remaniés	2	5	1	7	4	1	7	5	5	2	2	3	3	0	0	4	0	4	3	7
<b>Somme des palynomorphes remaniés</b>	<b>26</b>	<b>20</b>	<b>22</b>	<b>21</b>	<b>22</b>	<b>18</b>	<b>37</b>	<b>50</b>	<b>34</b>	<b>16</b>	<b>28</b>	<b>44</b>	<b>32</b>	<b>25</b>	<b>26</b>	<b>22</b>	<b>31</b>	<b>39</b>	<b>25</b>	<b>45</b>
Réseaux organiques de foraminifères	0	0	0	10	11	6	7	4	18	13	16	14	31	8	20	17	8	15	16	11
<i>Pediasium</i>	0	0	0	0	0	0	1	0	0	0	0	0	0	0	0	0	0	0	0	0
<i>Halodinium</i>	2	1	1	1	3	0	4	1	0	1	0	0	5	5	2	5	3	3	0	2

Profondeur (cm)	20	21	22	23	24	25	26	27	28	29	30	31	32	33	34	35	36	37	38
<i>Picea</i>	1	5	4	3	5	2	5	5	4	1	13	6	6	4	8	3	9	5	1
<i>Pinus</i>	3	4	3	3	3	1	5	3	4	1	3	0	6	3	4	4	3	2	3
<i>Tsuga</i>	0	0	0	0	0	0	2	0	0	0	0	0	0	0	1	0	0	0	0
<i>Betula</i>	1	1	0	1	0	1	0	2	2	0	1	4	1	3	2	1	1	2	1
<i>Carya</i>	0	0	0	0	0	0	0	0	0	0	0	0	0	0	0	1	0	0	0
<i>Corylus</i>	0	0	0	0	0	0	0	0	0	0	0	0	1	0	0	0	0	0	2
<i>Fagus</i>	0	0	0	0	0	0	0	0	0	0	0	0	0	0	0	1	0	0	0
<i>Fraxinus</i>	0	0	0	0	0	0	0	0	0	0	0	0	0	0	0	0	0	0	1
<i>Quercus</i>	0	0	0	1	0	0	0	0	0	1	0	0	0	0	0	2	0	0	0
<i>Tilia</i>	0	0	0	0	0	0	0	1	0	0	0	0	0	0	0	0	0	0	0
<i>Alnus</i>	0	0	0	0	2	1	0	1	2	5	0	2	0	0	0	0	1	1	0
Ericaceae	0	0	0	0	1	0	0	0	0	0	0	0	0	0	0	0	0	0	0
<i>Salix</i>	0	0	0	0	0	2	0	0	0	0	0	0	0	0	0	0	0	0	0
Liguliflorae	0	0	0	0	1	0	0	0	0	0	0	0	0	0	0	0	0	0	0
Tubuliflorae	0	0	0	0	0	0	0	0	0	0	0	0	0	0	0	0	0	0	0
Chenopodiaceae	0	0	0	0	0	0	0	1	0	0	0	0	0	0	0	0	0	0	0
Poacea	0	0	0	1	0	0	0	0	1	0	0	0	1	0	0	0	0	0	0
Autre pollen	0	0	3	0	0	0	0	0	0	0	1	0	0	0	0	0	0	0	0
<b>Somme des pollens</b>	5	9	10	9	12	7	11	12	13	8	17	12	16	11	16	11	14	12	7
<i>Lycopodium</i>	2	2	0	2	3	0	5	3	1	2	5	4	3	2	1	0	3	4	8
<i>Sphagnum</i>	0	1	2	2	6	0	2	2	3	2	2	2	0	2	1	0	2	7	0
Spores monolètes	3	1	2	2	5	0	3	5	2	7	0	3	2	6	2	1	3	3	5
Spores trilètes	2	5	8	2	4	5	5	8	12	16	8	12	5	6	8	4	6	2	3
<b>Somme des spores</b>	7	9	12	8	18	5	15	18	18	27	15	21	10	16	12	5	14	16	16
Grains de pollen d'angiospermes remaniés	0	0	0	1	2	0	0	1	1	0	0	4	1	0	2	1	1	0	0
Grains de pollen de gymnospermes remaniés	7	5	6	4	4	5	9	10	7	6	7	8	16	6	8	9	10	6	6
Spores remaniées	13	13	27	26	26	12	30	47	36	33	19	10	7	23	25	10	19	19	13
Acritarches	7	14	7	10	17	8	13	15	15	23	16	10	2	13	7	12	17	9	5
Dinokystes remaniés	6	6	7	7	6	3	14	8	11	8	14	5	10	4	9	6	8	9	3
<b>Somme des palynomorphes remaniés</b>	33	38	47	48	55	28	66	81	70	70	56	37	36	46	51	38	55	43	27
Réseaux organiques de foraminifère	18	9	24	28	36	27	6	15	76	29	26	23	21	30	22	8	30	21	5
<i>Pediastrum</i>	0	0	0	0	0	0	0	0	0	0	0	0	0	0	0	0	0	0	0
<i>Halodinium</i>	3	0	0	1	4	1	4	6	16	3	3	6	5	2	0	1	5	1	0

**Tableau A.3** Dénombrement des palynomorphes de la carotte PS2863-1

Profondeur (cm)	1.5	5	9	13	17	21	25	29	33	37	41	45	49	53	57	60.5	65	69	73
<i>Abies</i>	0	0	0	0	0	0	0	0	0	0	0	0	0	0	0	0	0	0	1
<i>Picea</i>	0	4	9	6	3	3	5	7	11	4	15	3	17	12	5	2	3	2	4
<i>Pinus</i>	0	0	2	2	4	4	5	2	3	0	0	9	6	10	1	4	2	2	4
<i>Tsuga</i>	0	1	0	0	0	1	0	0	0	0	2	1	0	2	0	1	0	0	1
<i>Acer</i>	0	0	0	0	0	1	0	0	0	0	0	0	0	0	0	0	0	0	0
<i>Betula</i>	1	1	0	0	2	2	2	0	4	1	3	2	0	1	0	2	0	2	4
<i>Carya</i>	0	0	0	0	0	0	0	0	0	0	0	0	0	0	0	0	0	0	0
<i>Corylus</i>	0	1	0	0	0	0	1	0	1	0	0	0	0	0	1	0	0	0	2
<i>Fagus</i>	0	0	0	0	0	0	0	0	0	0	0	0	0	0	0	0	0	0	0
<i>Fraxinus</i>	0	0	0	0	0	0	0	0	2	0	1	0	0	1	0	0	0	0	0
<i>Quercus</i>	0	0	0	0	0	0	1	0	0	0	0	0	0	0	0	0	0	0	1
<i>Tilia</i>	0	0	0	0	0	0	0	0	0	0	0	0	0	0	0	0	0	0	0
<i>Alnus</i>	0	1	0	0	1	1	0	0	4	3	1	0	0	1	0	1	0	0	1
<i>Myrica</i>	0	0	0	0	0	0	0	0	0	0	0	0	0	0	0	0	0	0	0
<i>Ilex</i>	0	0	0	0	0	0	0	0	0	0	0	0	0	0	0	0	0	0	0
<i>Salix</i>	0	0	0	0	0	0	0	0	0	0	0	0	0	0	0	0	2	0	2
Type <i>Ambrosia</i>	0	0	0	0	0	0	0	0	0	0	0	0	0	0	0	0	0	0	0
<i>Artemisia</i>	0	0	0	0	0	0	0	0	0	0	0	0	0	0	0	0	0	1	0
<i>Liguliflorae</i>	0	0	0	0	0	0	0	0	0	0	1	0	0	0	0	0	0	0	0
<i>Tubuliflorae</i>	0	0	0	0	0	0	0	0	0	0	0	0	0	0	0	0	1	0	1
Brassicaceae	0	0	0	0	0	0	0	0	0	0	0	0	1	0	0	0	0	0	0
Chenopodiaceae	0	0	0	0	0	0	0	0	0	0	0	0	0	0	0	0	0	0	0
Poacea	0	0	0	0	2	0	0	0	0	0	1	0	0	0	0	0	0	0	2
Autre pollen	0	0	0	0	0	0	0	5	0	6	0	0	4	0	0	1	0	2	
<b>Somme des pollens</b>	1	8	11	8	12	13	14	9	30	8	30	16	23	31	7	10	9	7	25
<i>Lycopodium</i>	0	0	1	1	0	3	0	5	8	2	11	13	3	12	6	5	6	4	1
<i>Sphagnum</i>	1	2	2	0	0	2	4	2	5	2	5	5	2	9	2	7	0	1	6
Spores monolètes	1	1	0	0	2	5	5	5	9	1	5	13	5	20	8	9	6	7	12
Spores trilètes	0	1	3	1	5	2	4	0	8	6	11	2	1	2	0	3	1	1	13
<b>Somme des spores</b>	2	4	6	2	7	12	13	12	30	11	32	33	11	43	16	24	13	13	32
Grains de pollen d'angiospermes	0	0	0	0	0	0	1	0	0	2	2	12	1	9	4	9	4	2	3
Grains de pollen de gymnospermes	4	0	1	1	5	3	10	8	1	4	16	53	19	15	16	11	10	9	11
Spores remaniées	4	1	6	4	13	13	9	8	12	12	32	105	20	48	15	32	37	34	34
Acratarches	5	2	0	3	10	5	9	9	9	9	12	17	8	20	9	19	13	4	16
Dinokystes remaniés	1	2	1	1	10	5	4	7	10	2	24	45	28	28	18	10	18	16	21
<b>Somme des palynomorphes remaniés</b>	14	5	8	9	38	26	33	32	32	29	86	232	76	120	62	81	82	65	85
Réseaux organiques de foraminifères	9	24	13	15	11	77	48	29	50	43	116	146	17	88	24	66	25	69	121
<i>Pediastrium</i>	0	0	0	0	0	0	0	0	0	0	2	4	0	1	1	1	1	0	
<i>Haladinium</i>	0	0	1	2	0	6	3	0	3	1	3	20	10	36	19	11	32	24	22

Profondeur (cm)	77	81.5	85	89	93	97	101	104	109	112	116	120	124	128	132	136	140	144	148
<i>Abies</i>	2	2	3	1	1	0	2	15	9	7	10	15	13	12	25	28	17	29	49
<i>Picea</i>	4	3	2	0	6	3	8	27	37	23	52	27	12	10	16	17	31	55	47
<i>Pinus</i>	1	1	0	0	2	3	4	21	27	25	45	11	6	5	13	9	10	75	117
<i>Tsuga</i>	0	0	0	0	2	2	0	2	6	1	0	2	0	1	4	4	7	11	11
<i>Acer</i>	0	0	0	0	0	1	0	0	0	0	1	0	0	0	0	0	0	0	0
<i>Betula</i>	4	3	0	0	1	2	3	9	7	9	23	4	1	1	0	2	3	1	0
<i>Carya</i>	0	0	0	0	0	0	0	2	2	0	2	1	1	0	0	0	0	0	0
<i>Corylus</i>	0	0	0	0	0	0	0	2	0	1	0	0	1	0	0	0	0	0	0
<i>Fagus</i>	0	0	0	0	0	0	0	0	0	0	0	0	0	0	0	0	0	0	2
<i>Fraxinus</i>	0	0	0	0	0	0	0	0	1	0	0	0	0	0	4	2	4	3	5
<i>Quercus</i>	0	0	1	1	0	1	0	0	0	0	0	0	1	1	0	0	0	0	0
<i>Tilia</i>	0	0	0	0	0	0	0	0	0	0	1	0	0	0	0	0	0	0	0
<i>Alnus</i>	2	0	0	0	0	1	1	3	3	5	3	0	0	0	0	1	0	0	0
<i>Myrica</i>	0	0	0	0	0	0	0	0	0	0	0	0	0	0	0	0	0	0	0
<i>Ilex</i>	0	0	0	0	0	0	0	1	0	0	3	0	0	0	0	2	0	3	5
<i>Salix</i>	0	1	0	0	2	0	1	0	0	2	2	2	0	0	0	0	1	1	0
Type <i>Ambrasia</i>	0	0	0	0	0	0	0	0	0	0	0	1	0	0	0	0	0	0	0
<i>Artemisia</i>	0	0	0	0	0	0	0	0	0	0	0	0	0	0	0	0	0	0	0
Liguliflorae	0	0	0	0	0	0	0	0	1	0	0	1	1	0	0	1	4	0	0
Tubuliflorae	0	0	0	0	0	0	0	0	0	0	2	0	0	0	0	0	3	1	0
Brassicaceae	0	0	0	0	0	0	0	0	2	8	9	4	5	12	10	5	15	1	1
Chenopodiaceae	0	0	0	0	0	0	0	0	3	1	8	9	5	2	6	10	10	3	0
Poaceae	2	0	1	0	0	0	0	0	0	0	0	2	2	0	0	1	1	0	0
Autre pollen	0	2	2	0	0	1	2	9	1	0	12	8	1	1	0	0	0	1	0
<b>Somme des pollens</b>	<b>15</b>	<b>12</b>	<b>9</b>	<b>2</b>	<b>14</b>	<b>15</b>	<b>20</b>	<b>92</b>	<b>99</b>	<b>81</b>	<b>173</b>	<b>87</b>	<b>50</b>	<b>48</b>	<b>78</b>	<b>82</b>	<b>105</b>	<b>194</b>	<b>224</b>
<i>Lycopodium</i>	0	1	0	0	0	1	0	3	0	4	5	4	0	0	0	0	2	3	2
<i>Sphagnum</i>	8	3	1	0	4	3	2	9	21	14	27	12	8	3	16	11	10	6	0
Spores monolètes	10	6	6	0	5	1	1	10	22	9	16	15	9	5	18	5	6	11	3
Spores trilètes	14	7	1	0	3	8	7	35	25	28	18	7	18	16	6	4	1	11	8
<b>Somme des spores</b>	<b>32</b>	<b>17</b>	<b>8</b>	<b>0</b>	<b>12</b>	<b>13</b>	<b>10</b>	<b>57</b>	<b>68</b>	<b>51</b>	<b>66</b>	<b>39</b>	<b>35</b>	<b>24</b>	<b>40</b>	<b>20</b>	<b>19</b>	<b>31</b>	<b>13</b>
Grains de pollen d'angiospermes	3	3	5	0	4	4	10	19	17	19	42	39	27	18	32	37	104	59	11
Grains de pollen de gymnospermes	17	7	4	3	13	13	27	73	71	24	52	48	106	191	123	33	52	76	109
Spores remaniées	48	27	15	11	34	29	80	140	90	49	133	145	548	693	556	63	63	82	22
Acritharches	17	8	5	0	5	5	11	15	6	3	7	11	66	95	61	4	1	1	0
Dinokystes remaniés	31	24	5	1	14	14	31	48	51	15	21	49	184	294	196	8	10	33	24
<b>Somme des palynomorphes remaniés</b>	<b>116</b>	<b>69</b>	<b>34</b>	<b>15</b>	<b>70</b>	<b>65</b>	<b>159</b>	<b>295</b>	<b>235</b>	<b>109</b>	<b>255</b>	<b>292</b>	<b>931</b>	<b>1291</b>	<b>968</b>	<b>145</b>	<b>230</b>	<b>251</b>	<b>166</b>
Réseaux organiques de foraminifère	42	9	4	0	0	6	37	26	0	5	8	5	10	14	15	0	3	18	8
<i>Pediasium</i>	3	1	1	0	0	1	1	10	9	12	22	19	12	5	10	20	17	15	21
<i>Haladinium</i>	16	3	0	0	3	1	0	3	10	3	14	8	15	18	11	5	0	9	8

<b>Profondeur (cm)</b>	<b>152</b>	<b>156</b>	<b>160</b>	<b>164</b>	<b>169</b>	<b>174</b>	<b>178</b>	<b>183</b>
<i>Abies</i>	8	14	19	2	3	4	7	3
<i>Picea</i>	25	66	65	23	16	0	5	2
<i>Pinus</i>	55	250	79	78	94	34	38	17
<i>Tsuga</i>	4	10	9	8	4	0	1	0
<i>Acer</i>	0	1	0	0	0	3	0	0
<i>Betula</i>	0	14	14	9	1	3	2	1
<i>Carya</i>	0	0	0	0	0	0	0	0
<i>Corylus</i>	0	1	1	0	0	2	0	0
<i>Fagus</i>	0	0	0	0	0	0	0	0
<i>Fraxinus</i>	3	11	9	2	1	0	0	3
<i>Quercus</i>	0	0	1	1	0	3	0	1
<i>Tilia</i>	0	0	0	0	0	0	0	0
<i>Alnus</i>	0	9	6	1	2	1	0	1
<i>Myrica</i>	0	0	1	0	1	1	0	0
<i>Ilex</i>	3	7	5	0	0	0	0	1
<i>Salix</i>	0	0	1	3	0	0	0	0
Type <i>Ambrasia</i>	0	1	4	0	0	0	0	0
<i>Artemisia</i>	0	6	3	0	0	0	0	0
<i>Liguliflorae</i>	4	4	3	5	0	0	0	0
<i>Tubuliflorae</i>	0	0	0	4	0	0	0	1
<i>Brassicaceae</i>	0	16	12	4	2	0	0	0
<i>Chenopodiaceae</i>	2	16	15	5	0	0	0	1
<i>Poacea</i>	2	0	1	0	0	0	0	1
Autre pollen	1	19	6	3	1	0	1	3
<b>Somme des pollens</b>	<b>107</b>	<b>444</b>	<b>254</b>	<b>148</b>	<b>125</b>	<b>51</b>	<b>54</b>	<b>35</b>
<i>Lycopodium</i>	0	2	9	3	0	1	0	1
<i>Sphagnum</i>	12	44	30	14	9	10	3	3
Spores monolètes	15	14	10	13	7	1	5	2
Spores trilètes	11	17	14	16	13	10	8	7
<b>Somme des spores</b>	<b>38</b>	<b>77</b>	<b>63</b>	<b>46</b>	<b>29</b>	<b>22</b>	<b>16</b>	<b>13</b>
Grains de pollen d'angiospermes	38	63	52	19	13	4	11	5
Grains de pollen de gymnospermes	81	125	65	92	186	92	69	33
Spores remaniées	62	148	98	315	331	159	282	68
Acritarches	1	6	3	57	26	3	5	10
Dinokystes remaniés	11	24	22	37	142	23	44	35
<b>Somme des palynomorphes remaniés</b>	<b>193</b>	<b>366</b>	<b>240</b>	<b>520</b>	<b>698</b>	<b>281</b>	<b>411</b>	<b>151</b>
Réseaux organiques de foraminifère	6	93	50	82	5	0	2	2
<i>Pediastrum</i>	7	26	11	9	0	0	3	1
<i>Halodinium</i>	0	14	3	1	0	0	1	0

**Tableau A.4** Dénombrement des dinokystes de la carotte MSM5/5-712-2

Profondeur (cm)	10	14	18	22	26	30	34	38	42	46	50	54	58	62	66	70	74	78	82	86	90	94	98	102	106
<i>Achomosphaera</i> sp.	0	0	0	0	0	0	0	0	0	0	0	0	0	0	0	0	0	0	0	0	0	0	0	0	0
<i>Ataxodinium choane</i>	0	0	0	0	0	0	0	1	0	0	0	0	0	0	0	0	0	0	0	0	0	0	0	0	0
<i>Bitectatodinium tepikiense</i>	1	1	0	0	2	0	0	0	0	1	1	0	0	0	3	0	0	1	1	0	0	1	0	0	0
<i>Bitectatodinium spongiculum</i>	0	0	0	0	0	0	0	0	0	0	0	0	0	0	0	0	0	0	0	0	0	0	0	0	0
<i>Impagidinium aculeatum</i>	0	0	0	0	0	0	0	0	0	0	0	0	0	0	0	0	0	0	0	0	0	0	0	0	0
<i>Impagidinium pallidum</i>	3	4	0	0	1	2	1	4	7	1	2	3	7	2	8	4	5	1	0	0	0	5	3	2	2
<i>Impagidinium paradoxum</i>	0	0	0	0	0	0	0	0	0	0	0	0	0	0	0	0	0	0	0	0	0	0	0	0	0
<i>Impagidinium patulum</i>	0	0	0	0	0	0	0	0	0	0	0	0	0	0	0	0	0	0	0	0	0	0	0	0	0
<i>Impagidinium spharicum</i>	0	0	1	0	0	2	0	1	0	3	0	0	4	0	1	0	0	0	4	0	1	0	1	0	0
<i>Impagidinium</i> spp.	0	0	0	0	0	0	0	0	0	0	0	0	0	0	0	0	0	0	0	0	0	0	0	0	0
<i>Lingulodinium</i>	0	0	0	0	0	0	0	0	0	0	0	0	0	0	0	0	0	0	0	0	0	0	0	0	0
<i>Nematospaeropsis</i>	6	27	3	45	6	23	13	29	13	7	21	21	23	29	34	40	13	17	10	30	15	39	30	17	15
<i>Operculodinium</i>	252	613	177	472	208	295	333	404	370	456	340	368	308	352	368	461	368	306	299	325	256	384	269	362	215
<i>Operculodinium israelianum</i>	0	0	0	0	0	0	0	0	0	0	0	0	0	0	0	0	0	0	0	0	0	0	0	0	0
<i>Polyshaeridium zoharyi</i>	0	0	0	0	0	0	0	0	0	0	0	0	0	0	0	0	0	0	0	0	0	0	0	0	0
<i>Spiniferites membranaceus</i>	0	0	0	0	0	0	0	0	0	0	0	0	0	0	0	0	0	0	0	0	0	0	0	0	0
<i>Spiniferites elongatus</i>	4	9	2	15	6	3	5	5	7	9	8	1	4	5	15	10	15	9	8	5	11	17	7	16	5
<i>Spiniferites ramosus</i>	3	6	1	6	4	1	2	4	4	3	6	1	4	2	7	13	4	12	2	12	3	10	9	7	7
<i>Spiniferites mirabilis</i>	3	1	0	1	0	0	0	0	0	0	0	0	3	3	1	0	0	0	0	0	0	0	0	1	0
<i>Spiniferites</i> spp.	0	0	0	2	2	0	0	1	1	0	1	0	0	2	4	0	1	1	2	0	0	0	1	0	0
Cyst of <i>Pentapharsodinium</i>	0	2	0	3	0	4	0	0	4	0	4	2	6	5	9	1	5	1	7	1	1	0	4	3	10
<i>Islandinium minutum</i>	27	19	14	38	30	31	7	18	32	20	32	8	32	32	37	18	23	15	18	28	69	24	32	8	51
<i>Islandinium cezare</i>	0	0	0	1	0	0	0	0	1	0	0	0	0	0	0	0	0	0	0	0	0	0	0	0	0
<i>Echinidinium karaense</i>	0	0	0	0	0	0	0	0	0	0	0	0	0	0	0	0	0	0	0	0	0	0	0	0	0
<i>Brigantedinium</i> spp.	14	10	7	77	5	7	3	5	8	12	9	10	7	34	10	14	14	11	16	21	7	13	10	4	12
<i>Selenopemphix nephroides</i>	0	0	0	0	0	1	0	0	0	0	0	0	0	0	0	1	0	0	0	0	0	0	0	0	0
<i>Selenopemphix quanta</i>	2	0	0	0	0	0	0	0	0	1	0	0	0	0	0	0	0	0	0	0	0	0	0	0	1
<i>Trinovantedinium applanatum</i>	0	1	0	0	0	3	0	1	0	0	1	0	0	0	0	1	2	1	0	0	0	0	0	0	0
<i>Qinquecuspis concreta</i>	0	0	0	0	0	0	0	0	0	0	0	0	0	0	0	0	0	0	0	0	0	0	0	0	0
<i>Polykrikos schwartzii</i>	0	0	0	0	1	0	0	0	0	0	0	0	0	0	0	0	0	0	0	0	0	0	0	0	0
<i>Protoperdinium</i>	0	0	0	0	0	0	0	0	0	0	0	0	0	0	0	0	0	0	0	0	0	0	0	0	0
<b>Somme des dinokystes</b>	<b>315</b>	<b>693</b>	<b>205</b>	<b>660</b>	<b>265</b>	<b>372</b>	<b>364</b>	<b>473</b>	<b>447</b>	<b>S13</b>	<b>425</b>	<b>414</b>	<b>395</b>	<b>466</b>	<b>499</b>	<b>564</b>	<b>450</b>	<b>375</b>	<b>367</b>	<b>422</b>	<b>363</b>	<b>493</b>	<b>366</b>	<b>420</b>	<b>318</b>

Profondeur (cm)	110	114	118	122	126	130	134	138	142	146	150	154	158	162	165	170	174	178	182	186	190	194
<i>Achomosphaera</i> sp.	0	0	0	0	0	0	0	0	0	0	0	0	0	0	0	0	0	0	0	0	0	0
<i>Ataxodonium choane</i>	1	0	0	1	0	0	0	0	0	0	0	1	0	0	0	1	0	3	0	0	0	0
<i>Bitectatodinium tepikiense</i>	0	1	3	2	0	0	0	1	0	1	1	0	0	0	0	2	0	0	0	1	1	0
<i>Bitectatodinium spongicium</i>	0	0	0	0	0	0	0	0	0	0	0	0	0	0	0	0	0	0	0	0	0	0
<i>Impagidinium aculeatum</i>	0	0	0	0	0	0	0	1	0	0	0	0	0	0	0	0	0	0	0	0	0	0
<i>Impagidinium pallidum</i>	4	1	2	0	7	4	5	1	4	7	4	0	8	2	3	2	7	8	11	1	3	4
<i>Impagidinium paradoxum</i>	0	0	0	0	0	0	0	0	0	0	0	0	0	0	0	0	0	0	0	0	0	0
<i>Impagidinium patulum</i>	0	0	0	0	0	0	0	0	1	0	0	0	0	0	0	0	0	0	0	0	0	0
<i>Impagidinium sphaericum</i>	1	1	2	0	0	2	1	0	0	3	0	1	1	1	1	2	3	2	0	0	1	1
<i>Impagidinium</i> spp.	0	0	0	0	0	0	0	0	0	0	0	0	0	0	0	0	0	0	0	0	0	0
<i>Lingulodinium</i>	0	0	0	0	0	0	0	0	0	0	0	0	0	0	0	0	0	0	1	0	1	0
<i>Nematosphaeropsis</i>	22	22	43	55	59	41	80	55	72	75	117	70	100	122	169	111	121	84	95	60	134	35
<i>Operculodinium</i>	277	266	340	386	271	284	293	245	273	275	185	111	157	135	136	113	120	106	122	68	116	26
<i>Operculodinium israelianum</i>	0	0	0	0	0	0	0	0	0	0	0	0	0	0	0	0	0	0	0	0	0	0
<i>Polyshaeridium zoharyi</i>	0	0	0	0	0	0	0	0	0	0	0	0	0	0	0	0	0	0	0	0	0	0
<i>Spiniferites membranaceus</i>	0	0	0	0	0	0	0	0	0	0	0	0	0	0	0	0	0	0	0	0	0	0
<i>Spiniferites elongatus</i>	13	16	11	18	5	15	13	8	3	9	16	11	7	9	16	19	14	26	29	6	18	6
<i>Spiniferites ramosus</i>	3	3	17	6	2	2	14	5	8	8	11	5	11	5	8	4	5	14	13	0	18	2
<i>Spiniferites mirabilis</i>	1	0	1	2	1	1	1	1	2	1	2	0	0	0	1	0	1	1	3	0	4	0
<i>Spiniferites</i> spp.	4	0	0	2	1	3	1	0	0	2	3	2	1	5	2	4	3	5	3	5	3	2
Cyst of <i>Pentapharsodinium</i>	3	6	3	0	3	1	6	1	0	3	1	6	1	2	1	4	11	3	4	3	12	3
<i>Islandinium minutum</i>	32	42	42	72	34	29	15	30	11	18	11	26	26	16	8	55	70	93	84	49	63	39
<i>Islandinium cezare</i>	0	0	0	0	0	0	0	0	0	0	0	0	0	0	0	3	0	0	0	0	0	0
<i>Echinidinium karaense</i>	0	0	0	0	0	0	0	0	0	0	0	0	1	0	0	0	0	0	0	0	0	0
<i>Brigantedinium</i> spp.	13	4	11	13	16	4	11	2	11	7	32	3	41	11	3	17	9	24	16	11	21	5
<i>Selenopempix nephroides</i>	0	0	0	0	0	0	0	0	0	0	0	0	0	0	0	0	0	0	0	0	0	0
<i>Selenopempix quanta</i>	0	0	0	0	0	1	0	0	0	0	0	0	0	0	0	0	0	0	0	0	1	0
<i>Trinovantedinium applanatum</i>	0	0	0	0	0	0	1	1	0	0	1	0	0	0	0	0	1	0	0	0	0	0
<i>Qinquecuspis concreta</i>	0	0	0	0	0	0	0	0	0	0	0	0	0	0	0	0	0	0	0	0	0	0
<i>Polykrikos schwartzii</i>	0	0	0	0	0	0	1	0	0	0	0	0	0	0	0	0	0	0	0	0	0	0
<i>Protoperidinium</i>	0	0	0	0	0	1	0	0	0	0	0	0	0	0	0	0	0	0	0	0	0	0
<b>Somme des dinokystes</b>	<b>374</b>	<b>362</b>	<b>475</b>	<b>557</b>	<b>399</b>	<b>388</b>	<b>442</b>	<b>351</b>	<b>385</b>	<b>409</b>	<b>384</b>	<b>236</b>	<b>355</b>	<b>308</b>	<b>348</b>	<b>334</b>	<b>368</b>	<b>369</b>	<b>381</b>	<b>204</b>	<b>396</b>	<b>123</b>

Profondeur (cm)	198	202	206	210	214	218	222	226	230	234	238	242	246	250	254	258	262	266	270	274
<i>Achomosphaera</i> sp.	0	0	0	0	0	0	0	0	0	0	0	0	0	0	0	0	0	0	0	0
<i>Ataxodinium choane</i>	0	2	0	0	1	0	2	0	0	0	0	1	1	0	0	1	1	0	0	2
<i>Bitectatadinium tepikense</i>	0	1	2	1	2	0	2	0	3	3	1	1	1	0	6	1	2	0	2	2
<i>Bitectotadinium spongiculum</i>	0	0	0	0	0	0	0	0	0	0	0	0	0	0	0	0	0	0	0	0
<i>Impagidinium aculeatum</i>	0	0	0	0	0	0	0	0	0	0	0	0	0	0	0	0	0	0	0	0
<i>Impagidinium pallidum</i>	5	5	10	5	1	0	0	0	2	0	1	0	0	0	0	3	3	0	2	0
<i>Impagidinium paradoxum</i>	0	0	0	0	0	0	0	0	0	0	0	0	0	0	0	1	0	0	0	0
<i>Impagidinium patulum</i>	0	0	1	0	0	0	0	1	0	1	0	0	2	0	0	0	0	0	0	0
<i>Impagidinium sphaericum</i>	1	0	6	2	5	0	1	0	6	0	3	1	11	0	3	1	8	2	2	3
<i>Impagidinium</i> spp.	1	0	0	0	0	0	0	0	0	0	0	0	1	0	1	0	1	0	0	0
<i>Lingulodinium</i>	0	0	0	0	0	0	0	0	1	0	0	0	0	0	1	0	0	0	0	0
<i>Nematosphaeropsis</i>	140	84	168	54	106	27	86	4	109	85	41	25	84	20	99	53	78	23	80	112
<i>Operculodinium</i>	89	57	85	22	76	16	63	9	78	55	38	21	68	26	49	33	50	21	47	78
<i>Operculodinium israelianum</i>	0	0	0	0	0	0	0	0	0	0	0	0	0	0	0	0	0	0	0	0
<i>Polyshaeridium zoharyi</i>	0	0	0	0	0	0	0	0	0	0	0	0	0	0	0	0	0	0	0	0
<i>Spiniferites membranaceus</i>	0	0	0	0	0	0	0	0	0	0	0	0	0	0	0	0	0	0	0	0
<i>Spiniferites elongatus</i>	41	33	14	7	7	1	21	2	11	15	9	4	9	5	26	9	14	8	8	21
<i>Spiniferites ramosus</i>	20	6	21	5	15	2	29	0	23	10	16	1	10	1	17	16	12	10	11	12
<i>Spiniferites mirabilis</i>	6	0	7	0	2	1	4	0	3	0	2	0	0	0	2	0	0	0	2	0
<i>Spiniferites</i> spp.	0	2	4	2	2	5	5	0	2	4	2	2	5	3	2	2	1	0	2	3
Cyst of <i>Pentapharsodinium</i>	4	8	5	5	9	2	5	0	7	9	8	11	3	4	9	9	9	3	12	15
<i>Islandinium minutum</i>	59	52	65	23	74	37	78	23	83	77	118	26	131	42	141	63	125	59	120	92
<i>Islandinium cezare</i>	0	3	0	0	0	2	0	0	0	0	1	0	5	0	4	0	14	0	12	4
<i>Echinidinium karaense</i>	0	0	0	0	0	0	0	0	0	0	0	0	0	0	0	0	0	0	0	0
<i>Brigantedinium</i> spp.	11	14	16	6	14	7	14	15	24	24	7	4	26	7	21	9	17	11	31	20
<i>Selenopempix nephroides</i>	1	0	0	0	0	0	0	0	1	2	1	0	3	0	0	0	0	0	0	1
<i>Selenopempix quanta</i>	1	0	0	0	0	0	0	0	0	0	0	0	0	0	0	0	0	0	1	0
<i>Trinovantedinium appланatum</i>	4	0	1	0	2	0	0	0	0	1	0	1	0	0	0	0	0	0	0	1
<i>Qinquecuspis concreta</i>	0	0	1	0	0	0	0	0	0	0	0	0	0	0	0	0	0	0	0	0
<i>Polykrikos schwartzii</i>	0	0	0	0	0	0	0	0	0	0	0	0	0	0	0	0	0	0	0	0
<i>Protoperidinium</i>	0	0	0	0	0	0	0	0	0	0	0	0	0	0	0	0	0	0	0	0
<b>Somme des dinokystes</b>	<b>383</b>	<b>267</b>	<b>406</b>	<b>132</b>	<b>316</b>	<b>100</b>	<b>310</b>	<b>54</b>	<b>353</b>	<b>286</b>	<b>248</b>	<b>101</b>	<b>358</b>	<b>107</b>	<b>384</b>	<b>200</b>	<b>331</b>	<b>142</b>	<b>331</b>	<b>369</b>

Profondeur (cm)	278	282	290	298	306	314	322	330	338	346	354	362	370	378	386	394	402	410	418	426	434	442	450
<i>Achomosphaera</i> sp.	0	0	0	0	0	0	0	0	0	0	0	0	0	0	0	0	0	0	0	0	0	0	0
<i>Ataxodinium choane</i>	2	0	0	0	0	0	0	0	0	0	0	0	0	0	0	0	0	0	0	0	0	0	0
<i>Bitectatodinium tepikiense</i>	3	0	0	0	0	0	2	0	2	0	3	1	4	3	5	8	2	3	3	1	5	3	2
<i>Bitectatodinium spongicum</i>	0	0	0	0	0	0	0	0	0	0	0	0	0	0	0	0	0	0	0	0	0	0	0
<i>Impagidinium aculeatum</i>	0	0	0	0	0	0	0	0	0	0	0	0	0	0	0	0	0	0	0	0	0	0	1
<i>Impagidinium pollidum</i>	3	2	0	0	0	0	0	8	7	0	6	2	1	0	1	1	0	0	1	2	0	0	0
<i>Impagidinium paradoxum</i>	0	0	0	0	0	0	0	0	0	0	0	0	0	0	0	0	0	0	0	0	0	0	0
<i>Impagidinium patulum</i>	0	0	0	0	0	0	0	0	0	0	0	0	0	0	0	0	0	0	0	0	0	0	0
<i>Impagidinium sphaericum</i>	6	4	1	2	3	0	0	0	0	2	0	1	0	0	0	0	1	0	0	0	1	0	1
<i>Impagidinium</i> spp.	1	0	0	0	1	0	0	0	0	0	0	0	0	0	0	0	0	0	0	0	0	0	0
<i>Lingulodinium</i>	0	0	0	0	1	0	0	0	0	0	0	0	0	0	0	0	0	0	0	0	0	0	0
<i>Nematosphaeropsis</i>	97	83	34	37	184	93	73	61	29	32	46	61	37	4	5	9	15	22	30	17	23	13	21
<i>Operculodinium</i>	48	35	25	8	36	27	40	61	26	33	20	22	103	61	68	134	16	16	52	25	49	40	47
<i>Operculodinium israelianum</i>	0	0	0	0	0	0	0	0	0	0	0	0	0	0	0	0	0	0	0	0	0	0	0
<i>Polyshaeridium zoharyi</i>	0	0	0	0	0	0	0	0	0	0	0	0	0	0	0	0	0	0	0	0	0	0	0
<i>Spiniferites membranaceus</i>	0	0	0	0	0	0	0	0	0	0	0	0	0	0	0	0	0	0	0	0	0	0	0
<i>Spiniferites elongatus</i>	26	16	2	9	8	2	9	12	4	7	5	9	49	83	51	73	26	51	51	47	48	34	51
<i>Spiniferites ramosus</i>	8	6	1	3	1	2	2	5	1	2	6	8	22	5	7	47	58	69	74	57	38	48	23
<i>Spiniferites mirabilis</i>	1	0	0	0	1	2	0	0	0	0	0	0	0	0	0	0	0	0	0	0	0	0	0
<i>Spiniferites</i> spp.	1	0	1	2	0	2	2	1	0	1	1	0	3	3	3	1	2	5	3	2	1	1	0
Cyst of <i>Pentapharsodinium</i>	9	12	0	5	0	1	10	14	4	23	30	31	39	19	51	27	29	34	36	40	26	46	42
<i>Islandinium minutum</i>	98	53	10	23	107	110	146	131	58	161	89	17	18	10	8	3	28	26	35	20	19	10	21
<i>Islandinium cezare</i>	3	0	0	0	0	0	0	5	2	0	7	10	5	2	0	3	0	0	0	0	0	0	0
<i>Echinidinium karaense</i>	0	0	0	0	0	0	0	0	0	0	0	0	0	0	0	0	0	0	0	0	0	0	0
<i>Brigantedinium</i> spp.	19	18	5	13	15	23	15	36	34	47	110	157	38	134	104	36	141	97	60	105	114	126	94
<i>Selenopempix nephroides</i>	0	0	0	1	1	1	0	0	0	0	0	0	0	0	0	0	0	0	0	0	0	0	0
<i>Selenopempix quanta</i>	0	0	0	0	0	0	0	2	1	0	1	1	6	2	4	2	2	3	1	4	3	5	5
<i>Trinovantedinium appanatum</i>	1	0	0	1	0	0	0	0	0	0	0	0	1	1	0	0	0	0	0	0	0	0	0
<i>Qinquecuspis concreta</i>	0	0	0	0	0	0	0	0	0	0	0	0	0	0	0	0	0	0	0	0	0	0	0
<i>Polykrikos schwartzii</i>	0	0	0	0	0	1	0	0	0	0	0	0	0	0	0	0	0	0	0	0	0	0	0
<i>Protoperidinium</i>	0	0	0	0	0	0	0	0	0	0	0	0	0	0	0	0	0	0	0	0	0	0	0
<b>Somme des dinokystes</b>	<b>326</b>	<b>229</b>	<b>79</b>	<b>104</b>	<b>358</b>	<b>266</b>	<b>312</b>	<b>333</b>	<b>158</b>	<b>323</b>	<b>322</b>	<b>322</b>	<b>317</b>	<b>329</b>	<b>311</b>	<b>335</b>	<b>321</b>	<b>325</b>	<b>348</b>	<b>322</b>	<b>326</b>	<b>327</b>	<b>310</b>

Profondeur (cm)	458	466	474	482	490	500	507	514	521	528	536	542	549	556	563	570	577	585	593	601	608	616	624	632	640
<i>Achromosphaera</i> sp.	0	0	0	0	0	0	0	0	0	0	0	0	0	0	0	0	0	0	0	0	0	0	0	0	0
<i>Ataxodinium choane</i>	0	0	0	0	0	0	0	0	0	0	0	0	0	0	0	0	0	0	0	0	0	0	0	0	0
<i>Bitectatodinium tepikense</i>	2	3	4	6	2	1	1	3	2	3	0	0	1	1	0	4	0	1	1	2	26	25	34	6	4
<i>Bitectatodinium spongicium</i>	0	0	0	0	0	0	0	0	0	0	0	0	0	0	0	0	0	0	0	0	0	0	0	0	0
<i>Impagidinium aculeatum</i>	0	0	0	0	0	0	0	0	0	0	0	0	0	0	0	0	0	0	0	0	0	0	0	0	0
<i>Impagidinium pallidum</i>	0	0	0	0	0	0	0	0	0	0	0	1	0	0	1	0	0	0	0	0	1	0	0	0	0
<i>Impagidinium paradoxum</i>	0	0	0	0	0	0	0	0	0	0	0	0	0	0	0	0	1	0	0	0	0	0	0	0	0
<i>Impagidinium patulum</i>	0	0	0	0	0	0	0	0	0	0	0	0	0	0	2	0	0	0	0	0	0	0	0	0	0
<i>Impagidinium sphaericum</i>	0	0	0	0	0	0	0	0	0	0	0	0	0	0	0	0	0	0	0	0	1	0	0	0	0
<i>Impagidinium</i> spp.	0	0	0	0	0	0	0	0	0	0	0	0	0	0	0	0	0	0	0	0	0	0	0	0	0
<i>Lingulodinium</i>	0	0	0	0	0	0	0	0	0	0	0	0	0	0	0	0	0	0	0	0	0	0	0	0	0
<i>Nematosphaeropsis</i>	4	1	3	0	1	1	1	1	4	2	6	1	2	1	1	1	1	1	1	0	1	0	0	8	5
<i>Operculodinium</i>	48	32	20	29	11	40	3	8	10	10	4	19	8	8	14	22	9	9	11	13	16	61	33	45	27
<i>Operculodinium israelianum</i>	0	0	0	0	0	0	0	0	0	0	0	0	0	0	0	0	0	0	0	0	0	0	0	0	0
<i>Polyshaeridium zoharyi</i>	0	0	0	0	0	0	0	0	0	0	0	0	0	0	0	0	0	0	0	0	0	0	0	0	0
<i>Spiniferites membranaceus</i>	0	0	0	0	0	0	0	0	0	0	0	0	0	0	0	0	0	0	0	0	0	0	0	0	0
<i>Spiniferites elongatus</i>	23	44	49	69	26	57	18	20	6	4	2	3	2	0	3	1	0	1	1	0	0	1	5	1	7
<i>Spiniferites ramosus</i>	10	2	1	0	1	0	2	1	2	2	1	3	0	3	0	0	0	0	0	0	0	2	12	1	2
<i>Spiniferites mirabilis</i>	0	0	0	0	0	0	0	0	0	0	0	0	0	0	0	0	0	0	0	0	0	0	0	0	0
<i>Spiniferites</i> spp.	0	0	0	0	0	1	2	1	1	0	0	0	0	1	0	0	0	0	0	0	0	0	1	0	0
Cyst of <i>Pentapharsodinium</i>	77	71	57	22	15	21	2	0	0	3	0	0	0	0	1	0	0	0	0	2	1	0	5	16	12
<i>Islandinium minutum</i>	31	7	24	36	23	25	47	41	40	13	15	5	12	0	2	5	2	12	4	6	0	7	0	20	27
<i>Islandinium cezare</i>	0	0	0	0	0	0	0	0	0	0	0	1	0	0	0	0	0	0	0	0	0	0	0	0	0
<i>Echinidinium karaense</i>	0	0	0	0	0	0	0	0	0	0	0	0	0	0	0	0	0	0	0	0	0	0	0	0	0
<i>Brigantedinium</i> spp.	123	146	156	152	223	154	241	238	237	260	281	164	278	276	182	79	95	127	60	71	0	199	0	205	211
<i>Selenopempix nephraides</i>	0	0	0	0	0	0	0	0	0	0	0	0	0	0	0	0	0	0	0	0	0	0	0	0	0
<i>Selenopempix quanta</i>	5	2	3	0	1	3	3	0	1	0	0	0	0	2	0	0	0	0	0	1	0	0	0	0	8
<i>Trinovantedinium applanatum</i>	0	0	0	0	0	0	0	0	0	1	0	0	0	0	0	0	0	0	0	0	0	0	0	1	0
<i>Qinquecuspis concreta</i>	0	0	0	0	0	0	0	0	0	0	0	0	0	0	0	0	0	0	0	0	0	0	0	0	0
<i>Polykrikos schwartzii</i>	0	0	0	0	0	0	0	0	0	0	0	0	0	0	0	0	0	0	0	0	0	0	0	0	0
<i>Protoperidinium</i>	0	0	0	0	0	0	0	0	0	0	0	0	0	0	0	0	0	0	0	0	0	0	0	0	0
Somme des dinokystes	323	308	317	314	303	303	320	313	300	300	305	202	302	293	207	113	107	151	78	95	44	297	90	303	303

Profondeur (cm)	648	656	664	672	680	688	696	704	712	720	728	736	744	752	760	768	776	
<i>Achomosphaera</i> sp.	0	0	0	0	0	0	0	0	3	0	3	1	0	1	2	2	0	
<i>Ataxodinium chaone</i>	0	0	0	0	0	0	0	0	0	0	0	0	0	0	0	0	0	
<i>Bitectatodinium tepikense</i>	2	1	0	1	0	1	2	1	33	15	34	39	41	73	34	36	18	
<i>Bitectatodinium spongiculum</i>	0	0	0	0	0	0	0	0	0	0	0	0	1	0	0	2	0	
<i>Impagidinium aculeatum</i>	0	0	0	0	0	0	0	0	0	0	0	0	1	0	0	0	0	
<i>Impagidinium pallidum</i>	0	0	0	0	0	0	0	0	1	0	0	0	0	0	0	0	0	
<i>Impagidinium paradoxum</i>	0	0	0	0	1	0	0	0	0	0	2	0	1	1	0	0	0	
<i>Impagidinium patulum</i>	0	0	0	1	0	0	0	0	0	0	0	0	0	0	0	0	0	
<i>Impagidinium sphaericum</i>	0	0	0	0	0	0	0	0	2	0	0	1	1	0	0	0	0	
<i>Impagidinium</i> spp.	0	0	0	0	0	0	0	0	0	0	0	0	0	0	0	0	0	
<i>Lingulodinium</i>	0	0	0	0	0	0	0	0	1	0	0	1	2	0	1	6	3	
<i>Nematosphaeropsis</i>	7	1	1	2	6	0	3	3	1	3	5	4	1	1	0	0	2	
<i>Operculodinium</i>	17	13	6	12	17	15	17	12	49	32	47	47	41	30	38	18	25	15
<i>Operculodinium israelianum</i>	0	0	0	0	0	0	0	0	0	0	2	1	0	0	0	0	0	
<i>Polyshaeridium zoharyi</i>	0	0	0	0	0	0	0	0	0	0	0	2	0	1	0	0	0	
<i>Spiniferites membranaceus</i>	0	0	0	0	0	0	0	0	1	0	0	0	0	1	0	0	0	
<i>Spiniferites elongatus</i>	1	2	29	7	47	1	4	0	1	4	2	3	3	0	1	3	1	
<i>Spiniferites ramosus</i>	0	0	0	4	1	2	0	4	9	8	11	14	5	6	3	8	5	
<i>Spiniferites mirabilis</i>	0	0	0	0	0	0	0	0	0	0	1	3	0	3	0	0	2	
<i>Spiniferites</i> spp.	0	0	0	0	0	0	0	0	1	6	2	4	1	2	1	0	3	
Cyst of <i>Pentapharsodinium</i>	5	8	1	1	6	2	1	0	8	5	7	19	25	4	1	5	6	
<i>Islandinium minutum</i>	18	17	30	13	18	32	11	6	6	1	0	1	0	3	1	2	2	
<i>Islandinium cezare</i>	0	0	0	0	0	0	0	0	1	1	0	0	0	1	0	1	0	
<i>Echinidinium karaense</i>	0	0	0	0	0	0	0	0	0	0	0	0	0	0	0	0	0	
<i>Brigantedinium</i> spp.	264	266	248	269	206	246	135	114	33	4	30	5	123	24	31	5	0	
<i>Selenopempix nephroides</i>	0	0	0	0	0	0	0	0	0	0	0	0	0	0	0	0	0	
<i>Selenopempix quanta</i>	11	1	0	0	3	3	0	0	0	0	0	0	0	0	0	0	0	
<i>Trinovantedinium applanatum</i>	0	0	0	0	0	0	0	0	0	2	4	1	0	0	0	1	0	
<i>Qinquecuspis concreta</i>	0	0	0	0	0	0	0	0	0	0	0	0	0	0	0	0	0	
<i>Polykrikos schwartzii</i>	0	0	0	0	0	0	0	0	0	0	0	0	0	0	0	0	0	
<i>Protoperidinium</i>	0	0	0	0	0	0	0	0	0	0	0	0	0	0	0	0	0	
<b>Somme des dinokystes</b>	<b>325</b>	<b>309</b>	<b>315</b>	<b>310</b>	<b>305</b>	<b>302</b>	<b>173</b>	<b>140</b>	<b>150</b>	<b>81</b>	<b>150</b>	<b>141</b>	<b>234</b>	<b>159</b>	<b>93</b>	<b>96</b>	<b>57</b>	

**Tableau A.5** Dénombrement des dinokystes de la carotte PS2863-2BC

Profondeur (cm)	0	1	2	3	4	5	6	7	8	9	10	11	12	13	14	15	16	17	18	19	20	21	22	23
<i>Ataxodinium choane</i>	0	0	0	0	0	0	0	0	0	0	0	0	0	0	0	0	0	0	0	0	0	0	0	0
<i>Bitectatadinium tepikiense</i>	0	0	2	0	0	0	0	0	0	0	0	0	1	0	0	0	1	0	1	0	1	1	1	1
<i>Impagidinium pallidum</i>	18	15	15	26	24	15	29	43	31	24	38	30	21	18	14	14	21	28	22	26	33	27	15	15
<i>Impagidinium paradoxum</i>	0	0	0	0	0	0	0	0	0	0	0	0	0	0	0	0	0	0	0	0	0	0	0	0
<i>Impagidinium patulum</i>	0	0	4	0	0	0	0	0	0	0	0	0	0	0	0	0	0	0	0	0	0	0	0	0
<i>Impagidinium sphaericum</i>	0	0	0	0	0	0	0	0	1	0	1	0	2	1	0	0	5	0	1	0	2	2	0	0
<i>Nematosphaeropsis</i>	41	57	39	27	78	33	46	72	29	42	49	57	46	36	37	31	22	39	41	34	49	44	41	35
<i>Operculodinium</i>	272	259	286	269	537	265	271	393	270	278	352	334	297	290	309	265	276	289	322	318	353	261	299	272
<i>Spiniferites elongatus</i>	6	7	10	1	10	9	4	10	4	4	8	5	1	3	4	4	2	5	6	7	8	3	2	5
<i>Spiniferites ramosus</i>	1	1	2	1	2	0	0	3	3	1	0	0	1	2	3	0	1	1	6	2	3	3	4	2
<i>Spiniferites</i> spp.	3	3	3	2	3	2	1	1	6	3	7	7	0	0	1	2	5	5	7	8	4	5	7	4
Cyst of <i>Pentapharsodinium</i>	22	32	11	8	7	6	2	17	5	4	15	14	3	3	3	4	6	4	3	8	8	6	9	5
<i>Islandinium minutum</i>	0	0	0	16	21	15	22	3	1	7	3	27	47	31	16	9	22	18	11	1	6	5	1	18
<i>Islandinium cezare</i>	0	0	0	4	1	2	0	0	0	0	0	0	0	2	0	0	0	0	0	0	0	0	0	0
<i>Brigantedinium</i> spp.	3	3	0	12	20	4	15	5	4	7	9	15	7	9	3	2	3	3	0	1	4	1	2	4
<i>Selenopemphix quanta</i>	1	0	0	0	0	1	0	0	1	0	1	1	0	0	0	0	0	0	0	0	0	0	0	0
<i>Trinovantedinium</i>	0	0	0	0	0	0	0	0	0	0	0	0	0	0	0	0	0	0	0	0	0	0	0	0
<b>Somme des dinokystes</b>	<b>367</b>	<b>377</b>	<b>372</b>	<b>366</b>	<b>703</b>	<b>352</b>	<b>390</b>	<b>547</b>	<b>354</b>	<b>371</b>	<b>482</b>	<b>491</b>	<b>424</b>	<b>397</b>	<b>391</b>	<b>331</b>	<b>358</b>	<b>398</b>	<b>418</b>	<b>407</b>	<b>468</b>	<b>358</b>	<b>383</b>	<b>361</b>

<b>Profondeur (cm)</b>	<b>24</b>	<b>25</b>	<b>26</b>	<b>27</b>	<b>28</b>	<b>29</b>	<b>30</b>	<b>31</b>	<b>32</b>	<b>33</b>	<b>34</b>	<b>35</b>	<b>36</b>	<b>37</b>	<b>38</b>
<i>Ataxodinium choane</i>	0	0	0	0	0	1	0	0	0	0	0	1	0	1	0
<i>Bitectatodinium tepikiense</i>	0	1	2	2	1	1	1	1	0	0	0	3	1	0	0
<i>Impagidinium pallidum</i>	14	12	15	17	19	14	17	21	19	19	18	11	12	10	6
<i>Impagidinium paradoxum</i>	0	0	0	0	1	0	0	0	0	0	0	0	0	1	0
<i>Impagidinium patulum</i>	0	0	0	1	0	0	0	0	1	0	0	0	0	0	0
<i>Impagidinium sphaericum</i>	1	0	2	1	1	0	2	2	1	2	4	2	1	3	0
<i>Nematosphaeropsis</i>	30	18	38	29	33	43	43	37	30	64	65	76	76	103	116
<i>Operculodinium</i>	248	258	306	262	231	244	275	234	278	229	230	260	221	214	180
<i>Spiniferites elongatus</i>	7	2	11	8	6	4	10	11	13	7	6	11	10	9	7
<i>Spiniferites ramosus</i>	4	2	4	8	4	3	4	5	6	8	10	4	5	8	10
<i>Spiniferites spp.</i>	7	5	11	5	3	7	11	2	6	11	6	5	6	6	8
Cyst of <i>Pentapharsodinium</i>	10	12	9	6	12	16	15	3	5	9	12	15	7	13	17
<i>Islandinium minutum</i>	28	20	4	4	29	20	22	21	9	4	5	1	22	4	5
<i>Islandinium cezare</i>	1	0	0	0	1	0	0	0	0	0	0	0	1	2	0
<i>Brigantedinium spp.</i>	7	3	3	3	14	3	5	4	6	0	4	4	5	0	1
<i>Selenopempix quanta</i>	0	0	0	0	0	1	0	0	0	0	0	0	0	0	0
<i>Trinovantedinium</i>	0	0	0	0	0	0	0	0	0	0	0	0	0	1	0
<b>Somme des dinokystes</b>	<b>357</b>	<b>333</b>	<b>405</b>	<b>346</b>	<b>355</b>	<b>357</b>	<b>405</b>	<b>341</b>	<b>374</b>	<b>353</b>	<b>361</b>	<b>393</b>	<b>367</b>	<b>375</b>	<b>350</b>

**Tableau A.6** Dénombrement des dinokystes de la carotte PS2863-1

Profondeur (cm)	1.5	5	9	13	17	21	25	29	33	37	41	45	49	53	57	60.5	65	69	73
<i>Achomasphoera</i> sp.	0	0	0	0	0	0	0	0	0	0	0	0	0	0	0	0	0	0	0
<i>Ataxodinium choane</i>	0	0	0	0	0	0	1	0	0	0	0	0	0	2	0	0	1	0	0
<i>Bitectatodinium tepikiense</i>	0	0	1	0	0	0	1	0	0	0	1	0	0	0	0	0	0	0	2
<i>Impagidinium aculeatum</i>	0	0	0	0	0	0	0	0	0	0	0	0	0	0	0	0	0	0	0
<i>Impagidinium pallidum</i>	21	21	18	17	21	18	22	5	11	5	17	4	11	11	4	3	6	5	22
<i>Impagidinium paradoxum</i>	0	0	0	1	0	0	0	0	0	0	1	0	0	0	0	1	0	0	0
<i>Impagidinium patulum</i>	0	0	0	0	0	0	0	0	0	0	0	0	1	0	0	0	0	0	0
<i>Impagidinium sphaericum</i>	0	1	3	0	4	1	0	3	2	1	6	6	3	1	4	1	3	3	2
<i>Lingulodinium machaerophorum</i>	0	0	0	0	0	0	0	0	0	0	0	0	0	0	0	0	0	0	0
<i>Nematosphaeropsis labyrinthus</i>	37	47	32	40	28	29	50	118	188	17	216	112	114	151	110	135	133	158	129
<i>Operculodinium centrocarpum</i>	240	313	311	282	281	262	238	196	114	24	138	65	63	64	81	43	42	42	47
<i>Spiniferites membranaceus</i>	0	0	0	0	0	0	1	0	0	0	1	0	0	0	0	0	0	0	0
<i>Spiniferites delicatus</i>	0	0	0	0	0	0	2	0	0	0	0	0	0	0	0	0	0	0	0
<i>Spiniferites elongatus</i>	2	5	2	1	16	8	6	9	17	2	25	25	34	37	41	34	28	33	45
<i>Spiniferites ramosus</i>	0	2	4	4	1	6	4	7	11	2	9	27	25	22	27	21	36	17	28
<i>Spiniferites belerius</i>	0	0	0	0	0	0	0	0	0	0	0	0	0	0	0	0	0	0	0
<i>Spiniferites bentorii</i>	0	0	0	0	0	0	0	0	0	0	0	0	0	0	0	0	0	0	0
<i>Spiniferites lazus</i>	0	0	0	0	0	0	1	0	1	0	0	0	0	0	0	0	0	0	0
<i>Spiniferites mirabilis</i>	0	0	0	0	0	0	0	0	0	0	0	0	0	1	0	0	0	0	0
<i>Spiniferites spp.</i>	3	1	5	4	11	8	5	5	13	4	8	5	5	9	7	4	0	4	6
<i>Tectatodinium pellitum</i>	0	0	0	0	0	0	0	0	0	0	0	0	0	0	0	0	0	0	0
Cyst of <i>Pentapharsodinium dalei</i>	19	5	6	4	9	8	4	7	19	2	67	63	94	54	51	46	68	17	21
<i>Islandinium minutum</i>	16	24	5	3	1	17	16	10	2	4	5	1	4	16	5	2	7	27	32
<i>Islandinium cezare</i>	2	2	0	1	0	0	1	0	0	0	0	0	0	0	1	0	0	2	4
<i>Brigantedinium</i> spp.	2	12	4	4	3	10	6	7	7	2	10	25	8	9	1	7	8	7	11
<i>Lejeuneacysta</i> spp.	0	0	0	0	0	0	0	0	0	0	2	0	0	0	0	0	0	0	0
<i>Selenopemphix quanta</i>	0	0	0	0	0	0	0	0	0	0	0	0	0	0	0	0	0	0	1
<i>Trinovantedinium applanatum</i>	0	0	0	0	0	2	1	1	2	0	3	0	2	1	0	1	0	1	0
Cyst of <i>Protoperidinium americanum</i>	0	0	0	0	0	0	0	0	0	0	0	0	0	0	0	0	0	0	0
Somme des dinokystes	342	433	391	361	375	369	359	368	387	63	509	333	364	378	332	298	332	316	350

Profondeur (cm)	77	81.5	85	89	93	97	101	104	109	112	116	120	124	128	132	136	140	144	148
<i>Achomosphaera</i> sp.	0	0	0	0	0	3	0	1	0	0	0	0	0	1	0	0	0	0	0
<i>Ataxodinium choane</i>	0	0	0	0	0	0	0	0	0	0	0	0	0	0	0	0	0	0	0
<i>Bitectatodinium tepikense</i>	3	2	2	0	0	1	0	6	4	1	6	1	0	0	0	0	1	0	0
<i>Impagidinium aculeatum</i>	0	1	0	0	0	0	0	0	0	0	0	0	0	0	0	0	0	0	0
<i>Impagidinium pallidum</i>	11	2	0	1	0	0	0	0	0	0	0	0	0	1	1	0	0	0	0
<i>Impagidinium paradoxum</i>	0	1	0	0	0	0	0	0	0	0	0	0	0	0	0	0	0	0	0
<i>Impagidinium patulum</i>	0	0	0	0	0	0	0	0	0	0	0	0	0	0	0	0	0	0	0
<i>Impagidinium sphaericum</i>	0	1	1	0	1	1	0	0	0	0	0	0	0	0	0	0	0	1	0
<i>Lingulodinium machaerophorum</i>	0	0	0	0	0	0	0	0	0	0	0	0	1	4	0	0	0	0	0
<i>Nematosphaeropsis labyrinthus</i>	121	126	56	54	61	93	9	9	4	8	4	3	1	1	6	1	0	0	0
<i>Oberculodinium centrocarpum</i>	34	44	25	18	41	68	81	37	36	46	17	12	15	19	17	2	1	13	3
<i>Spiniferites membranaceus</i>	0	0	0	0	0	0	0	0	0	0	0	0	0	0	0	0	0	0	0
<i>Spiniferites delicatus</i>	0	0	0	0	0	0	0	0	0	0	0	0	0	1	0	0	0	0	0
<i>Spiniferites elongatus</i>	38	75	78	83	102	100	157	150	147	119	63	3	2	7	25	25	17	12	5
<i>Spiniferites ramosus</i>	39	48	145	161	92	72	10	13	3	0	0	2	1	2	1	0	0	2	0
<i>Spiniferites belerius</i>	0	0	0	0	1	0	1	0	0	0	0	0	0	0	0	0	0	0	0
<i>Spiniferites bentorii</i>	0	0	0	0	0	0	0	0	0	0	0	0	0	1	0	0	0	0	0
<i>Spiniferites lazus</i>	0	0	0	0	0	0	0	0	0	0	1	0	0	0	0	0	0	0	0
<i>Spiniferites mirabilis</i>	0	0	0	0	0	0	0	1	0	0	0	0	0	0	0	0	0	0	0
<i>Spiniferites</i> spp.	13	7	12	4	30	18	6	3	0	0	0	0	3	4	1	0	0	1	0
<i>Tectatodinium pellitum</i>	0	0	0	0	0	0	0	0	0	0	0	0	0	0	0	0	0	0	0
Cyst of <i>Pentapharsodinium dalei</i>	15	8	5	7	27	21	36	19	13	5	3	0	2	0	5	1	0	2	2
<i>Islandinium minutum</i>	17	2	0	0	0	0	0	1	0	1	7	5	5	12	24	8	10	11	0
<i>Islandinium cezare</i>	1	0	0	0	0	0	0	0	0	0	0	0	2	0	0	0	0	0	0
<i>Brigantedinium</i> spp.	29	11	9	2	3	5	31	59	100	157	243	291	285	222	254	317	272	277	304
<i>Lejeuneacysta</i> spp.	0	0	0	0	0	0	0	0	0	0	0	0	0	0	0	0	0	0	0
<i>Selenopempix quanta</i>	0	0	0	0	0	0	0	1	0	6	0	3	1	0	2	1	2	6	8
<i>Trinovantedinium appланatum</i>	2	0	0	0	1	1	0	2	1	0	0	0	0	0	0	0	0	0	0
Cyst of <i>Protoperidinium americanum</i>	1	0	0	0	0	0	0	1	0	0	0	0	0	0	0	0	0	0	0
<b>Somme des dinokystes</b>	<b>324</b>	<b>328</b>	<b>333</b>	<b>330</b>	<b>359</b>	<b>383</b>	<b>331</b>	<b>303</b>	<b>308</b>	<b>343</b>	<b>344</b>	<b>321</b>	<b>319</b>	<b>273</b>	<b>336</b>	<b>355</b>	<b>303</b>	<b>325</b>	<b>322</b>

Profondeur (cm)	152	156	160	164	169	174	178	183
<i>Achromosphaera</i> sp.	0	0	0	4	3	0	1	3
<i>Ataxodinium choane</i>	0	0	0	1	0	0	0	0
<i>Bitectatodinium tepikiense</i>	1	0	3	4	33	11	15	10
<i>Impagidinium aculeatum</i>	0	0	0	0	0	0	0	0
<i>Impagidinium pallidum</i>	0	1	0	0	0	0	0	1
<i>Impagidinium paradoxum</i>	1	1	0	0	0	0	0	2
<i>Impagidinium patulum</i>	0	0	0	0	0	0	0	0
<i>Impagidinium sphaericum</i>	0	0	1	0	0	0	0	0
<i>Lingulodinium machaerophorum</i>	1	0	0	0	0	0	0	0
<i>Nematosphaeropsis labyrinthus</i>	1	4	1	1	2	0	1	0
<i>Operculodinium centrocarpum</i>	2	10	13	26	78	7	30	22
<i>Spiniferites membranaceus</i>	0	0	0	0	0	1	0	0
<i>Spiniferites delicatus</i>	0	0	0	0	0	0	0	0
<i>Spiniferites elongatus</i>	0	9	0	0	4	0	0	1
<i>Spiniferites ramosus</i>	0	2	0	7	34	3	9	7
<i>Spiniferites belerius</i>	0	0	0	0	0	0	0	0
<i>Spiniferites bentorii</i>	0	0	0	0	0	0	0	0
<i>Spiniferites lazus</i>	0	0	0	0	0	0	0	0
<i>Spiniferites mirabilis</i>	0	0	0	0	1	0	0	1
<i>Spiniferites</i> spp.	1	0	1	4	9	2	1	2
<i>Tectatodinium pellitum</i>	0	0	0	0	1	0	0	0
Cyst of <i>Pentapharsodinium dalei</i>	0	5	4	6	9	2	3	3
<i>Islandinium minutum</i>	2	43	56	6	1	0	0	0
<i>Islandinium cezare</i>	0	2	1	0	0	0	0	0
<i>Brigantedinium</i> spp.	47	244	229	66	5	1	0	2
<i>Lejeuneacysta</i> spp.	0	0	0	0	0	0	0	0
<i>Selenopemphix quanta</i>	0	0	0	0	0	0	0	0
<i>Trinovantedinium applanatum</i>	0	0	0	0	0	0	0	0
Cyst of <i>Protoperdidinium americanum</i>	0	0	0	0	0	0	0	0
<b>Somme des dinokystes</b>	<b>56</b>	<b>321</b>	<b>309</b>	<b>125</b>	<b>180</b>	<b>27</b>	<b>60</b>	<b>54</b>

**Tableau A.7** Concentration des palynomorphes de la carotte MSM5/5-712-2

<b>Profondeur (cm)</b>	<b>10</b>	<b>14</b>	<b>18</b>	<b>22</b>	<b>26</b>	<b>30</b>	<b>34</b>	<b>38</b>	<b>42</b>	<b>46</b>	<b>50</b>	<b>54</b>	<b>58</b>	<b>62</b>	<b>66</b>	<b>70</b>	<b>74</b>	
Poids sec (g)	2.54	3.31	3.08	4.32	3.10	3.37	4.17	4.56	3.43	4.17	3.76	4.01	3.48	4.40	3.38	4.03	4.10	
Volume (mL)	5	5	5	5.5	5	5	5	6.5	5	5	5	5	5	5	5	5	5	
Nombre de <i>L. clavatum</i> /capsule	18583	18583	18583	18583	18583	18583	18583	18583	18583	18583	18583	18583	18583	18583	18583	18583	18583	
<i>L. clavatum</i> comptés	49	36	34	73	64	51	28	30	36	41	56	62	67	36	56	80	63	
Dinokystes/g	46942	107982	36384	38856	24853	40247	57867	64227	67210	55727	37518	30929	31455	54631	49053	32518	32356	
Dinokystes/cm <sup>2</sup> /an	400	1052	326	449	229	450	859	801	867	964	588	514	456	887	552	437	442	
Pollens/g	894	779	532	353	656	541	636	543	902	1304	1324	523	1433	1993	1966	577	1366	
Spores/g	298	312	710	235	750	757	636	272	752	109	706	374	717	352	786	0	575	
Palynomorphes remaniés/g	447	779	1065	235	375	433	954	0	451	217	441	1419	398	352	1278	692	575	
Réseaux organiques de foraminifères/g	8047	6700	5502	4533	7221	7681	4769	8011	9322	4671	4767	3287	5813	6800	8552	7726	6471	
<i>Pediastrum</i> /g	0	0	0	59	0	0	0	0	0	0	0	0	0	0	0	58	0	
<i>Haladinium</i> /g	298	779	0	353	188	433	318	407	601	435	265	299	319	352	590	288	0	
<b>Profondeur (cm)</b>	<b>78</b>	<b>82</b>	<b>86</b>	<b>90</b>	<b>94</b>	<b>98</b>	<b>102</b>	<b>106</b>	<b>110</b>	<b>114</b>	<b>118</b>	<b>122</b>	<b>126</b>	<b>130</b>	<b>134</b>	<b>138</b>	<b>142</b>	<b>146</b>
Poids sec (g)	3.48	3.66	3.81	3.40	4.14	3.54	3.63	3.13	3.51	3.55	3.83	3.71	3.83	3.05	4.09	3.40	3.97	3.28
Volume (mL)	5	5	5.5	5	5	5	5	5	5	5	5	5	5	5	5	5	5	5
Nombre de <i>L. clavatum</i> /capsule	18583	18583	18583	18583	18583	18583	18583	18583	18583	18583	18583	18583	18583	18583	18583	18583	18583	18583
<i>L. clavatum</i> comptés	70	70	90	83	112	64	87	87	103	118	139	114	154	739	97	93	113	107
Dinokystes/g	28572	26630	22882	23928	19759	30012	24710	21727	19233	16074	16576	24501	12575	3199	20702	20599	15943	21687
Dinokystes/cm <sup>2</sup> /an	330	325	264	270	273	494	417	314	314	265	294	422	224	45	394	326	582	758
Pollens/g	838	1234	542	989	561	1312	588	957	1131	666	803	1320	599	181	984	704	952	1432
Spores/g	381	508	108	527	240	246	471	1298	823	355	140	484	221	49	234	587	621	636
Palynomorphes remaniés/g	229	290	325	461	441	1230	176	1640	206	533	140	924	693	132	281	998	538	636
Réseaux organiques de foraminifère/g	4190	5442	6669	5405	4168	5166	1059	4714	2211	2797	3001	1628	4192	462	6323	4460	2112	4030
<i>Pediastrum</i> /g	0	0	0	0	40	0	0	0	0	0	0	0	0	0	0	0	0	0
<i>Haladinium</i> /g	76	0	217	132	120	82	59	410	154	178	105	396	158	66	328	59	124	106

<b>Profondeur (cm)</b>	<b>150</b>	<b>154</b>	<b>158</b>	<b>162</b>	<b>165</b>	<b>170</b>	<b>174</b>	<b>178</b>	<b>182</b>	<b>186</b>	<b>190</b>	<b>194</b>	<b>198</b>	<b>202</b>	<b>206</b>	<b>210</b>	<b>214</b>	<b>218</b>
Poids sec (g)	3.35	3.49	3.58	3.54	3.37	3.66	3.41	3.71	3.65	3.44	4.00	3.33	4.26	3.22	3.81	3.91	3.98	3.58
Volume (mL)	5	5	5	5	5	5	5	5	5	5	5	5	6	5	5	5	5	5
Nombre de <i>L. clavatum</i> /capsule	18583	18583	18583	18583	18583	18583	18583	18583	18583	18583	18583	18583	18583	18583	18583	18583	18583	18583
<i>L. clavatum</i> comptés	96	104	137	87	141	153	143	242	215	171	282	50	145	105	241	82	398	88
Dinokystes/g	2220	12093	13464	18564	13629	11099	14016	7642	9031	6453	6520	13717	11525	14678	8225	7658	3707	5905
Dinokystes/cm <sup>2</sup> /an	793	456	514	702	491	423	455	273	317	211	252	831	1558	1800	1193	1140	562	272
Pollens/g	1273	461	1593	1868	979	1628	2019	828	616	633	642	1561	1083	605	810	1044	727	827
Spores/g	637	769	569	663	313	1063	1181	269	284	633	461	781	421	1154	486	522	469	709
Palynomorphes remaniés/g	289	769	303	1266	78	1030	533	311	261	822	247	2565	361	770	365	1160	164	118
Réseaux organiques de foraminifère/g	6654	3792	3944	6630	1214	3954	5294	2982	3508	2372	4759	4907	5176	4288	2755	3249	3719	1831
<i>Pediastrum</i> /g	0	0	0	0	0	0	0	21	47	0	33	0	0	0	20	0	12	0
<i>Halodinium</i> /g	231	102	379	241	39	366	267	186	498	95	198	669	542	220	446	290	411	118
<b>Profondeur (cm)</b>	<b>222</b>	<b>226</b>	<b>230</b>	<b>234</b>	<b>238</b>	<b>242</b>	<b>246</b>	<b>250</b>	<b>254</b>	<b>258</b>	<b>262</b>	<b>266</b>	<b>270</b>	<b>274</b>	<b>278</b>	<b>282</b>	<b>290</b>	<b>298</b>
Poids sec (g)	3.73	3.42	4.05	3.54	4.37	3.20	3.72	3.32	4.65	3.66	3.46	3.47	3.50	3.44	3.46	3.71	3.48	4.08
Volume (mL)	5	5	5	5	5	5	5	5	6	5	5	5	5	5	5	5	5	6
Nombre de <i>L. clavatum</i> /capsule	18583	18583	18583	18583	18583	18583	18583	18583	18583	18583	18583	18583	18583	18583	18583	18583	18583	18583
<i>L. clavatum</i> comptés	250	103	332	274	334	83	348	170	164	182	271	91	282	215	411	133	62	156
Dinokystes/g	6173	2850	4879	5481	3157	7061	5135	3526	9352	5573	6558	8354	6235	9271	4255	8617	6804	3033
Dinokystes/cm <sup>2</sup> /an	293	126	251	250	178	287	247	149	468	259	293	374	277	412	187	449	357	154
Pollens/g	796	792	940	1591	445	1818	1004	923	2143	1198	911	1235	1055	1156	522	1392	431	671
Spores/g	518	317	456	824	535	629	316	692	536	725	991	529	866	754	561	753	947	525
Palynomorphes remaniés/g	737	369	263	211	204	210	244	198	414	836	594	647	339	829	379	828	517	175
Réseaux organiques de foraminifère/g	3305	633	3262	2223	2469	2377	2323	1516	4968	2313	4062	4412	4766	3944	2101	1505	517	233
<i>Pediastrum</i> /g	0	0	28	0	13	70	0	0	24	0	59	0	0	50	0	0	0	0
<i>Halodinium</i> /g	518	317	484	345	573	140	832	165	950	390	951	1000	1319	854	861	790	86	321

<b>Profondeur (cm)</b>	<b>306</b>	<b>314</b>	<b>322</b>	<b>330</b>	<b>338</b>	<b>346</b>	<b>354</b>	<b>362</b>	<b>370</b>	<b>378</b>	<b>386</b>	<b>394</b>	<b>402</b>	<b>410</b>	<b>418</b>	<b>426</b>	<b>434</b>	<b>442</b>
Poids sec (g)	3.90	3.41	4.40	4.08	4.15	4.27	4.22	4.82	4.32	4.79	4.34	4.39	5.12	5.37	3.59	4.77	2.81	4.35
Volume (mL)	5	5	5	5	5	5	5	5	5	5	5	5	5	5	5	4	5	5
Nombre de <i>L. clavatum</i> /capsule	18583	18583	18583	18583	18583	18583	18583	18583	18583	18583	18583	18583	18583	18583	18583	18583	18583	18583
<i>L. clavatum</i> comptés	162	149	139	97	212	104	245	189	728	106	194	203	62	45	79	56	114	53
Dinokystes/g	10542	9735	9491	15641	3334	13509	5792	6572	1875	12049	6870	6979	18775	24974	22824	22397	18915	26360
Dinokystes/cm <sup>2</sup> /an	620	501	630	169	37	153	114	362	92	664	340	350	1107	1534	1169	1230	1968	3669
Pollens/g	648	622	30	329	359	544	288	429	101	0	287	313	175	307	66	278	116	242
Spores/g	618	622	213	517	295	627	126	20	18	146	133	208	234	307	66	0	0	81
Palynomorphes remaniés/g	236	256	1582	1691	401	1840	1655	1755	1059	2307	1193	1354	1053	3151	1705	1669	2321	2983
Réseaux organiques de foraminifère/g	3063	2013	3498	2677	950	3179	1007	1674	432	476	442	63	351	538	918	696	754	564
<i>Pediastrum</i> /g	0	0	0	0	0	0	54	20	0	146	44	0	58	0	66	70	58	81
<i>Halodinium</i> /g	501	366	791	892	148	544	198	245	0	73	88	0	58	307	66	70	174	161
<b>Profondeur (cm)</b>	<b>450</b>	<b>458</b>	<b>466</b>	<b>474</b>	<b>482</b>	<b>490</b>	<b>500</b>	<b>507</b>	<b>514</b>	<b>521</b>	<b>528</b>	<b>536</b>	<b>542</b>	<b>549</b>	<b>556</b>	<b>563</b>	<b>570</b>	<b>577</b>
Poids sec (g)	4.02	4.99	3.01	3.89	3.90	2.25	4.81	5.71	5.45	7.21	5.77	5.62	5.30	6.33	5.71	5.93	6.14	5.75
Volume (mL)	4	5	3	4	4	2	5	5.5	5	4.5	5	5	5	5.5	5	5	5	5
Nombre de <i>L. clavatum</i> /capsule	18583	18583	18583	18583	18583	18583	18584	18584	18584	18584	18584	18584	18584	18584	18584	18584	18584	18584
<i>L. clavatum</i> comptés	45	38	94	96	292	282	148	106	134	204	333	392	775	702	1530	1279	977	915
Dinokystes/g	31870	31670	20235	15756	5127	8878	7915	9823	7960	3788	2904	2571	914	1262	623	507	350	378
Dinokystes/cm <sup>2</sup> /an	5225	5055	3314	2455	975	3472	2624	3400	3039	2024	1172	1006	323	509	237	211	143	152
Pollens/g	514	784	66	50	98	88	52	61	0	38	39	17	45	21	21	7	6	11
Spores/g	0	98	131	0	65	0	52	0	0	38	10	17	9	4	0	7	6	0
Palynomorphes remaniés/g	3701	1961	2431	5020	3070	3897	2403	3070	1526	2500	2323	2091	2990	2099	1371	1830	2100	1522
Réseaux organiques de foraminifère/g	514	980	197	398	98	234	0	184	51	76	97	34	14	0	0	20	6	7
<i>Pediastrum</i> /g	0	98	0	0	33	0	26	0	0	0	10	0	5	0	2	2	0	4
<i>Halodinium</i> /g	103	294	66	50	16	59	26	31	102	63	68	34	23	17	9	2	6	11

<b>Profondeur (cm)</b>	<b>585</b>	<b>593</b>	<b>601</b>	<b>608</b>	<b>616</b>	<b>624</b>	<b>632</b>	<b>640</b>	<b>648</b>	<b>656</b>	<b>664</b>	<b>672</b>	<b>680</b>	<b>688</b>	<b>696</b>	<b>704</b>	<b>712</b>
Poids sec (g)	5.87	5.46	5.44	5.29	6.02	5.97	5.24	7.04	7.13	7.61	6.36	5.30	6.37	10.64	5.41	5.42	5.49
Volume (mL)	5	5	5	5	5	5	5	5	6	7.5	6.5	5	5	10	5	5	5
Nombre de <i>L. clavatum</i> /capsule	18584	18584	18584	18584	18584	18584	18584	18584	18584	18584	18584	18584	18584	18584	18584	18584	18584
<i>L. clavatum</i> comptés	752	937	1114	2012	1482	1897	335	181	159	64	51	729	353	645	1947/ 684	1549/ 480	3012/ 1108
Dinokystes/g	636	283	291	77	618	148	3208	4421	5325	11785	18043	1492	2520	818	305	310	169
Dinokystes/cm <sup>2</sup> /an	260	103	110	27	259	61	1121	2164	2202	3988	315	16	33	9	3	3	2
Pollens/g	8	4	3	5	6	15	0	0	0	0	0	10	17	27	16	15	31
Spores/g	4	7	0	5	0	3	11	0	0	0	0	0	17	0	4	2	11
Palynomorphes remaniés/g	2157	2294	2327	635	460	451	995	1036	1163	1678	1604	1982	2313	1669	1612	1885	621
Réseaux organiques de foraminifère/g	21	15	6	23	333	0	498	438	311	0	57	10	58	11	16	18	109
<i>Pediastrum</i> /g	0	0	3	3	2	2	0	0	16	0	0	0	0	0	5	0	33
<i>Halodinium</i> /g	17	18	25	0	0	0	42	29	66	0	0	14	17	14	5	7	7

<b>Profondeur (cm)</b>	<b>720</b>	<b>728</b>	<b>736</b>	<b>744</b>	<b>752</b>	<b>760</b>	<b>768</b>	<b>776</b>
Poids sec (g)	5.58	6.99	6.67	6.09	5.52	5.53	5.69	4.86
Volume (mL)	5	6	5.5	5.5	5	5	5.5	5
Nombre de <i>L. clavatum</i> /capsule	18584	18584	18584	18584	18584	18584	18584	18584
<i>L. clavatum</i> comptés	2071	2011/ 913	1981/ 731	1800/ 692	2916	1764	1160	968
Dinokystes/g	141	198	198	397	183	177	270	225
Dinokystes/cm <sup>2</sup> /an	2	4	4	8	4	4	9	9
Pollens/g	63	50	48	42	29	63	121	40
Spores/g	16	18	10	34	13	11	17	16
Palynomorphes remaniés/g	455	984	888	1071	551	890	732	1051
Réseaux organiques de foraminifère/g	103	107	41	66	89	170	0	217
<i>Pediastrum</i> /g	8	4	18	31	2	4	0	12
<i>Halodinium</i> /g	5	1	6	3	1	6	0	0

**Tableau A.8** Concentration des palynomorphes de la carotte PS2863-2BC

Profondeur (cm)	0	1	2	3	4	5	6	7	8	9	10	11	12	13	14
Poids sec (g)	4.00	3.13	3.66	5.59	4.34	3.86	3.73	3.88	4.34	5.12	4.65	4.30	4.36	3.90	4.43
Volume (mL)	5.0	3.5	5.0	7.0	5.5	5.0	5.0	5.0	5.0	5.0	5.0	5.0	5.0	4.5	5.0
Nombre de <i>L. clavatum</i> /capsule	18584	18584	18584	18584	18584	18584	18584	18584	18584	18584	18584	18584	18584	18584	18584
<i>L. clavatum</i> comptés	140	201	129	75	175	43	134	145	101	116	110	121	78	90	67
Dinokystes/g	12174	11139	14630	16232	17206	39394	14493	18065	15018	11619	17501	17526	23187	21010	24500
Dinokystes/cm <sup>2</sup> /an	67	47	51	61	64	144	51	66	62	56	77	71	96	86	103
Pollens/g	76	226	123	76	75	50	119	120	12	49	69	155	77	100	68
Spores/g	76	158	136	100	24	0	38	105	12	59	58	97	30	48	43
Palynomorphes remaniés/g	862	591	865	931	538	2014	1375	1651	1442	501	1017	1571	1750	1323	1629
Réseaux organiques de foraminifères/g	0	0	0	444	269	671	260	132	764	407	581	500	1695	423	1253
<i>Pediastrum</i> /g	0	0	0	0	0	0	0	0	0	0	0	0	0	0	0
<i>Halodinium</i> /g	690	528	634	743	425	1556	1026	1282	1251	513	946	1352	1525	1147	1442

Profondeur (cm)	15	16	17	18	19	20	21	22	23	24	25	26	27	28	29
Poids sec (g)	4.61	4.31	4.36	5.58	4.33	3.73	4.05	4.60	3.60	4.04	4.41	3.76	4.77	3.37	4.93
Volume (mL)	5.5	5.0	5.0	5.0	5.5	4.0	4.5	5.5	4.5	5.0	5.5	4.5	5.5	5.0	5.5
Nombre de <i>L. clavatum</i> /capsule	18584	18584	18584	18584	18584	18584	18584	18584	18584	18584	18584	18584	18584	18584	18584
<i>L. clavatum</i> comptés	70	123	125	121	129	162	153	170	182	216	105	300	188	261	211
Dinokystes/g	19073	12548	13558	11511	13550	14401	10732	9106	10233	7604	13361	6666	7176	7494	6372
Dinokystes/cm <sup>2</sup> /an	76	51	56	61	51	64	46	36	39	29	51	26	29	24	27
Pollens/g	69	68	71	61	74	53	120	102	129	150	89	138	139	197	84
Spores/g	37	60	11	0	53	75	115	127	114	232	63	183	203	279	285
Palynomorphes remaniés/g	1268	1087	1329	688	1498	1015	1139	1117	1361	1172	1123	1086	1680	1478	1249
Réseaux organiques de foraminifère/g	980	280	511	441	366	554	270	571	794	767	1083	99	311	1604	518
<i>Pediastrum</i> /g	0	0	0	0	0	0	0	0	0	0	0	0	0	0	0
<i>Halodinium</i> /g	1062	937	1160	768	1179	946	1026	934	1089	946	901	909	1456	997	1121

Profondeur (cm)	30	31	32	33	34	35	36	37	38
Poids sec (g)	4.75	4.88	4.74	5.06	4.47	4.21	4.38	2.74	3.33
Volume (mL)	5.0	5.5	5.0	5.5	5.0	5.0	5.0	3.0	4.0
Nombre de <i>L. clavatum</i> /capsule	18584	18584	18584	18584	18584	18584	18584	18584	18584
<i>L. clavatum</i> comptés	181	156	262	197	204	277	300	483	462
Dinokystes/g	8754	8327	5598	6575	7350	6257	5185	5275	4231
Dinokystes/cm <sup>2</sup> /an	39	35	25	29	31	25	22	23	22
Pollens/g	167	138	164	111	184	127	162	211	117
Spores/g	145	235	105	166	138	56	162	290	255
Palynomorphes remaniés/g	1210	904	539	857	1038	605	777	605	326
Réseaux organiques de foraminifère/g	562	562	314	559	448	127	424	295	60
<i>Pediastrum</i> /g	0	0	0	0	0	0	0	0	0
<i>Halodinium</i> /g	1150	801	511	789	929	510	681	551	272

**Tableau A.9** Concentration des palynomorphes de la carotte PS2863-1

Profondeur (cm)	1.5	5	9	13	17	21	25	29	33	37	41	45	49	53	57	60.5	65
Poids sec (g)	4.68	3.92	3.87	4.18	4.49	5.60	5.23	5.06	5.09	4.88	4.85	4.94	4.46	4.63	4.82	4.60	5.04
Volume (mL)	5	4	4	4	4.5	6	5.5	5	5.5	5	5	5	5	5	5	5	5.5
Nombre de <i>L. clavatum</i> /capsule	18583	18583	18583	18583	18583	18583	18583	18583	18583	18583	18583	18583	18583	18583	18583	18583	18583
<i>L. clavatum</i> comptés	76	93	100	124	233	205	217	213	381	146	812	568	301	613	335	324	432
Dinokystes/g	17857	22098	18754	12939	6660	5977	5875	6339	3708	1644	2400	2204	5037	2474	3818	3718	2832
Dinokystes/cm <sup>2</sup> /an	88	103	86	64	31	26	26	30	16	8	14	13	28	15	55	51	39
Pollens/g	52	425	511	287	207	205	235	161	284	217	140	106	314	203	81	129	80
Spores/g	104	204	288	72	124	194	213	207	287	287	151	218	138	281	184	299	111
Palynomorphes	731	255	384	323	675	421	540	551	307	757	406	1535	1052	785	713	1010	700
Réseaux organiques de foraminifères/g	470	1225	624	538	195	1247	786	500	479	1122	547	966	235	576	276	823	213
<i>Pediastrum</i> /g	0	0	0	0	0	0	0	0	0	0	0	0	13	55	0	12	12
<i>Halodinium</i> /g	0	0	48	72	0	97	49	0	29	26	14	132	138	236	219	137	273

Profondeur (cm)	69	73	77	81.5	85	89	93	97	100.5	104	108.5	112	116	120	124	128	132
Poids sec (g)	4.85	4.78	4.56	5.60	4.81	5.19	5.74	6.00	5.26	5.69	5.88	5.87	6.20	5.42	4.74	4.86	5.27
Volume (mL)	5	5	5	5	4.5	5	5	6	5	5	5	5	5	5	5.0	5.0	5.0
Nombre de <i>L. clavatum</i> /capsule	18583	18583	18583	18583	18583	18583	18583	18583	18583	18583	18583	18583	18583	18583	18583	18583	18583
<i>L. clavatum</i> comptés	401	546	592	569	265	86	292	125	293	574	476	262	397	469	1008	1473	900
Dinokystes/g	3018	2492	2228	1914	4857	13746	3983	9497	3989	1723	2044	4146	2584	2348	1241	709	1316
Dinokystes/cm <sup>2</sup> /an	44	36	30	32	78	214	68	142	63	29	52	161	105	81	30	18	36
Pollens/g	64	176	105	70	131	69	152	363	245	521	657	983	1310	636	197	125	307
Spores/g	124	228	220	99	117	0	133	322	121	324	451	616	499	285	136	62	157
Palynomorphes	621	605	798	403	496	625	777	1612	1916	1677	1560	1318	1927	2136	3622	3351	3790
Réseaux organiques de foraminifère/g	659	861	289	53	58	0	0	149	446	148	0	60	60	37	39	36	59
<i>Pediastrum</i> /g	10	0	21	6	15	0	0	25	12	57	60	145	166	139	47	13	39
<i>Halodinium</i> /g	229	157	110	18	0	0	33	25	0	17	66	36	106	59	58	47	43

Profondeur (cm)	136	140	144	148	152	156	160	164	169	174	178	183						
Poids sec (g)	5.81	6.26	6.22	6.11	6.11	6.27	6.61	5.99	6.31	5.20	4.83	4.73						
Volume (mL)	5.5	5.0	5.0	5.0	5.0	5.0	5.0	5.5	4.5	4.5	4.5	4.0						
Nombre de <i>L. clavatum</i> /capsule	18583	18583	18583	18583	18583	18583	18583	18583	18583	18583	18583	18584						
<i>L. clavatum</i> comptés	294	238	157	265	298	1192/ 662	824/ 17	2492/ 914		3973	1645	5144	2143					
Dinokystes/g	3862	3777	6189	3696	572	798	1053	156	133	59	45	99						
Dinokystes/cm <sup>2</sup> /an	34	36	58	34	5	8	10	1	1	1	1	2						
Pollens/g	888	1313	3713	2575	1089	1105	866	184	93	110	40	64						
Spores/g	218	237	590	149	388	191	215	57	21	48	12	24						
Palynomorphes	1577	2867	4780	1905	1970	1639	1304	1766	517	610	308	277						
Réseaux organiques de foraminifère/g	0	37	343	92	61	231	170	102	4	0	1	4						
<i>Pediastrum</i> /g	218	212	286	241	71	65	38	11	0	0	0	0						
<i>Halodinium</i> /g	54	0	171	92	0	35	10	1	0	0	1	0						

## APPENDICE B

### RÉSULTATS DES RECONSTITUTIONS

**Tableau B1 :** Résultats des reconstitutions des conditions des eaux de surface de la carotte MSM5/5-712-2 à partir de la méthode des analogues modernes appliquée aux assemblages de dinokystes

**Tableau B2 :** Résultats des reconstitutions des conditions des eaux de surface de la carotte PS2863-2BC à partir de la méthode des analogues modernes appliquée aux assemblages de dinokystes

**Tableau B3 :** Résultats des reconstitutions des conditions des eaux de surface de la carotte PS2863-1 à partir de la méthode des analogues modernes appliquée aux assemblages de dinokystes

**Tableau B.1** Résultats des reconstitutions des conditions des eaux de surface de la carotte MSMS5/5-712-2 à partir de la méthode des analogues modernes appliquée aux assemblages de dinokystes

Profondeur (cm)	Température des eaux de surface en hiver (°C)	Température des eaux de surface en été (°C)	Salinité des eaux de surface en été (psu)	Couverture de glace de mer (mois/an)	Productivité (gC/m <sup>2</sup> yr)
10	0.9	3.2	34.0	2.0	139
14	1.5	3.9	34.0	1.5	152
18	0.0	2.8	33.7	3.5	131
22	0.4	7.5	33.5	1.4	173
26	-0.3	2.0	32.7	5.6	127
30	0.9	3.4	33.8	2.0	149
34	1.2	3.9	33.7	2.8	147
38	1.4	3.9	34.0	2.2	155
42	0.4	2.8	33.4	5.0	135
46	0.6	3.2	34.0	2.9	132
50	1.7	4.1	34.2	1.7	153
54	1.1	4.3	33.9	2.0	158
58	1.2	3.3	34.0	3.7	146
62	1.0	4.2	34.2	1.2	145
66	2.1	4.8	34.3	1.1	149
70	1.7	4.2	34.2	1.4	151
74	0.7	3.7	33.8	2.4	137
78	1.2	3.3	33.8	2.3	144
82	0.7	3.1	33.4	4.8	125
86	1.0	4.0	34.0	1.6	152
90	1.5	4.3	34.1	1.3	160
94	1.1	3.3	34.0	2.3	142
98	1.6	4.1	33.9	2.6	142
102	2.6	5.3	34.2	1.6	162
106	0.8	4.4	33.3	4.2	139
110	1.5	4.1	34.2	1.6	144
114	1.6	3.9	33.8	3.2	140
118	2.2	4.5	34.1	1.5	156
122	1.2	4.0	34.1	1.6	147
126	0.5	3.4	33.9	1.9	146
130	1.6	3.8	33.9	2.4	158
134	2.3	5.2	34.5	0.5	151
138	2.5	4.7	34.3	1.5	161
142	1.0	3.5	34.0	2.2	143
146	2.0	4.4	34.2	1.4	147
150	1.9	4.4	34.3	1.1	148
154	1.1	5.9	33.3	3.0	153
158	0.8	3.3	34.0	2.3	139
162	1.2	4.2	33.9	2.3	138
165	2.5	5.2	34.3	1.3	167
170	1.7	5.7	33.5	2.6	169
174	0.3	3.5	33.6	4.9	148
178	0.9	4.4	33.6	3.1	134
182	2.5	5.1	34.5	0.5	150
186	0.7	3.9	34.0	2.5	141
190	2.8	6.8	34.2	0.3	178
194	-0.2	3.0	33.5	5.6	143
198	3.3	5.5	34.5	0.5	162

Profondeur (cm)	Température des eaux de surface en hiver (°C)	Température des eaux de surface en été (°C)	Salinité des eaux de surface en été (psu)	Couverture de glace de mer (mois/an)	Productivité (gC/m²yr)
202	-0.4	3.3	33.4	4.6	143
206	2.2	5.2	34.5	0.6	154
210	0.4	3.2	33.8	3.2	142
214	2.3	6.6	33.8	1.4	170
218	0.4	9.9	32.1	1.6	235
222	2.3	8.6	33.4	1.5	219
226	-0.4	3.2	33.3	3.6	140
230	2.1	6.5	33.4	2.5	163
234	1.2	9.9	32.1	2.5	225
238	1.0	4.6	33.8	2.5	140
242	0.4	10.2	31.3	3.0	234
246	1.1	4.6	33.7	3.7	137
250	0.0	7.0	32.5	4.1	148
254	1.4	6.6	33.8	1.4	180
258	0.8	3.9	33.7	3.5	134
262	0.7	4.3	33.0	5.3	125
266	7.4	5.6	32.7	4.0	149
270	1.0	8.7	32.6	1.2	219
274	0.4	5.7	32.9	4.0	181
278	1.3	6.4	33.7	1.5	177
282	0.5	4.1	32.9	5.5	114
290	0.3	5.9	33.4	2.0	153
298	0.7	7.4	32.2	4.5	165
306	0.3	2.9	33.7	2.2	142
314	1.4	9.2	33.2	0.8	204
322	-1.5	1.1	30.9	9.3	91
330	-0.4	4.6	33.0	5.2	162
338	0.2	4.3	33.0	5.2	123
346	-1.0	2.3	33.1	6.9	140
354	-0.8	5.9	32.2	5.8	164
362	-0.5	9.4	30.5	3.4	267
370	-0.4	12.6	29.6	3.1	319
378	0.2	12.1	30.9	2.2	270
386	-0.2	11.7	31.0	2.4	255
394	2.7	12.2	32.4	0.8	297
402	-0.4	12.1	30.2	3.3	281
410	-0.3	12.5	30.3	3.2	268
418	-0.5	12.3	29.5	3.1	327
426	-0.4	12.5	30.3	3.3	265
434	-0.4	12.1	30.2	3.3	279
442	-0.4	12.1	30.2	3.3	278
450	-0.4	12.1	30.3	3.3	277
458	-0.4	12.1	30.3	3.3	278
466	-0.8	10.1	30.7	3.1	241
474	-0.3	10.6	30.7	3.4	260
482	-1.1	4.2	31.2	5.6	151
490	-0.6	8.0	30.9	4.5	221
500	-1.1	4.8	31.3	5.5	156

Profondeur (cm)	Température des eaux de surface en hiver (°C)	Température des eaux de surface en été (°C)	Salinité des eaux de surface en été (psu)	Couverture de glace de mer (mois/an)	Productivité (gC/m²yr)
507	-0.9	7.7	30.3	4.5	252
514	-1.1	4.4	31.7	6.1	135
521	-0.9	5.5	31.3	5.6	171
528	-0.9	5.0	31.5	5.7	161
536	-1.3	2.2	32.1	7.9	117
542	-0.8	3.4	32.5	6.1	136
549	-1.8	1.0	32.2	9.1	98
556	-1.5	0.8	30.9	9.3	90
563	-1.3	6.8	31.7	4.7	158
570	-0.8	4.7	32.6	4.6	142
577	-1.5	1.2	31.4	8.9	97
585	-1.4	2.6	32.4	7.1	123
593	-0.9	4.4	32.5	5.1	138
601	-0.5	7.2	30.1	4.1	266
608	3.5	8.6	33.4	2.4	191
616	-1.3	5.3	31.2	6.1	150
624	4.8	14.4	33.6	0.0	263
632	0.1	9.6	31.5	3.2	228
640	-0.6	10.3	30.3	3.9	264
648	-0.3	6.9	29.5	2.7	255
656	-1.0	4.8	31.5	5.3	176
664	-1.3	3.2	32.3	6.7	125
672	-1.2	4.8	31.5	5.5	152
680	-0.8	5.6	31.7	4.6	186
688	-1.1	4.3	30.7	6.9	172
696	-1.0	3.3	32.1	5.8	132
704	-0.2	5.0	32.1	4.7	157
712	1.4	15.4	31.2	0.4	292
720	0.1	13.8	30.9	1.7	279
728	3.3	15.6	32.0	0.5	287
736	3.6	16.5	32.0	0.0	315
744	0.8	14.8	31.0	0.7	280
752	1.5	15.5	31.0	0.1	299
760	0.3	13.0	31.1	1.7	241
768	2.4	15.4	31.9	0.0	307
776	4.2	16.1	32.3	0.0	322

**Tableau B.2** Résultats des reconstitutions des conditions des eaux de surface de la carotte PS2863-2BC à partir de la méthode des analogues modernes appliquée aux assemblages de dinokystes

Profondeur (cm)	Température des eaux de surface en hiver (°C)	Température des eaux de surface en été (°C)	Salinité des eaux de surface en été (psu)	Couverture de glace de mer (mois/an)	Productivité (gC/m <sup>2</sup> yr)
0	0.9	4.3	32.6	4.8	117
1	0.7	4.3	32.6	5.3	108
2	1.0	4.8	33.5	3.5	150
3	-0.6	2.2	33.1	6.4	139
4	2.2	5.8	34.7	2.0	166
5	1.1	4.7	34.2	4.6	155
6	-0.4	3.9	34.4	2.0	142
7	1.6	5.2	34.3	2.0	140
8	-0.3	3.5	32.9	3.7	133
9	1.5	5.2	34.1	1.7	156
10	0.5	4.4	33.4	2.5	158
11	1.2	5.1	34.5	1.8	145
12	-0.4	3.2	34.0	2.4	149
13	0.3	2.7	33.7	5.2	148
14	1.7	4.5	34.5	2.6	154
15	1.7	6.2	34.8	0.6	161
16	1.0	4.6	34.5	1.6	144
17	1.1	3.5	33.9	3.7	157
18	1.1	4.6	32.6	4.0	139
19	1.8	4.7	33.4	3.9	119
20	1.5	4.6	33.9	2.3	142
21	2.3	5.1	34.3	1.2	152
22	2.6	5.9	34.3	1.6	143
23	1.6	4.3	34.4	1.6	147
24	0.7	3.3	33.8	5.4	156
25	1.6	4.5	34.4	1.4	148
26	2.5	5.4	34.3	1.6	141
27	3.2	6.2	34.7	0.2	169
28	0.6	3.0	33.6	5.1	153
29	1.5	5.0	34.6	0.8	147
30	2.1	4.9	34.4	2.2	154
31	1.2	3.6	34.0	3.4	156
32	2.4	5.1	34.6	2.0	158
33	1.7	4.9	33.1	3.8	119
34	2.8	5.2	34.5	2.1	155
35	2.8	5.8	34.2	1.7	155
36	1.5	3.8	34.0	3.7	157
37	2.2	4.7	33.6	4.0	140
38	2.4	5.4	34.3	1.8	140

**Tableau B.3** Résultats des reconstitutions des conditions des eaux de surface de la carotte PS2863-1 à partir de la méthode des analogues modernes appliquée aux assemblages de dinokystes

Profondeur (cm)	Température des eaux de surface en hiver (°C)	Température des eaux de surface en été (°C)	Salinité des eaux de surface en été (psu)	Couverture de glace de mer (mois/an)	Productivité (gC/m <sup>2</sup> /yr)
1.5	0.2	3.2	33.8	4.7	143
5	-0.4	2.2	33.2	7.3	149
9	2.8	5.0	34.4	1.1	153
13	2.0	5.2	34.6	2.5	160
17	0.1	3.0	32.2	5.9	112
21	2.2	5.0	34.5	2.3	157
25	1.1	4.7	34.3	1.8	155
29	2.9	5.8	34.8	0.2	156
33	2.4	5.7	34.1	1.9	152
37	0.9	3.9	33.9	3.7	155
41	3.1	6.0	34.6	0.3	161
45	2.5	7.6	33.7	0.9	208
49	2.5	5.4	34.6	0.3	165
53	2.5	5.3	34.5	0.4	162
57	2.5	5.6	34.0	1.6	153
60.5	2.4	9.5	33.0	1.2	216
65	1.0	3.9	33.5	2.7	199
69	0.6	3.9	33.6	5.0	142
73	0.3	3.6	33.8	3.9	158
77	1.8	6.6	33.7	1.1	176
81.5	1.5	10.5	32.3	1.7	235
85	1.4	10.7	32.1	1.8	237
89	3.5	7.8	33.9	1.7	212
93	0.5	12.3	31.2	2.2	264
97	0.6	12.1	31.3	2.2	257
100.5	0.8	9.9	32.0	1.7	246
104	2.4	11.5	32.7	0.6	251
108.5	-0.1	7.4	31.4	3.2	199
112	2.2	6.9	33.0	3.1	201
116	-0.8	4.8	32.0	5.2	159
120	-1.5	1.8	31.8	8.1	105
124	-1.2	8.2	30.3	4.5	204
128	-0.9	6.0	31.9	5.0	161
132	-1.0	6.4	31.3	4.3	195
136	-1.4	2.7	31.3	8.2	142
140	-1.3	1.0	31.8	9.1	103
144	-0.9	7.8	29.9	5.0	252
148	-0.9	6.0	29.9	5.6	243
152	-1.2	5.7	31.2	5.5	160
156	-1.6	1.7	31.8	7.4	120
160	-1.7	-0.5	31.0	10.7	72
164	0.0	13.7	31.1	0.6	248
169	3.1	16.1	32.0	0.1	318
174	3.1	13.9	32.9	0.5	283
178	5.8	13.5	33.9	0.0	270
183	4.8	14.7	33.3	0.0	301

## BIBLIOGRAPHIE GÉNÉRALE

- Aagaard-Sørensen, S., Husum, K., Hald, M., Marchitto, T. et Godtliebsen, F. (2014a). Sub sea surface temperatures in the Polar North Atlantic during the Holocene: Planktic foraminiferal Mg/Ca temperature reconstructions. *The Holocene*, 24(1), 93-103.
- Aagaard-Sørensen, S., Husum, K., Werner, K., Spielhagen, R.F., Hald, M. et Marchitto, T.M. (2014b). A Late Glacial–Early Holocene multiproxy record from the eastern Fram Strait, Polar North Atlantic. *Marine Geology*, 355, 15-26.
- Bauch, H.A., Erlenkeuser, H., Spielhagen, R.F., Struck, U., Matthiessen, J., Thiede, J. et Heinemeier, J. (2001). A multiproxy reconstruction of the evolution of deep and surface waters in the subarctic Nordic seas over the last 30,000 yr. *Quaternary Science Reviews*, 20(4), 659-678.
- Baumann, K.-H. et Matthiessen, J. (1992). Variations in surface water mass conditions in the Norwegian Sea: evidence from Holocene coccolith and dinoflagellate cyst assemblages. *Marine Micropaleontology*, 20(2), 129-146.
- Guiot, J. (1990). Methodology of the last climatic cycle reconstruction in France from pollen data. *Palaeogeography, Palaeoclimatology, Palaeoecology*, 80(1), 49-69.
- Hald, M., Andersson, C., Ebbesen, H., Jansen, E., Klitgaard-Kristensen, D., Risebrobakken, B., Salomonsen, G.R., Sarnthein, M., Sejrup, H.P. et Telford, R.J. (2007). Variations in temperature and extent of Atlantic Water in the northern North Atlantic during the Holocene. *Quaternary Science Reviews*, 26(25-28), 3423-3440.
- Hald, M., Dokken, T. et Mikalsen, G. (2001). Abrupt climatic change during the last interglacial–glacial cycle in the polar North Atlantic. *Marine Geology*, 176(1), 121-137.
- Hillaire-Marcel, C., Maccali, J., Not, C. et Poirier, A. (2013). Geochemical and isotopic tracers of Arctic sea ice sources and export with special attention to the Younger Dryas interval. *Quaternary Science Reviews*, 79, 184-190.

- Jessen, S.P., Rasmussen, T.L., Nielsen, T. et Solheim, A. (2010). A new Late Weichselian and Holocene marine chronology for the western Svalbard slope 30,000–0 cal years BP. *Quaternary Science Reviews*, 29(9), 1301-1312.
- Lucchi, R.G., Sagnotti, L., Camerlenghi, A., Macrì, P., Rebesco, M., Pedrosa, M.T. et Giorgetti, G. (2015). Marine sedimentary record of Meltwater Pulse 1a along the NW Barents Sea continental margin. *arktos*, 1(1), 7.
- Maslowski, W., Marble, D., Walczowski, W., Schauer, U., Clement, J.L. et Semtner, A.J. (2004). On climatological mass, heat, and salt transports through the Barents Sea and Fram Strait from a pan-Arctic coupled ice-ocean model simulation. *Journal of Geophysical Research: Oceans*, 109(C3).
- Matthiessen, J. et Baumann, A. (1997). Dinoflagellate cyst records from the East Greenland continental margin during the last 15,000 years: implications for paleoceanographic reconstructions. Dans Hass, C. & Kaminski, M.(eds.): *Micropaleontology and Paleoceanography from the northern North Atlantic.- Gryzbowski Foundation Special Publication* (Vol. 5, p. 149-165).
- McManus, J.F., Francois, R., Gherardi, J.-M., Keigwin, L.D. et Brown-Leger, S. (2004). Collapse and rapid resumption of Atlantic meridional circulation linked to deglacial climate changes. *Nature*, 428(6985), 834-837.
- Müller, J. et Stein, R. (2014). High-resolution record of late glacial and deglacial sea ice changes in Fram Strait corroborates ice–ocean interactions during abrupt climate shifts. *Earth and Planetary Science Letters*, 403, 446-455.
- Müller, J., Werner, K., Stein, R., Fahl, K., Moros, M. et Jansen, E. (2012). Holocene cooling culminates in sea ice oscillations in Fram Strait. *Quaternary Science Reviews*, 47, 1-14.
- Rasmussen, T.L., Forwick, M. et Mackensen, A. (2012). Reconstruction of inflow of Atlantic Water to Isfjorden, Svalbard during the Holocene: Correlation to climate and seasonality. *Marine Micropaleontology*, 94-95, 80-90.
- Rasmussen, T.L., Thomsen, E., Ślubowska, M.A., Jessen, S., Solheim, A. et Koç, N. (2007). Paleoceanographic evolution of the SW Svalbard margin (76°N) since 20,000 14C yr BP. *Quaternary Research*, 67(1), 100-114.
- Risebrobakken, B., Dokken, T., Smedsrød, L.H., Andersson, C., Jansen, E., Moros, M. et Ivanova, E.V. (2011). Early Holocene temperature variability in the Nordic Seas: The role of oceanic heat advection versus changes in orbital forcing. *Paleoceanography*, 26(4).

- Rosell-Melé, A. et Comes, P. (1999). Evidence for a Warm Last Glacial Maximum in the Nordic Seas or an example of shortcomings in UK37'and UK37 to estimate low sea surface temperature? *Paleoceanography*, 14(6), 770-776.
- Rosell-Melé, A., Bard, E., Emeis, K.C., Grieger, B., Hewitt, C., Müller, P.J. et Schneider, R.R. (2004). Sea surface temperature anomalies in the oceans at the LGM estimated from the alkenone-U37K' index: comparison with GCMs. *Geophysical Research Letters*, 31(3).
- Sarnthein, M., Jansen, E., Weinelt, M., Arnold, M., Duplessy, J.C., Erlenkeuser, H., Flatøy, A., Johannessen, G., Johannessen, T. et Jung, S. (1995). Variations in Atlantic surface ocean paleoceanography, 50°-80° N: A time-slice record of the last 30,000 years. *Paleoceanography*, 10(6), 1063-1094.
- Ślubowska-Woldengen, M., Koç, N., Rasmussen, T.L., Klitgaard-Kristensen, D., Hald, M. et Jennings, A.E. (2008). Time-slice reconstructions of ocean circulation changes on the continental shelf in the Nordic and Barents Seas during the last 16,000 cal yr B.P. *Quaternary Science Reviews*, 27(15-16), 1476-1492.
- Ślubowska-Woldengen, M., Rasmussen, T.L., Koç, N., Klitgaard-Kristensen, D., Nilsen, F. et Solheim, A. (2007). Advection of Atlantic Water to the western and northern Svalbard shelf since 17,500calyr BP. *Quaternary Science Reviews*, 26(3-4), 463-478.
- Spielhagen, R.F., Werner, K., Sørensen, S.A., Zamelczyk, K., Kandiano, E., Budeus, G., Husum, K., Marchitto, T.M. et Hald, M. (2011). Enhanced modern heat transfer to the Arctic by warm Atlantic water. *Science*, 331(6016), 450-453.
- Van Nieuwenhove, N., Baumann, A., Matthiessen, J., Bonnet, S. et de Vernal, A. (2016). Sea surface conditions in the southern Nordic Seas during the Holocene based on dinoflagellate cyst assemblages. *The Holocene*, 26(5), 722-735.
- Werner, K., Spielhagen, R.F., Bauch, D., Hass, H.C. et Kandiano, E. (2013). Atlantic Water advection versus sea-ice advances in the eastern Fram Strait during the last 9 ka: Multiproxy evidence for a two-phase Holocene. *Paleoceanography*, 28(2), 283-295.
- Werner, K., Spielhagen, R.F., Bauch, D., Hass, H.C., Kandiano, E. et Zamelczyk, K. (2011). Atlantic Water advection to the eastern Fram Strait — Multiproxy evidence for late Holocene variability. *Palaeogeography, Palaeoclimatology, Palaeoecology*, 308(3-4), 264-276.

- Zamelczyk, K., Rasmussen, T.L., Husum, K., Godtliebsen, F. et Hald, M. (2014). Surface water conditions and calcium carbonate preservation in the Fram Strait during marine isotope stage 2, 28.8-15.4 kyr. *Paleoceanography*, 29(1), 1-12.
- Zamelczyk, K., Rasmussen, T.L., Husum, K., Haflidason, H., de Vernal, A., Ravna, E.K., Hald, M. et Hillaire-Marcel, C. (2012). Paleoceanographic changes and calcium carbonate dissolution in the central Fram Strait during the last 20 ka. *Quaternary Research*, 78(3), 405-416.